2018

ELUCIDATON OF THE PYSICAL AND CHEMICAL PROPERTIES OF CYTOCHROME C – CARDIOLIPIN INTERACTIONS

Margaret Marie Elmer-Dixon

ELUCIDATON OF THE PYSICAL AND CHEMICAL PROPERTIES OF CYTOCHROME *C* – CARDIOLIPIN INTERACTIONS

By

MARGARET MARIE ELMER-DIXON

B.S. Theoretical Physics/Applied Math/Physics, Loyola University Chicago, Chicago, IL, 60660
M.S. Applied Physics, De Paul University, Chicago, IL, 60614

Dissertation

Presented in partial fulfillment of the requirements
for the degree of

Doctorate of Philosophy
In Biochemistry & Biophysics

The University of Montana
Missoula, MT

July 2018

Approved by:

Scott Whittenburg, Dean of The Graduate School
Graduate School

Bruce Bowler, Director of Chemistry & Biochemistry Program
Department of Chemistry & Biochemistry

J. B. Alexander (Sandy) Ross, Committee Member
Department of Chemistry & Biochemistry

Stephen R. Sprang, Committee Member
Department of Chemistry & Biochemistry

Mike DeGrandpre, Committee Member
Department of Chemistry & Biochemistry

Travis Hughes, Committee Member
Department of Chemistry & Biochemistry

Abstract

Elmer-Dixon, Margaret M. Ph. D., Summer 2018 Biochemistry & Biophysics

Elucidation of the Physical and Chemical Properties of Cytochrome *c* - Cardiolipin Interactions

Chairperson: Bruce E. Bowler

Recently, the electron transport protein Cytochrome *c* (Cyt*c*) was shown to interact with the mitochondrial lipid cardiolipin (CL) during the initial stages of the intrinsic apoptotic pathway. This interaction is characterized by the protein binding and oxidation of cardiolipin on the concave surface of the outer leaflet of the inner mitochondrial membrane. To date, this interaction has been studied with a variety of methods and techniques reporting varied and often conflicting findings characterizing the nature and extent of the protein-lipid interaction. Cyt*c* has been hypothesized to interact with cardiolipin electrostatically, hydrophobically and through hydrogen bonding and is thought to partially to completely unfold and imbed in the membrane during the interaction or remain folded on the membrane surface. This thesis aims to (1) quantitatively assess the electrostatic protein-lipid interaction, (2) characterize the cationic amino acid constituents that comprise the electrostatic protein binding site, (3) address the impact of membrane curvature on (a) lipid packing and (b) protein binding. Here, we present a complete analysis of electrostatic Cyt*c*-CL binding to both yeast and human variants of the protein. Using a new technique for lipid quantification, we characterize the interaction of the protein with membrane surfaces with high reproducibility. Our findings strongly suggest a biphasic response of the protein when exposed to CL with attenuated unfolding of the human variant with respect to the yeast variant. Alanine scanning was used to elucidate the electrostatic constituents of the anionic site. Lysines 72, 73, 86 and 87 were shown to be involved in CL binding but do not completely characterize electrostatic binding site. We also show that CL preferentially partitions to concave surfaces and that this preferential localization attenuates the interaction of Cyt*c* with the outer leaflet of mixed lipid vesicles. Lastly, we demonstrate the role of membrane curvature for electrostatically bound Cyt*c*. Here, Cyt*c* conformational rearrangements are attenuated on concave CL surfaces. The nature of the binding is intrinsically different with a concerted structural rearrangement observed on concave surfaces as opposed to the biphasic electrostatically-driven conformational rearrangement seen on convex outer leaflets.

Acknowledgements

The successful completion of this behemoth of a project would not have been possible without the support, guidance and mentoring of a large group of people. First and foremost, I would like to thank my advisor, Dr. Bruce Bowler. A great mentor teaches you to question everything, including yourself. Dr. Bowler has shown me how to be a critical, thoughtful scientist and for the opportunity to work with him, I am forever grateful.

Thank you to all past and present members of the Bowler lab. This work has taken considerable time and effort and being able to work cooperatively as a team has facilitated much of this work. Levi, Dustin, Haotian, Harmen, Moses and Shiloh, our conversations have inspired many of the experimental designs and analyses presented here as well as helped me avoid proceeding with some of my less successful ideas.

Thank you especially to Ziqing Xie. I could not have been more fortunate to find and work with a more dedicated undergraduate researcher. Your willingness to perform the so many of the important experimental preparations made completing this project possible.

I would like to thank my committee members, Dr. Mike DeGrandpre, Dr. Sandy Ross, Dr. Steve Sprang and Dr. Travis Hughes. From our initial meeting, your insight and expertise has been invaluable for experimental development and analysis.

Finally, I would like to thank my friends and family for the support they unknowingly provided throughout my graduate career. Thank you to both Harmen and Beth for helping me complete my daily tasks in the last months of my pregnancy and first months of parenthood. Harmen, collaborating with you has been intellectually and professionally rewarding and entertaining. Thank you to so many of my faculty mentors (Andrea Stierle, Holly Thompson, Brooke Martin, and Kent Sugden). You have taught me how to be a good mentor to others through your actions and our conversations and provided me with an educational model and mentality I hope emulate in my own career.

Thank you to my parents, Carol and Paul Elmer for listening to me vent my frustrations at 5 a.m. and to really forcing me to be able to explain exactly what I do on a daily basis. Thank you especially to my husband T. Scott Dixon. Your love, understanding and support from half a world away when need be and here when possible have made completing my graduate studies a reality.

Table of Contents

List of Figures

List of Tables

List of Appendix Tables

CHAPTER 1: Introduction

1.1. Cytochrome *c* Biological Role in the Cell.

Cytochrome *c* (Cyt*c*) is a small globular heme protein found in high concentrations in the intermembrane space of mitochondria where it shuttles electrons between complex III and complex IV of the electron transport chain (Figure 1.1).[1–3] Peroxidase activity associated with energy harvesting in electron transport has been isolated to the heme active site at the center of the protein.[1] Structural analysis, in coordination with mutagenesis and stopped-flow[4,5], has shown that access to the heme active site is regulated by the flexible Ω-loop-D (residues 70-85, Figure 1.2). Further, loop opening, and thus heme access, is directly linked to enhanced peroxidase activity.

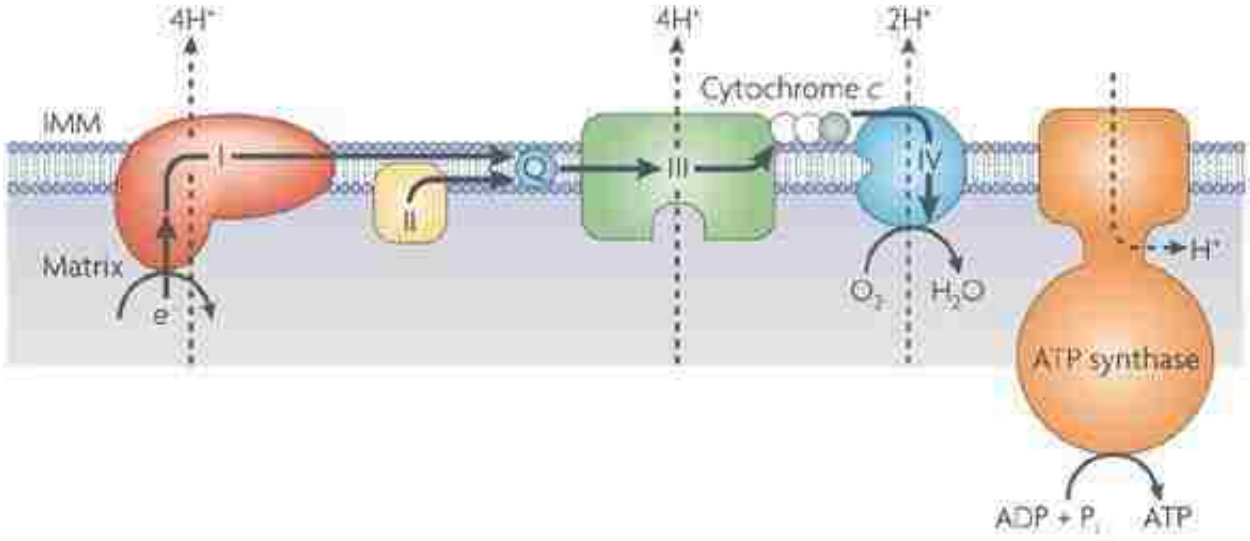

Figure 1.1. Cartoon of electron transport chain showing Cytochrome *c*'s role transporting electrons from complex III to complex IV on the surface of the inner mitochondrial membrane (IMM).[1]

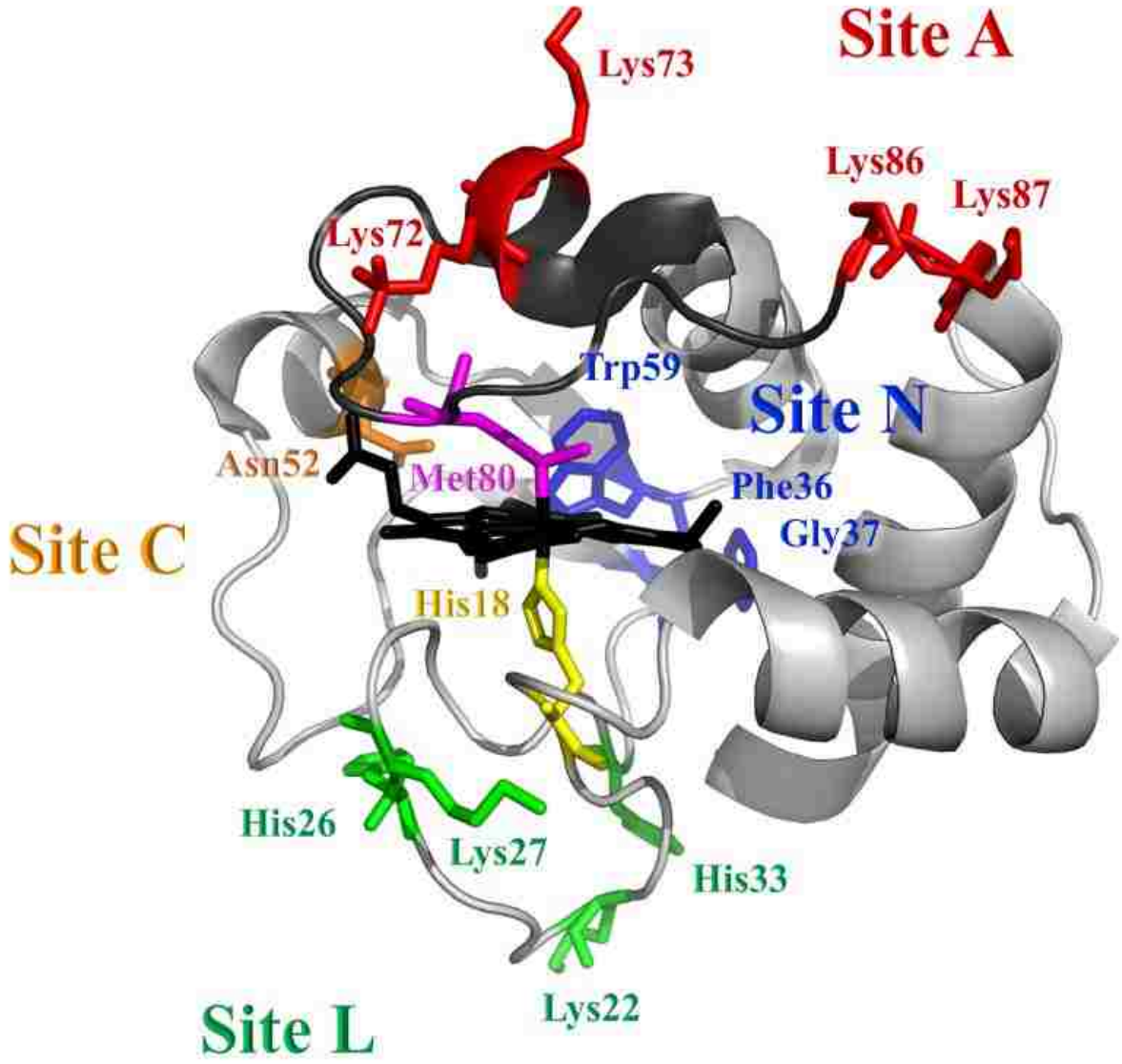

Figure 1.2. Cartoon of iso-1-yeast Cyt*c* corresponding to PDB 2YCC[6] produced using MacPymol. Heme center (Black sticks), tethered to protein by His18 (Yellow) and Met80 (Magenta). The flexible Ω-loop-D (residues 70-85, Dark Grey) controls direct access to the heme. The A site (Red) flanks Ω-loop-D above the heme while the L site (Green) sits below the heme. The C site (Orange) is hydrophobically buried adjacent to the heme. The N site (Blue) sits behind the heme toward the back of the heme crevice.

1.2.Cytochrome *c*'s Role in Apoptosis.

Recently, Cyt*c* was shown to have an additional role in the precursory steps of the intrinsic apoptotic pathway.[7–12] During apoptotic initiation, Cyt*c* binds and oxidizes the non-bilayer-forming lipid cardiolipin (CL) on the surface of the outer leaflet of the inner mitochondrial membrane in the cristae of the mitochondrion (Figure 1.3).[12,13] After oxidation, the protein loses affinity for the CL surface and dissociates from the membrane and exits the mitochondrion.[10–12] The exact mechanism for protein efflux from the mitochondrion is not clearly understood with several potential mechanisms of escape hypothesized.[10–12] Interestingly, CL is found in appreciable concentrations on the outer membrane of the mitochondrion suggesting a migration pathway may exist.[12]

The nature of the protein-lipid interaction between cationic Cyt*c* (+8 net charge) and CL (-2 headgroup charge) is not clearly understood and several conflicting models have been postulated to characterize the involvement of residues and regions on the protein, the structural orientation of the protein-lipid interaction, and the extent of protein interaction with the lipid and the membrane.[13–28]

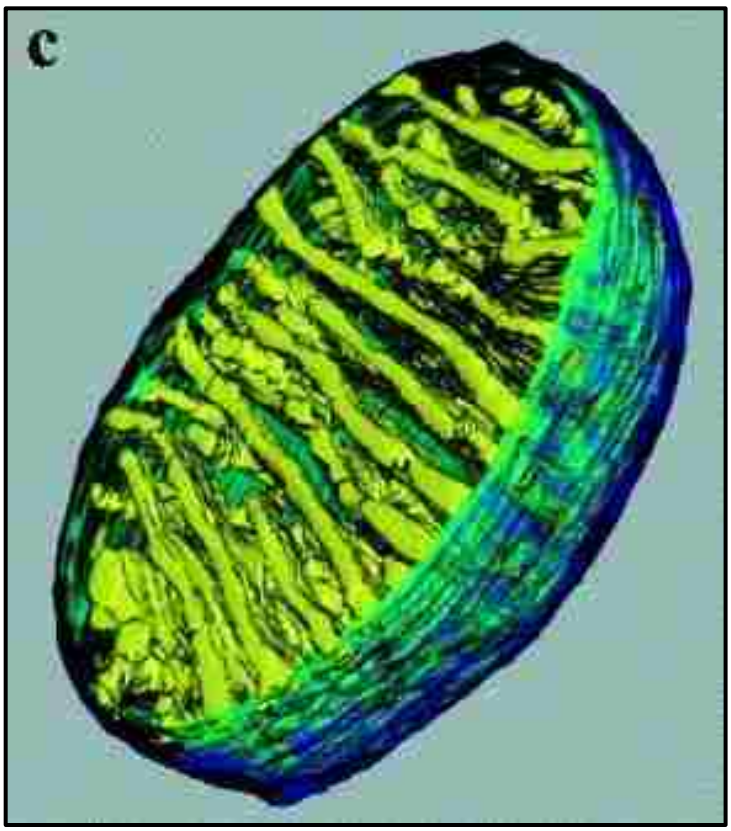

Figure 1.3. Composite three-dimensional model of chick cerebellum mitochondrion imaged using electron tomography. Outer membrane shown in blue and cristae, including both leaflets of the inner mitochondrial membrane, is displayed in yellow.[29]

1.3. Cardiolipin Binding Sites of Cytochrome *c*.

Four major regions of the protein have been hypothesized to function as binding sites during CL interaction. The anionic site, site A, resides on the flexible Ω-loop-D above the heme where it potentially regulates access to the heme loop crevice, the known site of peroxidation during electron transport (Figure 1.2).[14,23,30–32] This site is minimally characterized as electrostatically interacting with one lysine at residue 72.[14,23,30,31] Lysines at residues 73[14,23,30,31] and potentially 86 and 87 may also be constituents of this site.[32] The C site, comprised of a hydrophobically buried asparagine at residue 52, could potentially hydrophobically interact with buried CL acyl

chains (Figure 1.2).[14] The lipid-interacting or L site comprises the region below the heme and consists of histidines at positions 26 and 33 and lysines at positions 22, 25 and 27.[33] The L site is thought to interact with CL via both hydrogen bonding and electrostatic interactions (Figure 1.2).[33] Recently, a fourth site, the N site, has been characterized as Phe36, Gly37, Thr58, Trp59 and Lys60 (Figure 1.2).[34]

These four sites are not completely conserved across eukaryotes. Lysine at position 25, Thr58, as well as Lys60 are absent in yeast variants and may produce a varied response to lipid binding at the L site and N sites, respectively, when compared with higher order variants.[6,33,34]

1.4. Conformational Binding Models of Cytochrome *c*.

Two major conformations have been hypothesized to characterize protein structure during lipid interaction. The compact folded structure maintains the native Cyt*c* conformation, docking lipid headgroups at the exterior binding sites (A and L (See Figure 1.2)) while promoting acyl chain invagination into the heme loop crevice by maintaining a highly structured hydrophobic pocket around the heme.[15,21,34,35] The C site could further stabilize infiltration of acyl chains into the protein core through hydrophobic interaction.[14,21,31,36,37] Direct experimental evidence also supports a partially unfolded or extended conformer.[18,19,23–25,38] In this conformation, Ω-loop-D opens, promoting access to the heme active site. [18,19,23–25] Further structural rearrangement may encourage more contact between sites N, C and L with the membrane. Partial unfolding of the structure may also allow for partial burial of the protein into the hydrophobic region of the membrane.[38]

1.5. Environmental Contributions to Cytochrome *c*-Cardiolipin Binding.

To study this interaction, a wide variety of mimetic systems have been employed. Lipid composition has varied from pure cardiolipin systems[39] to mixed cardiolipin/neutral lipid systems[18,19] at varying concentrations. Further complicating the problem, a range of pHs from 7.0-8.0 are used.[14,18,19,33,35,39] Cyt*c* has a pH dependent conformer that further convolutes binding analyses. To complicate the matter further, hydrogen bonding is attributed to the L site due to the presence of histidines at the site, suggesting the site's involvement is a pH dependent phenomenon.[18,33] This variation in experimental design may be partially responsible for the diverse and conflicting results that have led to the characterization of four binding sites and two potential conformational models.

1.6. The Complexity and Consequences of *In Vitro* Experimental Design on Cytochrome *c*-Cardiolipin Binding.

The diverse array of model systems used to investigate Cyt*c*-CL binding makes direct comparison of experimental findings difficult at best. To investigate the intrinsic nature of the protein-lipid interaction, the true interaction of Cyt*c* with CL is necessary. Further, a systematic approach to experimental design is essential to make meaningful comparison of findings across a breadth of experiments possible.

Complex experimental design, multiple binding site involvement and multiple protein conformations have made extracting binding constants from lipid titrations nontrivial. Further, reported binding constants are often conflicting due to lack of analytical lipid quantification among other concerns. A simplified approach including reproducible, analytical analysis of site-specific involvement in lipid binding is needed to meaningfully analyze the Cyt*c*-CL system.

1.7. Cardiolipin's Structure Dictates Membrane Location and Functionality.

Cardiolipin is a large non-membrane-forming phospholipid consisting of two negatively charged phosphate headgroups and four acyl chains.[40] Tetraoleylcardiolipin (1',3'-bis[1,2-dioleoyl-sn-glycero-3-phospho]-glycerol) is the most stable form of cardiolipin, and the one generally used *in vitro*. It has four 18-carbon mono-unsaturated acyl chains (Figure 1.4).[7,12,19,39,41] Many variations of the lipid exist but are hard to work with and generally not used. The four unsaturated acyl chains have a larger cross-sectional area than the lipid's headgroup giving the bulk structure of the molecule a conic geometric shape and making it a non-membrane forming lipid.[40,42] Non-membrane forming lipids with smaller headgroups than tail cross sections can generally be found on the concave leaflet of curved membranes.[40,42,43] Cardiolipin is known to reside in high concentrations on the outer leaflet of the inner mitochondrial membrane.[7,13,41] This surface is concave in accordance with the preferred membrane surface dictated by the lipid's structure (Figure 1.3).

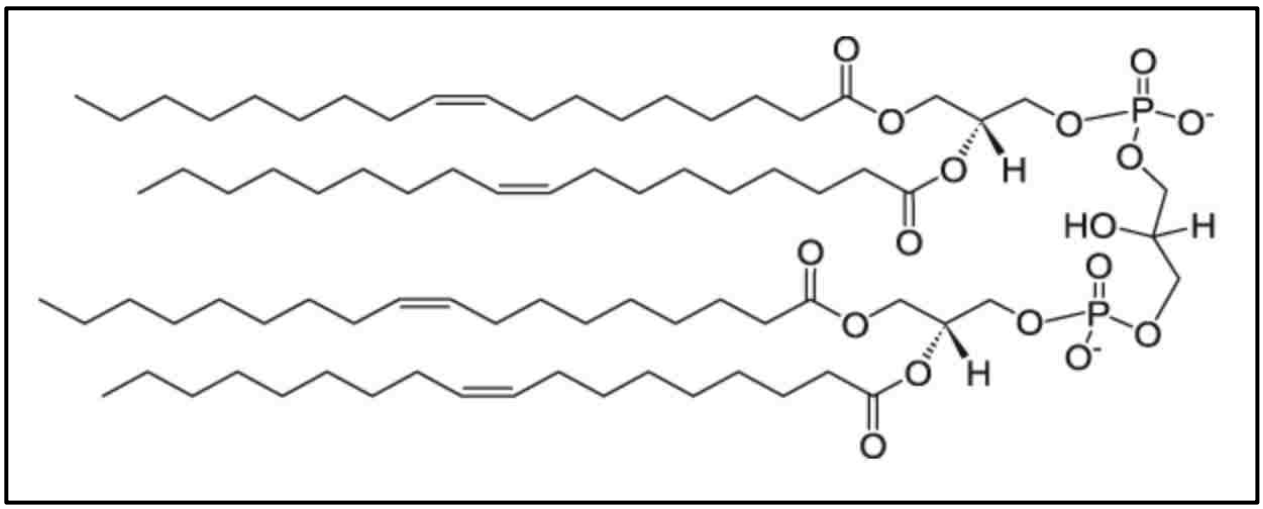

Figure 1.4. The most commonly researched form of Cardiolipin, Tetraoleylcardiolipin (1',3'-bis[1,2-dioleoyl-sn-glycero-3-phospho]-glycerol), imaged using ChemBioDraw courtesy of Avanti Polar Lipids (https://avantilipids.com/product/710335).

1.8. Experimental Considerations Ignore Cardiolipin's Preferred Membrane Location.

The majority of studies investigating Cyt*c*-CL interactions utilize mixed membrane systems generally consisting of CL and dioleoylphosphocholine (1,2-dioleoyl-sn-glycero-3-phoshocholine or DOPC)[13,15,17,21,22,24,25,27,44–46] (and occasionally other formulations[14,16,21,22,25,35]). Because CL's structure suggests a strong preference for the lipid to partition to the concave surface of membranes, careful consideration is needed when designing experiments with mixed lipid systems. Either the system designed needs to be characterized to verify the lipid of interest is in the location where the interaction is being studied or experimentation needs to occur on concave surfaces. DOPC is a well known, cylindrical membrane forming lipid with no preferred curvature-dependent localization.[40,47,48] Experiments using DOPC/CL formulations generally assume that both lipids mix homogeneously throughout the membrane without verifying lipid location. This basic assumption gives rise to concerns that Cyt*c* binding to these mixed systems may not truly be an investigation of CL binding. It should be noted that findings corresponding

to these mixed systems are often conflicting and difficult to compare. An analysis of CL location in mimetic systems would facilitate a better understanding of previously reported findings using mixed lipid membranes.

1.9. Experimental Considerations Ignore Cytochrome *c*'s Location in the Mitochondria and the Role of Membrane Curvature in Protein-Lipid Binding.

Cyt*c* is known to reside in high concentrations in the inner mitochondrial space surrounded by the cardiolipin rich, concave, outer leaflet of the inner mitochondrial membrane. The physiological environment where Cyt*c*-CL binding occurs[32] (the concave outer leaflet) and CL's hypothesized propensity for negatively curved surfaces strongly suggests that the true nature of the protein-lipid interaction is membrane curvature dependent. To date, one group has considered the membrane structural dependence on this interaction.[34] All other investigations of Cyt*c*-CL binding ignore membrane curvature, assume homogeneous lipid mixing and study protein binding to convex surfaces of memetic membranes.[13,14,26,27,32,35,44–46,49,50,15–17,21–25] While these studies are valuable for their isolation of regional contributions by the protein to lipid interaction, they do not begin to study the interaction in a physiologically relevant manner making their findings interesting but not necessarily meaningful. A comprehensive, analytical approach to protein binding to concave surfaces is needed to elucidate the complex physical and chemical interactions that govern Cyt*c*-CL binding.

GOALS

Goal 1: Create Method for Rapid Quantification of Lipids.

In an effort to quantitatively approach lipid-protein binding, a technique for rapid lipid quantification was developed to be used immediately before experimentation to ensure accurate analytical assessment of CL's involvement in binding. In Chapter 2, Mie scattering theory is used to derive a computational method to determine lipid concentration from scattering measurements acquired using a UV-Visible spectrophotometer for pure lipid and mixed lipid systems.

Goal 2: Investigate Species-dependent Electrostatic Binding of Cytochrome *c* to Cardiolipin.

Cytochrome *c* is highly conserved across eukaryotes yet its function varies from yeast, where it serves only in electron transport, to higher order organisms like mammals, where it is integral to both the electron transport chain and apoptotic pathway initiation. Further, the primary lysine attributed to the anionic site, site A, on Cyt*c* is completely conserved in all organisms.[51] Chapter 3 investigates the role of the primary A-site lysine at position 72 in both yeast and human variants of the protein during CL binding.

Goal 3: Characterize the Electrostatic Constituents of the Anionic Site on Cytochrome *c.*

With the varied approaches to study the Cyt*c*-CL interaction, it is unsurprising that a complete characterization of the anionic binding site of Cyt*c* has not been undertaken. In chapter 4, we quantitatively evaluate the electrostatic contributions by lysines in and around the anionic

site of model protein, yeast iso-1-Cyt*c* in an attempt to (1) characterize the binding site constituents and (2) elucidate the physical nature of the binding event.

Goal 4: Evaluate Cardiolipin's Preferred Location on Curved Surfaces with Variable Lipid Composition.

Cardiolipin is found in high concentrations on the concave surface that comprises the outer leaflet of the inner mitochondrial membrane in eukaryotes. Further, the structure of CL suggests that the lipid readily preferentially localizes on the concave leaflet of membranes. Yet, when investigating the Cyt*c*-CL interaction, most experiments assume homogenous mixing of DOPC and CL containing membranes between the inner (concave) and outer (convex) leaflets of vesicles when investigating protein-lipid binding on the convex surface of a mimetic membrane such as a vesicle. Chapter 5 investigates the preferred location of CL in membranes in a concentration dependent manner.

Goal 5: Investigate the Role of Cardiolipin Partitioning in Mixed Lipid Systems During Convex, Electrostatic, Cytochrome *c* Binding.

Using analytical techniques for evaluating electrostatic protein-lipid binding on membrane surfaces established in chapters 2 and 3, chapter 5 investigates the role of lipid partitioning in mixed lipid membranes on protein binding to convex surfaces.

Goal 6: Investigate the Role of Membrane Curvature on Electrostatic Cytochrome *c* – Cardiolipin Binding.

Cyt*c*-CL binding occurs on the concave surface of the inner mitochondrial membrane. Chapter 6 evaluates the physiological relevance of membrane surface curvature on protein-lipid binding.

1.10. REFERENCES

(1) Ow, Y. L. P.; Green, D. R.; Hao, Z.; Mak, T. W. Cytochrome c: Functions beyond Respiration. *Nature Reviews Molecular Cell Biology*. 2008.

(2) Dickerson, R. E.; Timkovich, R. *Cytochromes c, in The Enzymes*, 3rd ed.; Academic Press: New York, 1975.

(3) Pettigrew, G. W.; Moore, G. R. *Cytochromes c: Biological Aspects*; Springer-Verlag: New York.

(4) McClelland, L. J.; Mou, T.-C.; Jeakins-Cooley, M. E.; Sprang, S. R.; Bowler, B. E. Structure of a Mitochondrial Cytochrome c Conformer Competent for Peroxidase Activity. *Proceedings of the National Academy of Sciences of the United States of America* **2014**, *111* (18), 6648–6653.

(5) McClelland, L.; Seagraves, S.; Khan, M.; Cherney, M.; Bandi, S.; Culbertson, J.; Bowler, B. The Response of Ω-Loop D Dynamics to Truncation of Trimethyllysine 72 of Yeast Iso-1-Cytochrome c Depends on the Nature of Loop Deformation. *Journal of Biological Inorganic Chemistry* **2015**, *20* (5), 805–819.

(6) Berghuis, A. M.; Brayer, G. D. Oxidation State-Dependent Conformational Changes in Cytochrome C. *Journal of Molecular Biology* **1992**.

(7) Kagan, V. E.; Bayır, H. A.; Belikova, N. A.; Kapralov, O.; Tyurina, Y. Y.; Tyurin, V. A.; Jiang, J.; Stoyanovsky, D. A.; Wipf, P.; Kochanek, P. M.; Greenberger, J. S.; Pitt, B.; Shvedova, A. A.; Borisenko, G. Cytochrome c/Cardiolipin Relations in Mitochondria: A Kiss of Death. *Free Radical Biology and Medicine* **2009**, *46* (11), 1439–1453.

(8) Alvarez-Paggi, D.; Hannibal, L.; Castro, M. A.; Oviedo-Rouco, S.; Demicheli, V.; Tórtora, V.; Tomasina, F.; Radi, R.; Murgida, D. H. Multifunctional Cytochrome c: Learning New Tricks from an Old Dog. *Chemical Reviews* **2017**.

(9) Hannibal, L.; Tomasina, F.; Capdevila, D. A.; Demicheli, V.; Tórtora, V.; Alvarez-Paggi, D.; Jemmerson, R.; Murgida, D. H.; Radi, R. Alternative Conformations of Cytochrome c: Structure, Function, and Detection. *Biochemistry*. 2016.

(10) Liu, X.; Kim, C. N.; Yang, J.; Jemmerson, R.; Wang, X. Induction of Apoptotic Program in Cell-Free Extracts: Requirement for DATP and Cytochrome C. *Cell* **1996**, *86* (1), 147–157.

(11) Jiang, X. J.; Wang, X. D. Cytochrome C-Mediated Apoptosis. *Annual Review of Biochemistry* **2004**, *73*, 87–106.

(12) Orrenius, S.; Zhivotovsky, B. Cardiolipin Oxidation Sets Cytochrome c Free. *Nature chemical biology* **2005**, *1* (4), 188–189.

(13) Kagan, V. E.; Tyurin, V. A.; Jiang, J.; Tyurina, Y. Y.; Ritov, V. B.; Amoscato, A. A.; Osipov, A. N.; Belikova, N. A.; Kapralov, A. A.; Kini, V.; Vlasova, I. I.; Zhao, Q.; Zou, M.; Di, P.; Svistunenko, D. A.; Kurnikov, I. V; Borisenko, G. G. Cytochrome c Acts as a Cardiolipin Oxygenase Required for Release of Proapoptotic Factors. *Nat Chem Biol* **2005**, *1* (4), 223–232.

(14) Rytömaa, M.; Kinnunen, P. K. J. Evidence for Two Distinct Acidic Phospholipid-Binding Sites in Cytochrome C. *Journal of Biological Chemistry* **1994**, *269* (3), 1770–1774.

(15) Mandal, A.; Hoop, C. L.; Delucia, M.; Kodali, R.; Kagan, V. E.; Ahn, J.; Van Der Wel, P. C. A. Structural Changes and Proapoptotic Peroxidase Activity of Cardiolipin-Bound Mitochondrial Cytochrome C. *Biophysical Journal* **2015**, *109* (9), 1873–1884.

(16) Heimburg, T.; Marsh, D. Investigation of Secondary and Tertiary Structural-Changes of Cytochrome-C in Complexes with Anionic Lipids Using Amide Hydrogen-Exchange Measurements - an Ftir Study. *Biophysical Journal* **1993**, *65* (6), 2408–2417.

(17) Gorbenko, G. P.; Molotkovsky, J. G.; Kinnunen, P. K. J. Cytochrome c Interaction with Cardiolipin/Phosphatidylcholine Model Membranes: Effect of Cardiolipin Protonation. *Biophysical Journal* **2006**, *90* (11), 4093–4103.

(18) Pandiscia, L. A.; Schweitzer-Stenner, R. Coexistence of Native-like and Non-Native Partially Unfolded Ferricytochrome c on the Surface of Cardiolipin-Containing Liposomes. *Journal of Physical Chemistry B* **2015**, *119* (4), 1334–1349.

(19) Pandiscia, L. A.; Schweitzer-Stenner, R. Coexistence of Native-Like and Non-Native Cytochrome c on Anionic Liposomes with Different Cardiolipin Content. *Journal of Physical Chemistry B* **2015**.

(20) Sinibaldi, F.; Fiorucci, L.; Patriarca, A.; Lauceri, R.; Ferri, T.; Coletta, M.; Santucci, R. Insights into Cytochrome C-Cardiolipin Interaction. Role Played by Ionic Strength. *Biochemistry* **2008**, *47* (26), 6928–6935.

(21) Rytomaa, M.; Kinnunen, P. K. J. Reversibility of the Binding of Cytochrome c to Liposomes. Implications for Lipid-Protein Interactions. *Journal of Biological Chemistry* **1995**, *270* (7), 3197–3202.

(22) Tuominen, E. K. J.; Zhu, K.; Wallace, C. J. A.; Clark-Lewis, I.; Craig, D. B.; Rytömaa, M.; Kinnunen, P. K. J. ATP Induces a Conformational Change in Lipid-Bound Cytochrome C. *Journal of Biological Chemistry* **2001**, *276* (22), 19356–19362.

(23) Muenzner, J.; Pletneva, E. V. Structural Transformations of Cytochrome c upon Interaction with Cardiolipin. *Chemistry and Physics of Lipids* **2014**, *179*, 57–63.

(24) Hanske, J.; Toffey, J. R.; Morenz, A. M.; Bonilla, A. J.; Schiavoni, K. H.; Pletneva, E. V. Conformational Properties of Cardiolipin-Bound Cytochrome C. *Proceedings of the National Academy of Sciences of the United States of America* **2012**, *109* (1), 125–130.

(25) Hong, Y.; Muenzner, J.; Grimm, S. K.; Pletneva, E. V. Origin of the Conformational Heterogeneity of Cardiolipin-Bound Cytochrome C. *Journal of the American Chemical Society* **2012**, *134* (45), 18713–18723.

(26) Amacher, J. F.; Zhong, F.; Lisi, G. P.; Zhu, M. Q.; Alden, S. L.; Hoke, K. R.; Madden, D. R.; Pletneva, E. V. A Compact Structure of Cytochrome c Trapped in a Lysine-Ligated State: Loop Refolding and Functional Implications of a Conformational Switch. *Journal of the American Chemical Society* **2015**, *137* (26), 8435–8449.

(27) Muenzner, J.; Toffey, J. R.; Hong, Y.; Pletneva, E. V. Becoming a Peroxidase: Cardiolipin-Induced Unfolding of Cytochrome C. *Journal of Physical Chemistry B* **2013**, *117* (42), 12878–12886.

(28) Nantes, I. L.; Zucchi, M. R.; Nascimento, O. R.; Faljoni-Alario, A. Effect of Heme Iron Valence State on the Conformation of Cytochrome c and Its Association with Membrane Interfaces: A CD AND EPR INVESTIGATION . *Journal of Biological Chemistry* **2001**, *276* (1), 153–158.

(29) Frey, T. G.; Renken, C. W.; Perkins, G. A. Insight into Mitochondrial Structure and Function from Electron Tomography. *Biochimica et Biophysica Acta - Bioenergetics* **2002**, *1555* (1–3), 196–203.

(30) Sinibaldi, F.; Howes, B. D.; Droghetti, E.; Polticelli, F.; Piro, M. C.; Di Pierro, D.; Fiorucci, L.; Coletta, M.; Smulevich, G.; Santucci, R. Role of Lysines in Cytochrome C-Cardiolipin Interaction. *Biochemistry* **2013**, *52* (26), 4578–4588.

(31) Sinibaldi, F.; Milazzo, L.; Howes, B.; Piro, M.; Fiorucci, L.; Polticelli, F.; Ascenzi, P.; Coletta, M.; Smulevich, G.; Santucci, R. The Key Role Played by Charge in the Interaction of Cytochrome c with Cardiolipin. *JBIC Journal of Biological Inorganic Chemistry* **2017**, *22* (1), 19–29.

(32) Kostrzewa, A.; Páli, T.; Froncisz, W.; Marsh, D. Membrane Location of Spin-Labeled Cytochrome c Determined by Paramagnetic Relaxation Agents. *Biochemistry* **2000**, *39* (20), 6066–6074.

(33) Kawai, C.; Prado, F. M.; Nunes, G. L. C.; Di Mascio, P.; Carmona-Ribeiro, A. M.; Nantes, I. L. PH-Dependent Interaction of Cytochrome c with Mitochondrial Mimetic Membranes: The Role of an Array of Positively Charged Amino Acids. *Journal of Biological Chemistry* **2005**, *280* (41), 34709–34717.

(34) O'Brien, E. S.; Nucci, N. V.; Fuglestad, B.; Tommos, C.; Wand, A. J. Defining the Apoptotic Trigger: The Interaction of Cytochrome c and Cardiolipin. *Journal of Biological Chemistry* **2015**, *290* (52), 30879–30887.

(35) Rytomaa, M.; Mustonen, P.; Kinnunen, P. K. J. Reversible, Nonionic, and PH-Dependent Association of Cytochrome c with Cardiolipin-Phosphatidylcholine Liposomes. *Journal of Biological Chemistry* **1992**, *267* (31), 22243–22248.

(36) Tuominen, E. K. J.; Wallace, C. J. A.; Kinnunen, P. K. J. Phospholipid-Cytochrome c Interaction. Evidence for the Extended Lipid Anchorage. *Journal of Biological Chemistry* **2002**, *277* (11), 8822–8826.

(37) Sinibaldi, F.; Howes, B.; Piro, M.; Polticelli, F.; Bombelli, C.; Ferri, T.; Coletta, M.; Smulevich, G.; Santucci, R. Extended Cardiolipin Anchorage to Cytochrome c : A Model for Protein–Mitochondrial Membrane Binding. *JBIC Journal of Biological Inorganic Chemistry* **2010**, *15* (5), 689–700.

(38) McClelland, L. J.; Steele, H. B. B.; Whitby, F. G.; Mou, T. C.; Holley, D.; Ross, J. B. A.; Sprang, S. R.; Bowler, B. E. Cytochrome c Can Form a Well-Defined Binding Pocket for Hydrocarbons. *Journal of the American Chemical Society* **2016**.

(39) Elmer-Dixon, M. M.; Bowler, B. E. Site A-Mediated Partial Unfolding of Cytochrome c on Cardiolipin Vesicles Is Species-Dependent and Does Not Require Lys72. *Biochemistry* **2017**, *56* (36), 4830–4839.

(40) Burger, K. N. J. Greasing Membrane Fusion and Fission Machineries. *Traffic* **2000**, *1* (8), 605–613.

(41) Paradies, G.; Paradies, V.; De Benedictis, V.; Ruggiero, F. M.; Petrosillo, G. Functional Role of Cardiolipin in Mitochondrial Bioenergetics. *Biochimica et Biophysica Acta - Bioenergetics*. 2014, pp 408–417.

(42) Carnie, S.; Israelachvili, J. N.; Pailthorpe, B. A. Lipid Packing and Transbilayer Asymmetries of Mixed Lipid Vesicles. *BBA - Biomembranes* **1979**, *554* (2), 340–357.

(43) Marsh, D. *Handbook of Lipid Bilayers*; 2013.

(44) Pandiscia, L. A.; Schweitzer-Stenner, R. Salt as a Catalyst in the Mitochondria: Returning Cytochrome c to Its Native State after It Misfolds on the Surface of Cardiolipin Containing Membranes. *Chemical Communications* **2014**, *50* (28), 3674–3676.

(45) Vincelli, A. J.; Pottinger, D. S.; Zhong, F.; Hanske, J.; Rolland, S. G.; Conradt, B.; Pletneva, E. V. Recombinant Expression, Biophysical Characterization, and Cardiolipin-Induced Changes of Two Caenorhabditis Elegans Cytochrome c Proteins. *Biochemistry* **2013**, *52* (4), 653–666.

(46) Pandiscia, L. A.; Schweitzer-Stenner, R. Coexistence of Native-Like and Non-Native Misfolded Ferricytochrome C on the Surfac of Cardiolipin Containing Liposomes. *Biophysical Journal* **2015**, *108* (2, Supplement 1), 91a.

(47) Capponi, S.; Freites, J. A.; Tobias, D. J.; White, S. H. Interleaflet Mixing and Coupling in Liquid-Disordered Phospholipid Bilayers. *Biochimica et Biophysica Acta - Biomembranes* **2016**, *1858* (2), 354–362.

(48) Pathak, P.; London, E. The Effect of Membrane Lipid Composition on the Formation of Lipid Ultrananodomains. *Biophysical Journal* **2015**, *109* (8), 1630–1638.

(49) Soffer, J. B.; Fradkin, E.; Pandiscia, L. A.; Schweitzer-Stenner, R. The (Not Completely Irreversible) Population of a Misfolded State of Cytochrome c under Folding Conditions. *Biochemistry* **2013**, *52* (8), 1397–1408.

(50) Santucci, R.; Bongiovanni, C.; Mei, G.; Ferri, T.; Polizio, F.; Desideri, A. Anion Size Modulates the Structure of the A State of Cytochrome C. *Biochemistry* **2000**, *39* (41), 12632–12638.

(51) Margoliash, E., and Schejter, A. (1996) How does a small protein become so popular?: A succinct account of the development of our understanding of cytochrome *c*. In *Cytochromes C:* A Multidisciplinary Approach (Scott, R. A. and Mauk, A. G., Eds) pp 3-31, University Science Books, Sausalito, CA.

CHAPTER 2: Lipid Quantification

2.1. Rapid Quantification of Cardiolipin Lipid and Vesicle Concentration.

2.1.1. INTRODUCTION

Vesicles are made and used in a variety of biologically relevant experiments to elucidate and characterize membrane associated interactions. Existing methods for vesicle quantification are time consuming and costly. Commercially available particle-counting equipment can enumerate vesicles as small as 10 nm, but these devices are expensive. Phosphate analysis assays and inductively coupled plasma atomic emission spectroscopy (ICP) can measure phosphate headgroup concentration but are time consuming and destroy large amounts of sample [1–3] and thus are impractical for routine use. Because of these limitations, measurement of protein/membrane binding affinities via analytical vesicle titrations is expensive. Due to lipid oxidation in solution and membrane stability [4,5], it is essential that lipid and vesicle concentration be measured expeditiously. Here, we report a rapid and reliable method for vesicle quantification.

This quantification technique can be performed immediately before vesicle titrations of protein samples and does not destroy any of the vesicle stock solution. After initial validation, this technique requires only 15 minutes to quantify vesicles and lipids and uses common laboratory equipment and software. In this report, we apply the method to measurement of the concentration of 100% 18:1 cardiolipin (1',3'-bis[1,2-dioleoyl-*sn*-glycero-3-phospho]-*sn*-glycerol) vesicles of known radii, we then use existing physical parameters to extend this method to DOPC analysis demonstrating that the method is readily adapted for use with vesicles composed of any lipid with appropriate validation or calibration.

2.1.2. THEORETICAL CALCULATIONS

Quantifying lipids is difficult because they have no absorbance signature in a convenient region of the UV-Visible spectrum (Figure 2.1.1.). While lipids, themselves, do not characteristically absorb visible light, supramolecular structures like lipid vesicles scatter light in a size, wavelength, concentration and media dependent manner known as Mie scattering [6]. A UV-Vis spectrophotometer can be used to evaluate Mie Scattering as a function of wavelength. Knowing particle size, the wavelength and angle of exposure, as well as the refractive index of the medium, the concentration of particles in solution can be calculated. Methods for using Mie scattering theory to measure nanoparticle concentration [6,7] have been modified for application to cardiolipin and 1,2-dioleoyl-*sn*-glycero-3-phosphocholine (DOPC) vesicles so that vesicle and lipid concentration can be determined.

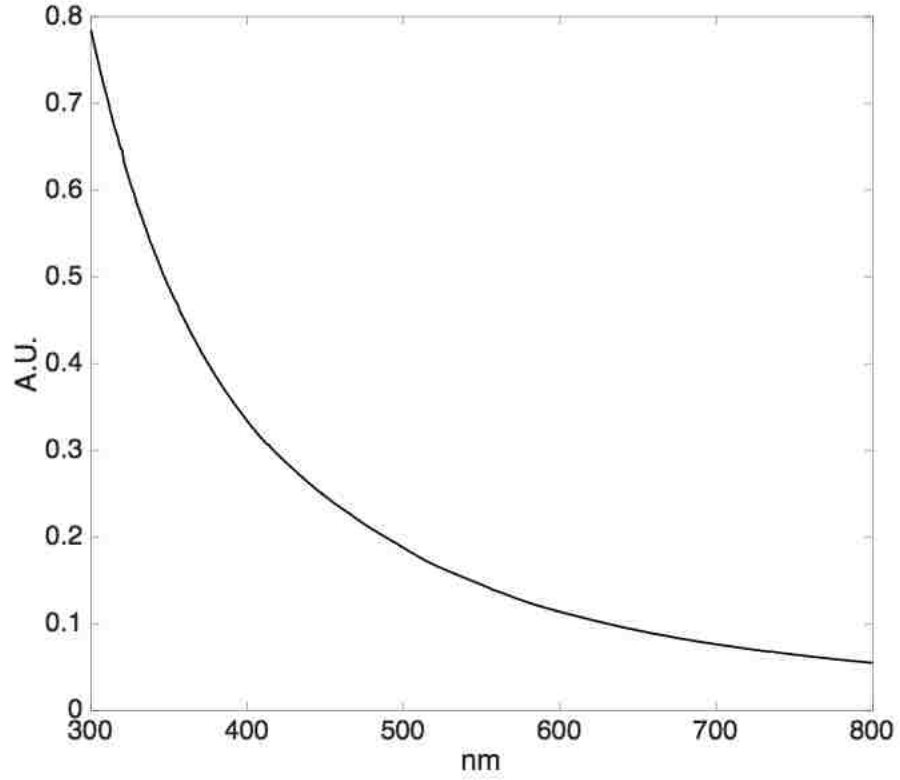

Figure 2.1.1. Scattering measurement of 136.6 nm extruded cardiolipin vesicles prepared at a concentration of 535 μM lipid (based on reported mass from manufacturer) in 20 mM TES Buffer, 0.1 mM EDTA, pH 8. The scattering curve demonstrates no intrinsic absorbance in the UV-Visible region of the electromagnetic spectrum for cardiolipin.

This method involves calculating the scattering cross section of vesicles of known size at an appropriate wavelength using Mie scattering theory, measuring the absorbance of the vesicle with a UV-Vis spectrophotometer and solving Beer's law for the particle concentration. Matlab code is provided in Appendix I.1 for the required calculations. To accurately calculate scattering due to vesicles, vesicle size, angle and wavelength of absorbance and the index of refraction of the medium are required. Furthermore, with appropriate validation or calibration, the number of lipids per vesicle can be determined, allowing total lipid concentration to be calculated.

To relate absorbance to the calculated scattering off of a non-absorbing vesicle, Beer's law must be expressed in terms of the scattering extinction coefficient, C_{ext} [6,7];

$$A(\lambda) = d \sum_i N_i C_{ext,i}(\lambda) \qquad \text{Eqn. 2.1.1}$$

where d is sample path length, N is the number of scattering centers and A is the total absorbance measured at a specific wavelength, λ.

The scattering extinction coefficient is expressed as [6,7]

$$C_{ext} = \frac{\lambda^2}{2\pi} \sum_{n=1}^{\infty} (2n+1)\, Re\{a_n + b_n\} \qquad \text{Eqn. 2.1.2}$$

where a_n and b_n are the differential expressions of Bessel functions

$$a_n = \frac{m\psi_n(mx)\psi_n'(x) - \psi_n(x)\psi_n'(mx)}{m\psi_n(mx)\xi_n'(x) - \xi_n(x)\psi_n'(mx)} \qquad \text{Eqn. 2.1.3a}$$

$$b_n = \frac{\psi_n(mx)\psi_n'(x) - m\psi_n(x)\psi_n'(mx)}{\psi_n(mx)\xi_n'(x) - m\xi_n(x)\psi_n'(mx)} \qquad \text{Eqn. 2.1.3b}$$

where ψ_n, is the Ricatti-Bessel Function, j(n), of the first kind, and ξ_n, is the Hankel function, h(n), of the first kind. The value, x is the size parameter relating vesicle radius, R, to wavelength;

$$x = \frac{2\pi Re(m) R}{\lambda} \qquad \text{Eqn. 2.1.4}$$

where wavelength, λ, is reported in the same units as the vesicle radius. The value m is the relative refractive index represented by the real, n_{Re}, and complex, n_{Im}, parts of the refractive index of the lipid and water.

$$m = \frac{n_{Re,lipid} + n_{Im,lipid}}{n_{Re,water} + n_{Im,water}} \qquad \text{Eqn. 2.1.5}$$

For cardiolipin. $n_{Re,lipid}$ was set to 1.46 [8], while $n_{Im,lipid}$ was approximated as $n_{Im,water}$ at 200 nm ($1x10^{-7}$, [9]). The wavelength dependence of $n_{Re,water}$ was calculated with Eqn. 2.1.6 [10],

$$n_{Re,water}(\lambda) = 1.31848 + \frac{6.662}{\lambda - 129.2} \qquad \text{Eqn. 2.1.6}$$

while $n_{Im,water}$ was approximated using the value at 200 nm reported above. Equations 2.1.2-2.1.6 were programmed into Matlab to solve Eqn. 2.1.1 for N, allowing calculation of vesicle concentration. Absorbance measurements taken with a Beckman Coulter DU 800 UV-Visible spectrophotometer were used in the calculation. Wavelengths were selected such that the value of x in Equation 2.1.4 was between 1 and 10. Wavelengths of 300-400 nm are ideal for measuring vesicle scattering off of 100-200 nm diameter vesicles.

2.1.3. EXPERIMENTAL METHODS

2.1.3.1. Fluorescein Vesicle Preparation.

Vesicles of cardiolipin (TOCL, Avanti Polar Lipids) were formed in the presence of high concentrations (~mM) of fluorescein dye in 20 mM TES, 0.1 mM EDTA at pH 8. Lipids were purchased in chloroform from Avanti. Lipids were initially dried under a steady stream of Argon for 2 hours to remove chloroform. The dried sample was reconstituted into the above specified buffer and vortexed for 1 minute. Lipid solutions then underwent a freeze/thaw/vortex cycle that was repeated 5 times. Lipids were then extruded with an Avanti Mini-extruder fitted with 200 nm membranes to form vesicles. Vesicle diameter was measured by DLS and found to be 136.6 nm. Fluorescein-filled vesicles were buffer exchanged to remove unencapsulated dye from the buffer using a 10,000 MWCO Amicon centrifugal ultrafiltration device. Samples were buffer exchanged multiple times until the flow through showed no detectable fluorescein (ε_{495} = 76,000

M^{-1} cm^{-1}) by UV-Vis spectroscopy. Vesicle size did not change during buffer exchange from that observed immediately after extrusion, as determined by DLS. The spectra of vesicle samples were collected at a series of dilutions. Total fluorescein concentration in the vesicle stock solution was calculated after adjusting for dilution. Vesicle inner volume was approximated by using the lipid size to estimate bilayer thickness, so that the measured vesicle diameter could be corrected for bilayer thickness (estimated as ~3.9 nm from the combined acyl chain and headgroup length of cardiolipin determined with MacPymol software, Schrödinger, Inc.). This estimation corresponds closely with recently published experimental data for cardiolipin bilayers (bilayer thickness ~3.7 nm[11]). Using inner volume per vesicle derived in this manner, the total initial solution volume and the fraction of absorbance remaining after buffer exchange, the vesicle concentration was calculated (Table 2.1.1.).

2.1.3.2. NBD Vesicle Preparation.

To calibrate lipid concentration to vesicle concentration, vesicles were doped with 5% NBD-labelled DOPC lipid (Avanti Polar Lipids), (for NBD, ε_{485} = 19,500 M^{-1} cm^{-1}). Cardiolipin(TOCL)/NBD-labelled DOPC vesicles were formed under the same conditions as stated above using Cardiolipin that was mixed with 5% mole ratio NBD-labelled DOPC lipid in chloroform. The resultant mixture was dried to remove chloroform before reconstitution in 20 mM TES buffer in 0.1 mM EDTA at pH 8.

Cardiolipin(TOCL)/NBD-DOPC mixtures were extruded using an Avanti mini extruder and their size was measured using DLS. NBD-DOPC lipid was assumed to fully incorporate into cardiolipin vesicles at a 5% mole ratio. The membranes of the extruder were colorless after vesicle extrusion, consistent with this assumption. The scattering and absorbance spectrum of the

NBD doped cardiolipin vesicles was measured from 200-800 nm at a series of dilutions (Figure 2.1.2.). The absorbance spectrum of free NBD in solution was also measured (Figure 2.1.2.). NBD absorbance was evaluated from the UV-Vis spectrum of vesicles (Figure 2.1.2.) and used to determine cardiolipin concentration. Cardiolipin concentration from three independently prepared samples is reported in Table 2.1.2. Lipid concentration was also evaluated from the scattering portion of the UV-Vis spectrum (Figure 2.1.2.) using vesicle concentration obtained from Mie scattering and the lipid density evaluated from the relative surface area of cardiolipin (129.8 $Å^2$, [1]) and the vesicle.

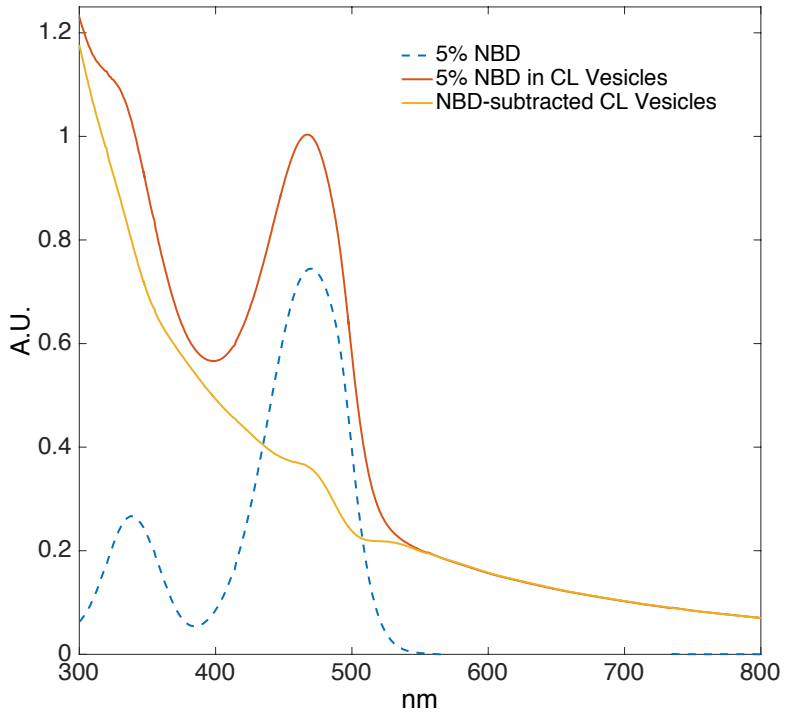

Figure 2.1.2. CL vesicles were prepared at 5% NBD mole ratio. Total absorbance was measured (red) and the NBD signal (blue, dashed) was subtracted to produce scattering due to vesicles (yellow). Scattering data were fit using equations 1-6 for wavelengths between 300-400 nm. Vesicles were measured to be 136 nm using DLS and lipid concentration per vesicle was approximated to be 1.75×10^5 lipids/vesicle based on ICP measurements.

2.1.3.3. ICP Sample Analysis to Measure Lipid Concentration.

Cardiolipin (TOCL, Avanti Polar Lipids) vesicles were prepared in 20 mM TES, 0.1 mM EDTA at pH 8 by extrusion through two 200 nm pore membranes using an Avanti Mini-extruder using the same lipid preparation as stated previously. Scattering and R_g (DLS) were measured for each sample before submission for ICP phosphorous analysis.

DOPC (Avanti Polar Lipids) vesicles were prepared in 20 mM TES, 0.1 mM EDTA at pH 8 by extrusion through two 100 nm pore membranes using an Avanti Mini-extruder using the same lipid preparation method as stated previously. Scattering and R_g (DLS) were measured for each sample before submission for ICP phosphorous analysis.

DLS was performed on extruded vesicles to measure particle size and vesicle concentration of the stock was calculated using the Matlab vesicle concentration calculator. Samples were then made from the stock at various concentrations. The corresponding vesicle concentration for each sample was calculated using the Matlab vesicle concentration calculator before submission for ICP phosphorous analysis. A cold digest (concentrated nitric acid, 12 hours) was used to remove both phosphorous atoms from the cardiolipin headgroup[2] and samples were analyzed on a Perkin Elmer 5300 DV ICP-OES using the 178.2 nm emission of phosphorous.

2.1.3.4. Method Validation.

Initial validation or calibration measurements are required before the Matlab vesicle concentration calculator (MVCC) can be used simply with absorbance data as input. Strong absorbing dyes were used to estimate vesicle and lipid concentration and relate these measurements to scattering measurements. All experiments were performed on a Beckman Coulter DU 800 UV-Visible spectrophotometer where the spectral range from 200 to 800 nm was monitored. A Malvern Zetasizer Dynamic Light Scattering (DLS) instrument was used to monitor vesicle size throughout the validation process. If a DLS instrument is not available, particle size can be measured with a UV-Vis spectrophotometer[7].

To validate the MVCC, vesicles were first quantified by labelling their interior with a strongly absorbing dye and measuring dye content after external dye was removed by extensive

washing. Knowing vesicle size (and thus internal volume) and initial dye concentration, vesicle concentration could be calculated from the decrease in dye absorbance after the wash step. Vesicles were formed in the presence of fluorescein (a strongly absorbing dye) to determine vesicle concentration. External fluorescein was removed from extruded vesicles by buffer exchange and the residual fluorescein concentration was calculated. This fluorescein concentration was related to inner volume of a vesicle to determine the total number of vesicles required to produce the fluorescein absorbance (Table 2.1.1.).

Next, the vesicle concentration was found using Mie scattering theory. To extract scattering data from spectra taken of fluorescein-filled vesicles, the fluorescein absorbance was subtracted from spectra collected after buffer exchange (Figure 2.1.3.). Scattering absorbance data between 300-400 nm were input into the Matlab vesicle concentration calculator because this spectral region has minimal fluorescein absorbance (Figure 2.1.3.) The vesicle concentration obtained is reported in Table 1. The vesicle concentration found using fluorescein is within an error of less than 8% of the vesicle found using Mie Scattering theory in three independent trials. Taking into account the error in approximating inner vesicle volume and extracting scattering absorbance from the raw absorbance data, the agreement is good, validating the use Mie scattering theory to calculate vesicle concentration.

Table 2.1.1.
Comparison of vesicle concentration calculated using fluorescein filled vesicles with that obtained from Mie scattering for the same vesicles.

Vesicle Concentration from Fluorescein Absorbance	Vesicle Concentration from Mie scattering	% Error
$4.8 \pm 0.1 \times 10^{17}$	$5.15 \pm .01 \times 10^{17}$	6.8
$5.0 \pm 0.1 \times 10^{17}$	$5.16 \pm .01 \times 10^{17}$	3.1
$4.8 \pm 0.1 \times 10^{17}$	$5.16 \pm .01 \times 10^{17}$	7.0

Concentrations reported in vesicles per L. Vesicle concentration measurements and calculations found for three independent trials. Error reported reflects error in absorbance measurements.

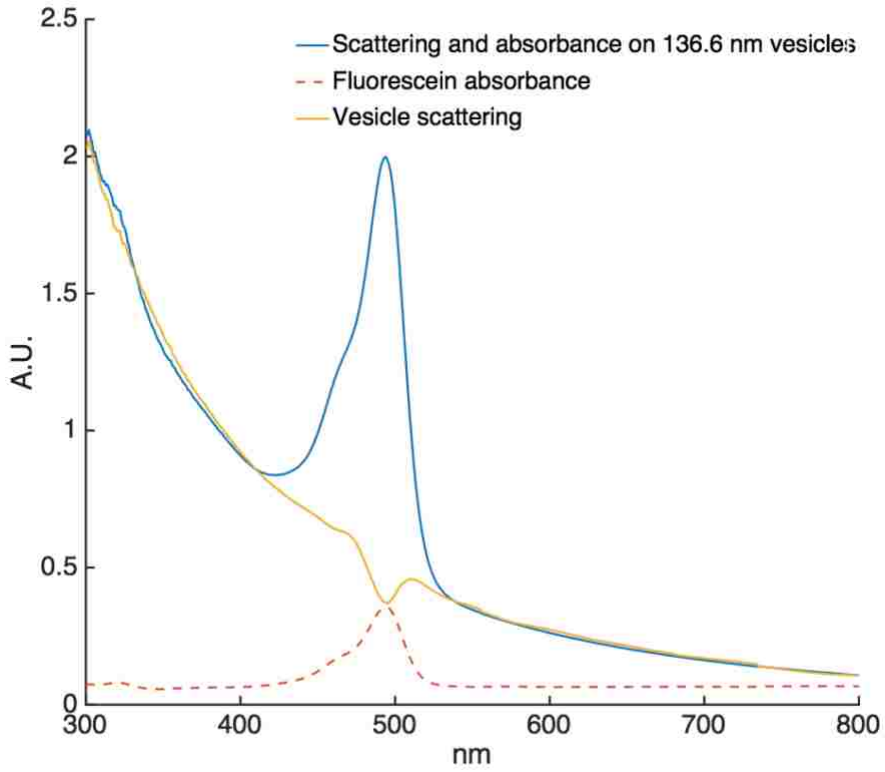

Figure 2.1.3. Fluorescein filled vesicle scattering and absorbance data of extruded vesicles measuring 136.6 nm in diameter using DLS (blue). Fluorescein intrinsic absorbance spectrum shown for diluted fluorescein stock used during vesicle preparation (dotted red). Scattering off vesicles after subtracting out absorbance due to fluorescein inside vesicles.

Having established that the number of vesicles per sample could be calculated, we carried out a second, independent set of experiments so that the MVCC could be calibrated to incorporate lipid density per vesicle to permit lipid concentration determination. In these experiments, lipid concentration per vesicle was measured using fluorescently labelled lipid to correlate vesicle concentration to lipid concentration. NBD-labelled DOPC lipid was used to dope Cardiolipin

vesicles and determine lipid concentration. Associated scattering data from absorbance measurements was used to calculate vesicle concentration and relate that to lipid concentration using Cardiolipin headgroup size as reported by Pan et al.[11] The lipid concentrations obtained from NBD absorbance and from Mie scattering theory from three independent trials are within 5% (Table 2.1.2.), confirming the validity of the surface area used for cardiolipin.

Table 2.1.2.
Comparison of lipid concentration calculated using NBD doped vesicles with that obtained from Mie scattering for the same vesicles.

Lipid Concentration from NBD Absorbance, M	Lipid Concentration from Mie scattering, M	% Error
$8.5 \pm 0.3 \times 10^{-4}$	$8.41 \pm .04 \times 10^{-4}$	1.1
$8.4 \pm 0.2 \times 10^{-4}$	$8.20 \pm .03 \times 10^{-4}$	2.4
$8.5 \pm 0.2 \times 10^{-4}$	$8.16 \pm .02 \times 10^{-4}$	4.4

Error evaluated as standard deviation of multiple spectra collected for each trial.

As an independent external method for lipid concentration calibration, ICP was used to measure phosphorous content of samples of pure cardiolipin vesicles. Samples were prepared for ICP as outlined in Supplementary Information. The correspondence between cardiolipin concentration obtained by phosphorous analysis and cardiolipin concentration calculated with the MVCC using the experimental value for cardiolipin surface area[11] to evaluate lipid density was consistently within <5% (Table A.1.).

To demonstrate the versatility of the MVCC, samples of DOPC were also submitted for ICP analysis and compared to MVCC calculated concentrations (TableA.1.). DOPC bilayer

thickness, headgroup surface area [11] and index of refraction [12] were used to calculate DOPC lipid concentration from scattering. Error between the MVCC and ICP was within <3% demonstrating the calculator's ability to accurately measure lipid concentration given the corresponding lipid physical parameters.

Lipid concentration, as determined using the reported manufacturer concentration, was compared to MVCC findings to analyze the necessity of a vesicle calculator in quantitative experiments. Significant deviations in concentration based on manufacturer specified lipid mass or concentration and ICP analysis are reported for all DOPC and TOCL samples in Table A.2. Error in concentration based on starting material and final ICP measurements were as high as 28%, whereas the correspondence between the ICP and MVCC values was always <5% (Table A.1.). Because of the vesicle formation process used, lipid had the potential of being lost in several steps demonstrating that concentration based on manufacturer reported lipid mass does not necessarily reflect final experimental concentration. This finding supports the use of the MVCC in reliably determining lipid concentration for quantitative experiments.

2.1.4. CONCLUSION

The Mie scattering-based method for vesicle quantification was designed to provide a quick, reliable, and cost effective analytical method, which after initial validation by absorbance and/or phosphorous analysis, can be implemented immediately before any experiment involving use of extruded vesicles. The method allows vesicle concentration to be accurately measured simply using UV- Vis measurements. Knowing the surface area of the lipid (validated or calibrated by absorbance or by phosphorous analysis), lipid concentration can also be obtained with the

MVCC. Due to the simplicity of the experimental setup, vesicle and lipid concentrations may be calculated quickly and without sample destruction, providing a reliable alternative for more time-consuming methods.

The wavelength measurement range is only limited by the size of the vesicle (thus size parameter, x (See Eq. 1.4)) and constraints of the detection device. When using extruded vesicles or vesicles with a well-defined radius, as was done here, DLS measurements are not necessary once vesicle size is established, although occasional spot- checking of the consistency of the extrusion process is recommended. While the region of 300-400 nm was used to measure vesicle scattering and calculate concentration, any convenient wavelength in the UV-Visible spectrum may be used provided the constraints on size parameter, x, are met from Eqn. (2.1.4). This technique uses the mean vesicle radius to determine C_{ext} for a scattering center. Table A.3. provides wavelength ranges for testing dependent on vesicle size for various vesicle compositions. It should be noted that for samples with large standard deviations in vesicle radius, theoretical vesicle calculations may have higher error.

The technique may be adopted for any pure lipid system. The above outlined technique should also work for mixed lipid systems, provided the refractive index of the mixed lipid vesicle is available. Finally, any buffer that does not appreciably change the index of refraction may be used provided it does not absorb significantly at the wavelength of detection. Modifications may be made to incorporate the adjusted index of refraction of the buffering media if needed.

A simplified version of the MVCC written in .m file format can be found in Appendix I.1 with associated instructions on the installation and running of the file. This version uses reported index of refraction, headgroup size and bilayer thickness to calculate lipid concentration for

TOCL, DOPC, POPC (1- palmitoyl-2-oleoyl-sn-glycero-3-phosphocholine) and POPG (1-palmitoyl-2-oleoyl-sn-glycero-3-phospho-(1’-rac-glycerol)).[8,11–15]

2. 2. Rapid quantification of vesicle concentration for DOPG/DOPC and Cardiolipin/DOPC mixed lipid systems of variable composition.

2.2.1. INTRODUCTION

Lipid bilayers in the form of micelles, vesicles and liposomes are important for studies of membrane associated biological interactions. More recently, they have been utilized for vaccine delivery.[16] Both fields use a diverse array of lipid compositions to form biologically relevant membranes.[16,17] To date, basic characterization of lipid systems has been time consuming and expensive.

Recent work by Elmer-Dixon and Bowler (See Chapter 2.1.)[18] described and validated a rapid, label-free, and non-destructive method to determine vesicle number and to generate lipid concentration in pure lipid systems composed of either 1,2-dioleoyl-sn-glycero-3-phosphocholine (DOPC) or cardiolipin (1',3'-bis[1,2-dioleoyl-sn-glycero-3-phospho]-sn-glycerol, TOCL). Using Mie scattering theory, Beer's law was applied to scattering, non-absorbing vesicles to calculate the number of vesicles scattering light.[6,18] A standard UV-Visible spectrophotometer was used to acquire absorbance measurements of the pure lipid vesicles. Knowing vesicle size and the refractive index of the lipid, vesicle concentration was calculated using a Matlab Vesicle Concentration Calculator (MVCC, code found in Appendix I.1).[18] Lipid concentration measurements using standard methods were used to calibrate the number of lipids per vesicle allowing the MVCC also to derive lipid concentration from the absorbance data. This paper extends the MVCC to allow calculation of vesicle number and lipid concentration for mixed lipid systems.

2.2.2. THEORETICAL CALCULATIONS

As previously noted,[18] quantification of lipids is difficult because they lack a characteristic absorbance in the UV-Visible spectrum. However, it is possible to quantify lipid-containing vesicles based on their light scattering properties, using Mie scattering theory. Knowing the lipid number per vesicle, a total lipid concentration can be calculated. Our previous work applied this approach to quantify vesicle and lipid concentrations for pure lipid systems of Cardiolipin and DOPC.[18] Simple modifications in the calculation of vesicle concentration from UV-Visible spectrophotometer scattering measurements can be implemented to extend the technique to mixed lipid systems.

The pure lipid vesicle quantification method of Elmer-Dixon and Bowler (see Chapter 2.1.)[18] requires that the physical characteristics of the pure lipid are known. Specifically, the MVCC requires that the lipid headgroup surface area, lipid bilayer thickness and refractive index of the lipid are known. Headgroup surface area and bilayer thickness are used to determine total vesicle surface area and approximate lipid packing in the membrane allowing calculation of the total number of lipids per vesicle given a known vesicle diameter. Refractive index is required as it dictates how light interacts with the non-absorbing vesicle surface leading to a deviation from its initial trajectory. Cardiolipin (TOCL) and DOPC have significantly different refractive indices (1.46[8] and 1.375,[12] respectively) resulting in differences in the absorbance due to scattering when the same number of vesicles for each pure lipid are scanned with a UV-Visible spectrophotometer. Refractive index prediction for heterogeneous systems from individual component refractive indices is well established for bulk liquid mixtures.[19] That said, the lipids comprising the system are constrained to the lipid bilayer at the surface of the vesicle. At the time of this publication, the authors are unaware of existing models to predict refractive index

from component refractive indices for mixed lipids on surfaces. To extend the MVCC to mixed lipid systems, we have developed and validated a model for approximating the refractive index of lipid mixtures.

The quantification of mixed lipid vesicles requires the use of a bilayer refractive index dependent on the composition of the mixed lipid system. Assuming that lipids readily incorporate into heterogeneous vesicles, a corresponding refractive index can be calculated based on the mole fraction of membrane constituents, the headgroup surface area of each lipid and the corresponding refractive index for that lipid. The mole fraction of each constituent lipid in the membrane only partially dictates the surface composition of a heterogeneous lipid membrane because the surface area of the headgroup of each constituent lipid can vary considerably. The mole fraction, x_i, of a lipid, ℓ_i, in a system of mixed composition is

$$x_i = \frac{[\ell_i]}{\sum_i [\ell_i]}. \qquad \text{Eqn. 2.2.1}$$

We define effective lipid headgroup surface area, $HDSA_{eff}$, as the mole fraction weighted sum of the actual surface areas of the constituent lipids, $HDSA_i$,

$$HDSA_{eff} = \sum_i x_i * HDSA_i \qquad \text{Eqn. 2.2.2}$$

Using $HDSA_{eff}$, the fractional surface area, P_i, for each lipid constituent is the mole fraction weighted surface area of each divided by $HDSA_{eff}$:

$$P_i = x_i * \frac{HDSA_i}{HDSA_{eff}} \quad .$$ Eqn. 2.2.3

Because the refractive index is expected to be proportional to fractional contribution of each lipid to lipid surface area, the effective refractive index of a mixed lipid system is the sum of refractive indices (RI_i) of the constituent lipids weighted by P_i:

$$RI = \sum_i RI_i * P_i. \quad \text{Eqn. 2.2.4}$$

Equations 1-4 have been used to modify the previously published Matlab code (Appendix I.2)[18] to incorporate the mixed lipid refractive index. The updated Matlab code, which we refer to as the Mixed Lipid Calculator (MLC), incorporates this method of evaluating RI for a mixed lipid vesicle, and is provided in supplementary information. Like the MVCC for pure lipid vesicles, the MLC requires absorbance measurements of scattering off of vesicles of known approximate size to calculate particle and lipid concentration using Beer's law.[6,18]

2.2.3. EXTERNAL VALIDATION.

To validate the above method for evaluating refractive index in mixed lipid systems, vesicle and lipid concentration calculations with the MLC were compared with direct measurements of lipid content using phosphorous analysis. Samples analyzed with the MLC were prepared and

sent for independent lipid concentration analysis using Inductively Coupled Plasma Atomic Emission Spectroscopy (ICP) to determine phosphorous content.

The previously reported MVCC was not tested and validated with pure DOPG vesicles using the known physical parameters of the lipid (Refractive index, headgroup surface area, bilayer thickness). Thus, before modifying the MVCC for use with mixed lipid systems containing DOPG, the MVCC was validated for pure DOPG vesicles using a headgroup surface area of 0.694 nm^2,[20] a bilayer thickness of 3.63 nm[20] and a refractive index of 1.359.[12]

Known amounts of DOPG (Avanti Polar Lipids, Inc), based on the manufacturer reported mass, were dried under a constant flow of compressed nitrogen to remove excess chloroform. Samples were then reconstituted in 20 mM TES buffer, 0.1 mM EDTA, pH 8 to yield a concentration based on the manufacturer reported mass (see Table A.4.). Samples were extruded to 100 nm diameter using an Avanti Mini-extruder. Vesicle diameter was verified with dynamic light scattering (DLS) measurements using a Malvern Zetasizer. A Beckman-Coulter DU 800 spectrophotometer was used to measure Mie scattering in standard absorbance mode for each sample at multiple wavelengths between 300 and 400 nm. The vesicle diameter and the Mie Scattering data were used to evaluate lipid concentration using the MVCC.[18] Samples were then submitted for independent ICP analysis. Table 2.2.1. compares the results for the two methods. The agreement between ICP and the MVCC is excellent.

Table 2.2.1.
Comparison of DOPG lipid concentration in 100 nm pure DOPG vesicles found using ICP and calculated from Mie scattering data using the MVCC.

DOPG lipid concentration measured using ICP, mM*	DOPG lipid concentration from Mie scattering (MVCC), mM†	% Error‡
1.16	1.14 ± 0.02	1.7%
0.94	0.89 ± 0.05	5.3%
0.20	0.21 ± 0.01	5.0%

*Based on phosphorous content obtained from ICP measurements (see Table A.4) after a cold digest to release phosphorous (see ref. [3])
†Error is the standard deviation from scattering measurements at different wavelengths
‡% Error for Mie scattering data versus ICP data

Samples of mixed lipid composition were then prepared to test the validity of the method of evaluating RI for mixed lipid vesicles implemented in the MLC. Known masses of DOPC were mixed with known masses of either Cardiolipin (CL) or DOPG (Avanti Polar Lipids, Inc) based on their manufacturer reported concentrations, and dried under a constant flow of compressed nitrogen to remove excess chloroform. Samples were then reconstituted in 20 mM TES buffer, 0.1 mM EDTA, pH 8 to yield a concentration based on the manufacturer reported mass (see Table A.5.). Concentrations for reconstitution were well above the known critical micelle concentration (CMC) for constituents of the mixture to ensure heterogeneous incorporation of lipids into vesicles.[21] Samples were extruded to 100 nm diameter using an Avanti Mini-extruder. Vesicle diameter was verified using DLS (Malvern Zetasizer). Mie scattering was measured with a Beckman-Coulter DU 800 spectrophotometer operating in standard absorbance mode. For each sample, multiple wavelengths between 300-475 nm were used to evaluate Mie scattering. Samples were then submitted for independent ICP analysis.

Table 2.2.2. reports lipid concentration and compares calculated total lipid concentration using Mie scattering to total concentration obtained by ICP measurements of phosphorous content. The average percent error between the values obtained by ICP and those calculated from Mie scattering with the MLC is 4.3%, providing a strong validation of our method for evaluating refractive index in mixed lipid systems. The concentrations from Mie scattering measurements are also mostly within one standard deviation of the concentrations obtained by phosphorous analysis (Table 2.2.2.). The method of evaluating RI for mixed lipid systems provides close agreement between ICP measurements and calculations from Mie scattering data with the MLC across a broad range of mixing ratios, indicating that the method of evaluating RI is general.

Table 2.2.2.
Comparison of total lipid concentrations of 100 nm DOPC:CL or DOPC:DOPG mixed lipid vesicles found using ICP and calculated with the MLC.

Mixed lipid vesicle content*	Total lipid concentration by ICP, mM†	Total lipid concentration from Mie scattering (MLC), mM‡	Calculated DOPC concentration (MLC), mM	Calculated CL or DOPG concentration (MLC), mM	% Error§
20% CL	0.93	0.95 ± 0.03	0.76	0.19	2.30
20% CL	1.26	1.37 ± 0.04	1.09	0.27	8.66
20% CL	2.28	2.47 ± 0.08	1.97	0.49	7.96
50% CL	0.58	0.54 ± 0.03	0.27	0.27	6.22
50% CL	0.35	0.35 ± 0.03	0.17	0.17	1.86
20% DOPG	1.07	1.09± 0.01	0.87	0.22	2.29
20% DOPG	0.38	0.37± 0.01	0.30	0.07	3.26
20% DOPG	0.75	0.79± 0.03	0.63	0.16	4.37
50% DOPG	1.06	1.08± 0.02	0.54	0.54	1.86

*Mole percent, the remainder being DOPC.
†Based on phosphorous content obtained from ICP measurements (see Table A.4) after a cold digest to release phosphorous (see ref. [3]).
‡Error is the standard deviation from scattering measurements at multiple wavelengths.
§% Error for Mie scattering data versus ICP data.

Due to the physical nature of the lipids investigated here, it is impossible to obtain scattering measurements based on specific lipids in a mixed lipid system using absorbance spectroscopy in the visible range of the electromagnetic spectrum. That being said, knowing the mole fraction of each constituent lipid from the mass of lipid used to prepare the vesicles, the concentration of each lipid can be calculated from the total lipid concentration. This indirect measurement permits quantification of individual lipid populations in mixed lipid systems using the MLC (see Table 2.2.2.). The close correlation between the lipid concentrations obtained by Mie scattering and ICP also indicates that the manufacturer-provided masses are fairly accurate and that losses of

material during extrusion (average percent error is 11.9 % for mixed lipid systems relative to ICP, see Table A.5) do not affect the mole fractions of lipids in the vesicles used to evaluate RI.

2.2.4. CONCLUSION

The modification of the MVCC to produce the MLC for mixed lipid systems provides a rapid, reliable, non-destructive quantification method for timely experimental characterization of lipid vesicles across a broad range of mixed lipid compositions. The method provides accurate lipid concentrations using a standard UV-Vis spectrophotometer making the technique accessible and affordable.

As discussed in our earlier report,[18] the optimal wavelength region for Mie scattering measurements depends on vesicle size. Further, with vesicle extrusion, DLS is not necessary once vesicle size is characterized for the system. The MLC has been validated for DOPC:DOPG and DOPC:CL mixed lipid vesicles, but can be extended to any other lipid if the headgroup surface area, the bilayer thickness and the refractive index of the lipid of interest is known. Finally, all lipid mixtures in this work were prepared well above the CMC.[21] If sample preparation for vesicle formation is near the transition temperature for a specific lipid or the CMC, the resultant vesicles may not be heterogeneous. In this case, the MLC may fail to accurately measure lipid concentration.

Matlab code for the MLC along with installation and user instructions can be found in Appendix I.2.

2.3. REFERENCES

(1) US Environmental Protection Agency. Determination of Metals and Trace Elements in Water and Wastes by Inductively Coupled Plasma-Atomic Emission Spectrometry. *US EPA* **1994**, *4*, 1–58.

(2) Saxena, V.; Nielsen, J. *Novel Integrated Bio-Optical System for Oxygen Saturation Measurement*; 2004; Vol. 5368.

(3) Rouser, G.; Fleischer, S.; Yamamoto, A. Two Dimensional Thin Layer Chromatographic Separation of Polar Lipids and Determination of Phospholipids by Phosphorus Analysis of Spots. *Lipids* **1970**, *5* (5), 494–496.

(4) Unsay, J. D.; Cosentino, K.; Subburaj, Y.; García-Sáez, A. J. Cardiolipin Effects on Membrane Structure and Dynamics. *Langmuir* **2013**, *29* (51), 15878–15887.

(5) Qiu, C.; Blanchard, G. J. Phospholipid Vesicle Stability and Temporal Variations in Acyl Chain Organization. *Spectrochimica Acta - Part A: Molecular and Biomolecular Spectroscopy* **2013**, *110*, 383–390.

(6) Bohren, Craig F, Huffman, D. R. *Absorption and Scattering of Light by Small Particles*; Bohren, C. F., Huffman, D. R., Eds.; Wiley-VCH Verlag GmbH: Weinheim, Germany, 1998.

(7) Haiss, W.; Thanh, N. T. K.; Aveyard, J.; Fernig, D. G. Determination of Size and Concentration of Gold Nanoparticles from UV-Vis Spectra. *Analytical Chemistry* **2007**, *79* (11), 4215–4221.

(8) Maniti, O.; Cheniour, M.; Lecompte, M. F.; Marcillat, O.; Buchet, R.; Vial, C.; Granjon, T. Acyl Chain Composition Determines Cardiolipin Clustering Induced by Mitochondrial Creatine Kinase Binding to Monolayers. *Biochimica et Biophysica Acta - Biomembranes* **2011**, *1808* (4), 1129–1139.

(9) G.M.Hale; M.R.Querry. Optical Constants of Water in the 200nm to 200mm Wavelength Region. *Appl. Opt.* **1973**, *12* (3), 555–563.

(10) Bashkatov, A. N.; Genina, E. A. Water Refractive Index in Dependence on Temperature and Wavelength: A Simple Approximation. In *Proc. SPIE 5068, Saratov Fall Meeting 2002: Optical Technologies in Biophysics and Medicine IV, 393 (October 14, 2003)*; 2003; Vol. 5068, pp 393–395.

(11) Pan, J.; Cheng, X.; Sharp, M.; Ho, C.-S.; Khadka, N.; Katsaras, J. Structural and Mechanical Properties of Cardiolipin Lipid Bilayers Determined Using Neutron Spin Echo, Small Angle Neutron and X-Ray Scattering, and Molecular Dynamics Simulations. *Soft Matter* **2014**, *11* (1), 130–138.

(12) Popplewell, J. F.; Swann, M. J.; Freeman, N. J.; McDonnell, C.; Ford, R. C. Quantifying the Effects of Melittin on Liposomes. *Biochimica et Biophysica Acta - Biomembranes*

2007, *1768* (1), 13–20.

(13) Kučerka, N.; Nieh, M.-P.; Katsaras, J. Fluid Phase Lipid Areas and Bilayer Thicknesses of Commonly Used Phosphatidylcholines as a Function of Temperature. *Biochimica et Biophysica Acta (BBA) - Biomembranes* **2011**, *1808* (11), 2761–2771.

(14) Murray, D. H.; Tamm, L. K.; Kiessling, V. Supported Double Membranes. *Journal of Structural Biology* **2009**, *168* (1), 183–189.

(15) Pan, J.; Cheng, X.; Sharp, M.; Ho, C.-S.; Khadka, N.; Katsaras, J. Structural and Mechanical Properties of Cardiolipin Lipid Bilayers Determined Using Neutron Spin Echo, Small Angle Neutron and X-Ray Scattering, and Molecular Dynamics Simulations. *Soft Matter* **2015**, *11* (1), 130–138.

(16) Schwendener, R. A. Liposomes as Vaccine Delivery Systems: A Review of the Recent Advances. *Therapeutic Advances in Vaccines* **2014**, *2* (6), 159–182.

(17) Akbarzadeh, A.; Rezaei-Sadabady, R.; Davaran, S.; Joo, S. W.; Zarghami, N.; Hanifehpour, Y.; Samiei, M.; Kouhi, M.; Nejati-Koshki, K. Liposome: Classification, Preparation, and Applications. *Nanoscale Research Letters* **2013**, *8* (1), 102.

(18) Elmer-Dixon, M. M.; Bowler, B. E. *Rapid Quantification of Cardiolipin and DOPC Lipid and Vesicle Concentration*; 2017; Vol. 520.

(19) Tasic, A. Z.; Djordjevic, B. D.; Grozdanic, D. K.; Radojkovic, N. Use of Mixing Rules in Predicting Refractive Indexes and Specific Refractivities for Some Binary Liquid Mixtures. *Journal of Chemical & Engineering Data* **1992**, *37* (3), 310–313.

(20) Pan, J.; Heberle, F. A.; Tristram-Nagle, S.; Szymanski, M.; Koepfinger, M.; Katsaras, J.; Kučerka, N. Molecular Structures of Fluid Phase Phosphatidylglycerol Bilayers as Determined by Small Angle Neutron and X-Ray Scattering. *Biochimica et biophysica acta* **2012**, *1818* (9), 2135–2148.

(21) Marsh, D. *Handbook of Lipid Bilayers*; 2013.

CHAPTER 3: Site A-mediated Partial Unfolding of Cytochrome *c* on Cardiolipin Vesicles Is Species Dependent and Does Not Require Lys72

3.1. INTRODUCTION

Cytochrome *c* (Cyt*c*) is well known to function as an electron transporter during respiration.[1] More recently, Cyt*c* was shown to be involved in the initiating steps of apoptosis.[2-4] This involvement requires the protein to dissociate from the inner mitochondrial membrane and exit mitochondria.[2-4] Before any of these steps can happen, the protein must oxidize cardiolipin (CL).[4, 5] Thus, the nature of Cyt*c*-CL binding, CL oxidation by Cyt*c* and subsequent dissociation of Cyt*c* from CL recently has been the subject of intense investigation.[6, 7] Cyt*c*-membrane interactions have been studied *in vitro* with a variety of memetic membrane systems using primarily mammalian Cyt*c*,[8-21] and in some cases, yeast iso-1-Cyt*c*.[22, 23] These studies use differing compositions of mixed lipid systems, salt and solution concentrations and detection techniques. These variations make direct comparison of protein response to lipid exposure between and among different studies difficult, if not impossible. Four binding sites, A (Figure 3.1, anionic site; lysines 72, 73, 86 and 87; electrostatic),[13, 14, 21] C (cardiolipin site; Asn52; hydrophobic),[13, 14] L (lysines 22 and 27, histidines 26 and 33; membrane fusion)[24] and N (novel site; Phe36, Gly37, Thr58, Trp59, Lys60)[25] have been characterized. However, few studies have attempted to analyze the binding at these sites in isolation or via mutagenesis methods.[26, 27] Similarly, few studies exist that directly compare binding behavior for Cyt*c* from different species.[22, 23]

Comparison of the binding of yeast iso-1-Cyt*c* versus human Cyt*c* to cardiolipin vesicles has the potential to provide important insight into how this interaction has evolved to optimize the

Cyt*c*-mediated switch that initiates the intrinsic pathway of apoptosis through peroxidation of cardiolipin. Yeast, while capable of releasing Cyt*c* from mitochondria under solution conditions that mimic apoptosis,[28] lacks many components of the intrinsic pathway of apoptosis, including the ability to interact with Apaf-1 to form a functional apoptosome.[32-34] Yeast iso-1-Cyt*c* has been free of the necessity of evolving to bind to Apaf-1, which has led to some changes in sequence that affect the charge distribution around site A. Mutating Glu62 to the yeast residue, Asn, in horse Cyt*c* leads to a 10-fold decrease in caspase activation.[34]

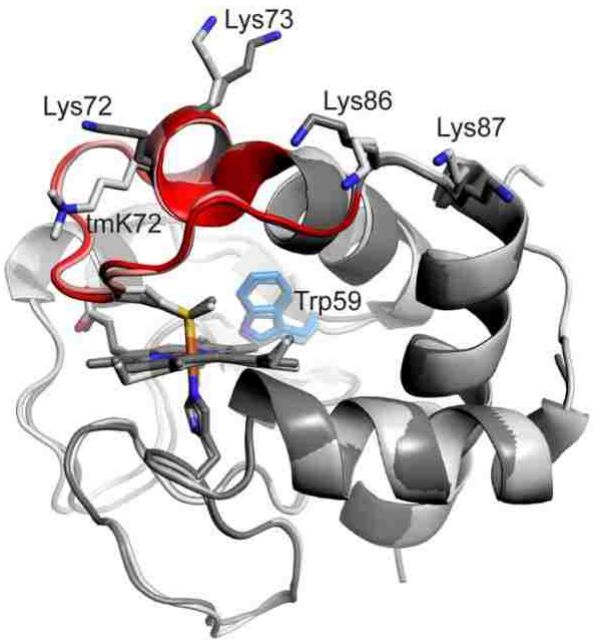

Figure 3.1. Overlay of yeast iso-1-Cyt*c* (PDB entry 2YCC;[29] light gray and salmon) and human Cyt*c* (PDB entry 3ZCF;[30] dark gray and red) aligned using Pymol.[31] Lys72 (trimethyllysine in yeast, tmK72), Lys73, Lys86 and Lys87, which have been implicated as constituents of site A, are show in light gray and dark gray stick models for yeast iso-1-Cyt*c* and human Cyt*c*, respectively. Ω-Loop-D (residues 70 – 85), which positions the Met80 heme ligand, is shown in salmon and red for yeast iso-1-Cyt*c* and human Cyt*c*, respectively. Trp59, seen behind the heme, is shown as a blue stick model. The heme and its ligands, Met80 and His18, are shown as light gray and dark gray stick models for yeast iso-1-Cyt*c* and human Cyt*c*, respectively.

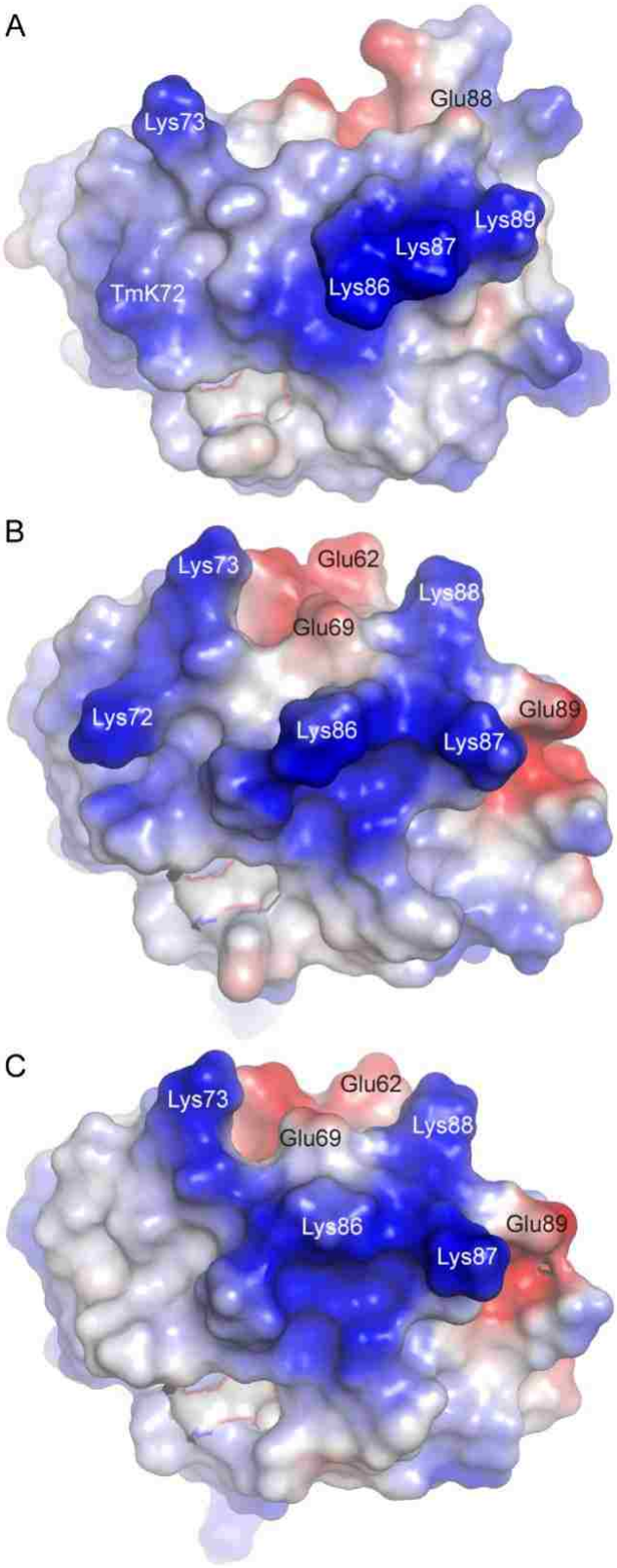

Figure 3.2. Surface electrostatics of site A in yeast iso-1-Cyt*c* versus human Cyt*c*. (A) yeast iso-1-Cyt*c* (PDB entry 2YCC),[29] (B) chain A of human Cyt*c* (PDB entry 3ZCF)[30] and (C) chain A of human K72A Cyt*c* (PDB entry 5TY3).[35] Electrostatic surface was generated with PyMol.[31] Positive, neutral and negative electrostatic surfaces are indicated by blue, white and red surfaces, respectively. Lysine and glutamate residues in or near site A are labelled.

This mutation contributes to a significant change in the continuity of the positive surface charge around site A (Figure 3.2), along with the additional mutation from Thr69 in yeast to Glu69 in mammals. The re-ordering of the cluster of charged residues at positions 86 – 90 that follow □-loop D (KKEKD in yeast iso-1-Cyt*c* and KKKEE in human Cyt*c*) also changes the charge distribution around site A (Figure 3.2A versus 2B) and has implications for ATP inhibition of CL binding.[23] Studies on the salt dependence of yeast iso-1-Cyt*c* versus horse Cyt*c* binding to 100% CL vesicles indicate that the electrostatic interaction with CL is much stronger for yeast iso-1-Cyt*c*,[23] indicating that these evolutionary changes significantly impact the Cyt*c*/CL interaction. However, this study was carried out at pH 7 and showed strong increases in light scattering when 100% CL vesicles were mixed with yeast iso-1-Cyt*c* and horse Cyt*c*. This behavior indicates that significant binding through site L, which leads to membrane fusion, was occurring under these conditions and thus the results do not report exclusively on site A binding. To address the evolution of Cyt*c*/CL binding specifically through site A, solution conditions to quantitatively investigate site A, in the absence of other binding sites, have been developed. CL vesicle binding to wild type human Cyt*c* (HuWT) and wild type yeast iso-1-Cyt*c* (yWT), using *Escherichia coli*-expressed iso-1-Cyt*c*, which lacks the native post-translational modification at K72 (ε-NH_2 is trimethylated in yeast[36]), has been characterized. The results show that site A binding to 100% CL vesicles is both similar and different for yeast iso-1-Cyt*c* and human Cyt*c*.

Recent studies on horse Cyt*c* variants have also indicated that Lys72 is a predominate contributor to CL/Cyt*c* binding at pH 7.[26, 27] The structure of human Cyt*c* carrying a K72A mutation shows the expected truncation of the charge surface usually assigned to site A (Figure 3.2B versus 3.2C). Thus, significant effects on site A binding might be expected. Recent work indicates that K72A mutations to yeast iso-1-Cyt*c*[37] and human Cyt*c*[35] can promote

conformational fluctuations that enhance the intrinsic peroxidase activity of these proteins. Thus, it is of interest to evaluate whether the enhanced conformational flexibility produced by the K72A mutation also affects binding through site A. The site A specific binding conditions developed here are also applied to K72A variants of yeast iso-1-Cyt*c* and human Cyt*c* (yK72A and HuK72A, respectively). Our results indicate that other nearby lysines can compensate for the loss of Lys72 from site A.

3.2. EXPERIMENTAL METHODS

3.2.1. Mutagenesis.

The yeast WT iso-1-cytochrome *c* was made using the QuikChange Lightning Site-Directed Mutagenesis kit (Agilent Technologies, Inc.) to mutate Ala72 to lysine (A72→K72) (primers: CATGTCAGAGTACTTGACTAACCCAAAGAAATATATTCCTGGTACCAGATGG and its reverse complement, from Invitrogen Life Technologies) in the pRbs_BTR1 plasmid[38] carrying the gene for the K72A variant of iso-1-Cyt*c*.[37] The pRbs_BTR1 plasmid[38] is a derivative of pBTR1[36, 39] with an optimized ribosomal binding sequence. pRbs_BTR1 co-expresses the iso-1-cytochrome *c* gene, *CYC1*, and the yeast heme lyase gene, *CYC3*, allowing covalent attachment of the heme in the cytoplasm during expression. After mutagenesis, mutant DNA was transformed into XL-10 Gold Competent *Escherichia coli* cells (Agilent Technologies). Cultures (5 mL) of individual clones were grown and the DNA extracted using a Wizard Genomic DNA Purification Kit (Promega Corp). Extracted DNA was submitted to the Murdock DNA Sequencing Facility (University of Montana, Missoula) for sequencing to confirm successful mutagenesis.

3.2.2. Protein Preparation.

The yeast iso-1-cytochrome *c* variants yWT and yK72A[37] were expressed from the pRbs_BTR1 plasmid. Human Cyt*c* variants, HuWT and HuK72A,[35] were expressed from the pBTR(HumanCc) plasmid, obtained from the Pielak laboratory at the University of North Carolina.[40] DNA plasmids for all mutants were transformed into *E. coli* BL21 competent cells (EdgeBio, Gaithersburg, MD). The yeast and human variants were expressed and purified using previously reported methods.[41-44] Final purification was by HPLC cation exchange (Uno S6, BioRad) using a previously described gradient.[41] Purified protein in the reduced state was oxidized using a 5-fold excess by weight of potassium ferricyanide followed by size exclusion chromatography using a Sephadex G-25 (GE Healthcare Life Sciences) column to separate oxidized Cyt*c* from ferricyanide. Protein concentration prior to experiments was determined by UV-Vis spectroscopy (Beckman Coulter DU 800 spectrophotometer) using the previously reported extinction coefficients of Cyt*c* at 339, 526.5, 541.75 and 550 nm.[45]

3.2.3. Lipid and Vesicle Preparation.

Cardiolipin (1',3'-bis[1,2-dioleoyl-*sn*-glycero-3-phospho]-*sn*-glycerol, TOCL) was purchased from Avanti Polar Lipids, Inc., Alabaster, AL and used in vesicle formation without further purification. Lipids were dried under Argon to remove chloroform before being reconstituted in 20 mM TES Buffer, 0.1 mM EDTA, pH 7 or pH 8, as specified. Lipids and buffer were vortexed for 1 minute then set in a warm bath for 9 minutes. This vortex/warm bath cycle was repeated 10 times. To form vesicles, the lipid solution underwent a freeze/thaw/vortex cycle five times. The vesicle solution was then extruded to the desired vesicle size using an Avanti mini-extruder with two 100 nm membranes. The size of the extruded vesicles was

measured using a Malvern Dynamic Light Scattering (DLS) instrument and found to be 102 ± 9 nm. Scattering measurements were performed using a Beckman Coulter DU 800 with a 10 mm pathlength Hellma micro-cuvette. Scattering measurements were used in coordination with DLS measurements to determine vesicle and lipid concentration using a previously reported technique based on Mie scattering.[46] Vesicles were used immediately after preparation to avoid issues related to vesicle stability. DLS measurements following experiments indicated no change in vesicle size.

3.2.4. Titration of Cyt*c* with Cardiolipin Vesicles.

Titrations were performed using a batch procedure. The main stock of freshly prepared vesicles was then used to make a set of dilutions at 2-fold the concentration required for each vesicle concentration in the titration curve. A 2-fold concentration protein stock was added to 2-fold concentration lipid for each titration point in a 1:1 ratio resulting in a solution at the desired protein and lipid concentrations. Samples were gently mixed by hand and incubated for 30 minutes before spectroscopic measurements. Experiments were performed in triplicate and each sample at each concentration point was prepared independently.

3.2.5. Absorption Spectroscopy.

A Beckman Coulter DU800 spectrophotometer was used to measure the UV-Vis spectrum during titrations of Cyt*c* with CL vesicles. A 10 mm pathlength Hellma micro-cuvette was used to measure absorption between 200 and 800 nm at a 1 nm step and 400 nm/min scan rate with a 5 nm bandwidth.

3.2.6. Circular Dichroism Spectroscopy.

An Applied Photophysics Chirascan circular dichroism (CD) spectrophotometer was used for Soret CD measurements. Spectral regions from 350-450 nm were measured with a Hellma 4x10 mm quartz cuvette utilizing the 4 mm pathlength. CD data were acquired using a 1 nm descending step, 1.8 nm bandwidth and a 3 second acquisition time at 25 °C. Three independent titrations were carried out for each protein. All spectra were smoothed using a 6th order Savitsky-Golay filter smoothing technique. The data points in Figure 3.7 of the Results are the average and standard deviation of the three independent trails for each of the four proteins studied.

3.2.7. Fluorescence Spectroscopy.

An Applied Photophysics Chirascan CD spectrophotometer was adapted for scanning fluorescence measurements. Tryptophan excitation was performed at 295 nm with a 5 nm bandwidth. A Helma 5x5 mm fluorescence cuvette was used during data acquisition. Excitation bleed-through was filtered using a 305 nm cutoff filter (Newport Corp.) and data were acquired using the scanning emission monochromator provided by Applied Photophysics. Emission spectra were measured from 320 - 500 nm using a 1 nm step and a 2.5 nm bandwidth with an acquisition time of 0.5 sec per step. A minimum of three independent trials were acquired for each Cyt*c* variant. Each trial was smoothed using a 6th order Savitsky-Golay filter smoothing technique before averaging data points from the three independent trials (See Figure 3.14, Results).

3.2.8. Data Fitting.

CD and fluorescence data for all Cyt*c* variants were fit to the simplest suitable model, a one site cooperative Langmuir-type equation (eq 3.1), where the spectroscopic value,

$$s(x) = \frac{s_o + s_1\left(\frac{x}{K_d(\text{app})}\right)^n}{1+\left(\frac{x}{K_d(\text{app})}\right)^n} \qquad \text{(eq 3.1)}$$

s(x), corresponds to the amplitude measured at the lipid to protein ratio, x, in the titration and s_0 and s_1 are the amplitudes of the initial and final states, respectively. In eq 3.1, K_d(app) is the apparent dissociation constant corresponding to the lipid concentration or lipid to protein ratio (LPR) required to induce half occupancy of the conformation associated with site A binding to CL and n is the associated Hill coefficient.

3.2.9. Guanidine Hydrochloride Induced Protein Unfolding Monitored by Fluorescence.

An Applied Photophysics Chirascan CD spectrophotometer adapted for scanning fluorescence monochromator measurements and coupled with a Hamilton Microlab 500 series auto-titrator was used to perform guanidine hydrochloride (GdnHCl) titrations monitored using Trp59 fluorescence. Tryptophan excitation was performed at 295 nm with a 5 nm bandwidth. A Hellma 4 mm x 10 mm quartz cuvette was used with excitation along the 4 mm pathlength and acquisition along the 10 mm pathlength. This cuvette accommodates a stir bar to ensure complete mixing during the titration. Excitation bleed-through was filtered as described for vesicle titrations. Emission spectra were measured from 320 - 500 nm as described for vesicle titrations. The autotitrator was setup to increase GdnHCl concentration variably in 0.05 to 0.1 M increments. Two protein stock solutions were prepared at 10 µM protein concentration in 1) 20 mM Tris Buffer, 40 mM NaCl, at pH 7 as well as 2) 6 M GdnHCl, 20 mM Tris Buffer, 40 mM

NaCl, at pH 7 and were stored at 4 °C until experimentation when the solutions were equilibrated to 25 °C. Protein stock with GdnHCl was auto-titrated into protein stock with no GdnHCl. After each increment of GdnHCl, the sample was stirred in the cuvette for 10 seconds and then left to rest for 100 seconds before data acquisition. Three independent trials were acquired for yWT iso-1-Cyt*c*.

3.3. RESULTS

3.3.1. Site A-specific Binding Conditions.

To create a simplified, controlled environment to investigate site A-specific CL binding, we optimized experimental conditions. Site A sits on the Ω-loop covering heme crevice access[1] and has been characterized as being comprised of Lys72 and Lys73,[13, 16] and sometimes lysines 86 and 87 (see Figures 3.1 and 3.2).[6, 21] Therefore, electrostatic interactions dominate. Both sites C and L diminish in importance above neutral pH.[14, 24] To isolate site A, binding studies were carried out in 20 mM TES buffer, 0.1 mM EDTA at pH 8. To further simplify binding, 100% CL vesicles formed with 1',3'-bis[1,2-dioleoyl-*sn*-glycero-3-phospho]-*sn*-glycerol (TOCL) were used.

To demonstrate that binding at site A is dominant at pH 8, we compared binding to 100% TOCL vesicles monitored by UV-Vis spectroscopy at pH 7 versus pH 8 using yWT iso-1-Cyt*c* and HuWT Cyt*c*. At pH 7, titrations of yWT iso-1-Cyt*c* with CL led to a substantial increase in light scattering as CL concentration increased (Figure 3.3A), as observed previously.[23] Similar observations are made with HuWT Cyt*c* at pH 7 (Figure 3.4A), although, the degree of light scattering is less pronounced. Thus, at pH 7, Cyt*c*-CL interactions produce large structures that generate scattering. This finding corresponds directly with Kawai *et al*.[24] who attributed

formation of large structures to vesicle fusion mediated by simultaneous binding to both sites A and L of Cyt*c*.

Deprotonation of ionizable residues contributing to site L eliminates this site above pH 7 in the membrane system used in this earlier study.[24] For 100% CL vesicles, titration of yWT iso-1-Cyt*c* and HuWT Cyt*c* at pH 8 led to no significant light scattering, indicating that site L no longer plays a role in binding at this pH (Figure 3.3B, Figure 3.4B). Thus, CL vesicle titrations at pH 8 should report on site A binding. While light scattering does not report directly on site C, pH dependent binding data for site C indicate that binding is almost completely eliminated when pH is raised to 7.

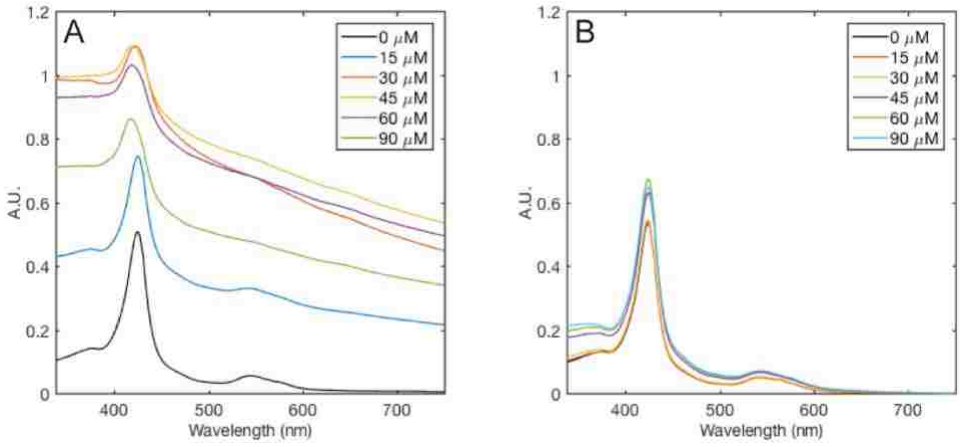

Figure 3.3. (A) UV-Vis absorbance of yWT iso-1-Cyt*c* in the presence of various concentrations of 100% CL lipid vesicles at pH 7, 25 °C. (B) UV-Vis absorbance of yWT iso-1-Cyt*c* in presence of various concentrations of 100% CL lipid vesicles at pH 8, 25 °C. Panel A shows signal shifted well above 0 A.U (absorbance units). across the spectrum for each titration point above 0 M CL total lipid concentration, indicative of scattering due to large lipid vesicles.

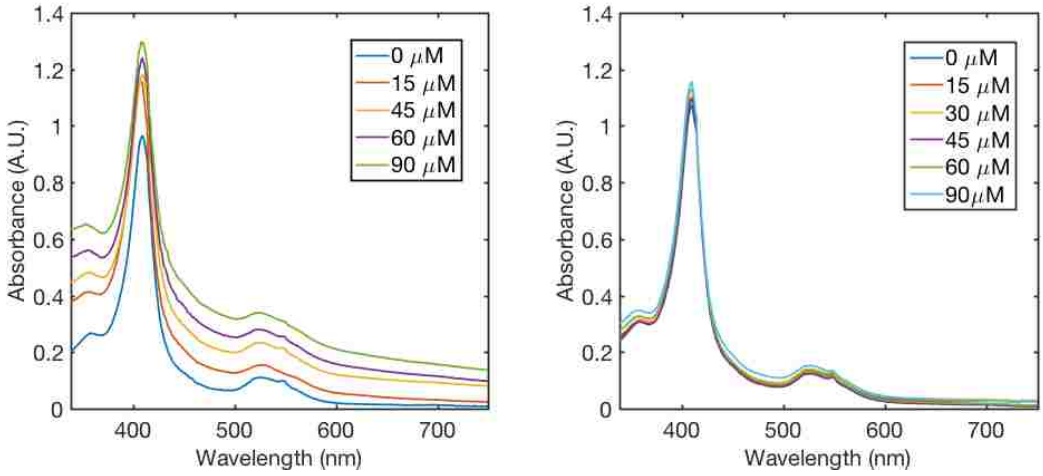

Figure 3.4. (A) UV-Vis absorbance of 97% oxidized HuWT Cyt*c* in the presence of various concentrations of 100% CL lipid vesicles at pH 7, 25 °C. (B) UV-Vis absorbance of HuWT Cyt*c* in presence of various concentrations of 100% CL lipid vesicles at pH 8, 25 °C. Panel A shows signal shifted well above 0 A.U. across the spectrum for each titration point above 0 M CL total lipid concentration indicative of scattering due to enlarged lipid vesicles.

3.3.2. Site A Binding Monitored by Heme Soret CD.

To assess Cyt*c*-CL binding analytically, 100 nm pure TOCL vesicles were formed by extrusion and vesicle and lipid concentrations were quantified utilizing a previously reported method for rapid lipid quantification.[46] We monitored the Soret region of Cyt*c* during titrations using CD spectroscopy, which probes the environment near the heme. Soret CD band signal shifts are indicative of heme crevice rearrangement due to binding at site A.

Soret CD from 350-450 nm demonstrates intrinsically different spectral signatures for human and yeast variants (Figure 3.5) at pH 8. HuWT shows a pronounced negative

trough at 418 nm while yeast has less obvious negative ellipticity at pH 8. At lower pH, the negative trough is prominent for yeast iso-1-Cyt*c*.[22] Previous studies on the Soret CD of the alkaline state of horse Cyt*c*[47] indicate that the reduced negative trough for yWT is consistent with population of the alkaline conformer at this pH (pK_{app} = 8 for the alkaline transition of yWT).[36, 38] The negative trough is more pronounced for yK72A than for yWT (compare black spectra in Figure 3.6 for yWT and yK72A), consistent with the higher pK_{app} of 8.6 for yK72A.[36] Furthermore, peaks and troughs do not occur at exactly the same wavelengths: the HuWT positive peak is at 405 nm while for yWT it is at 407 nm and HuWT shows a negative trough at 418 nm whereas for yWT it is at 422 nm.

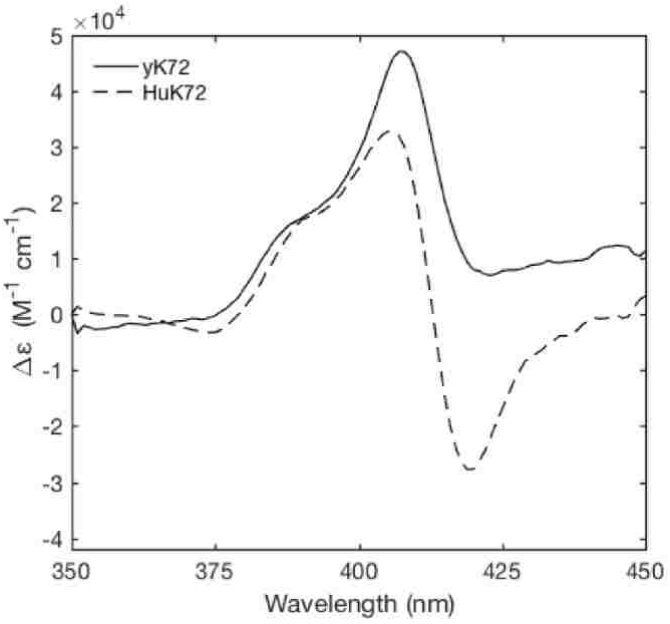

Figure 3.5. yWT iso-1-Cyt*c* (solid line) and HuWT Cyt*c* (dashed line) at 10 µM concentration in 20 mM TES buffer, 0.1 mM EDTA, pH 8. Spectra were acquired at 25 °C.

The Soret CD signal response to increased CL vesicle concentration also differs for human versus yeast iso-1-Cyt*c* (Figure 3.6). The negative trough near 420 nm initially decreases in magnitude for both yWT and HuWT. At higher CL concentrations, the negative trough re-emerges for yWT, leading to an isodichroic point (Figure 3.6). Neither the reemergence of the negative trough nor the isodichroic point are observed for HuWT. For yWT, the isodichroic point is not present for the first few data points, indicating a distinct process from that which occurs after the isodichroic point forms. This early phase is likely initial intermolecular binding and only modestly affects the Soret CD spectrum. This observation suggests that initial intermolecular binding does not strongly perturb the structure of the heme crevice, consistent with some previous reports.[11, 25] The binding process leading to the isodichroic point would then correspond to an intramolecular structural rearrangement on the surface of the vesicle. Structural rearrangements are expected to depend on available space on the membrane surface. For this reason, we analyze our data in terms of lipid to protein ratio (LPR). Only lipid available on the outer leaflet of the vesicle is used to calculate LPR, i.e. exposed LPR. Because the dissociation constants extracted from our data are due to structural rearrangements on the membrane surface rather than intermolecular association, they will be referred to as apparent dissociation constants, K_d(app).

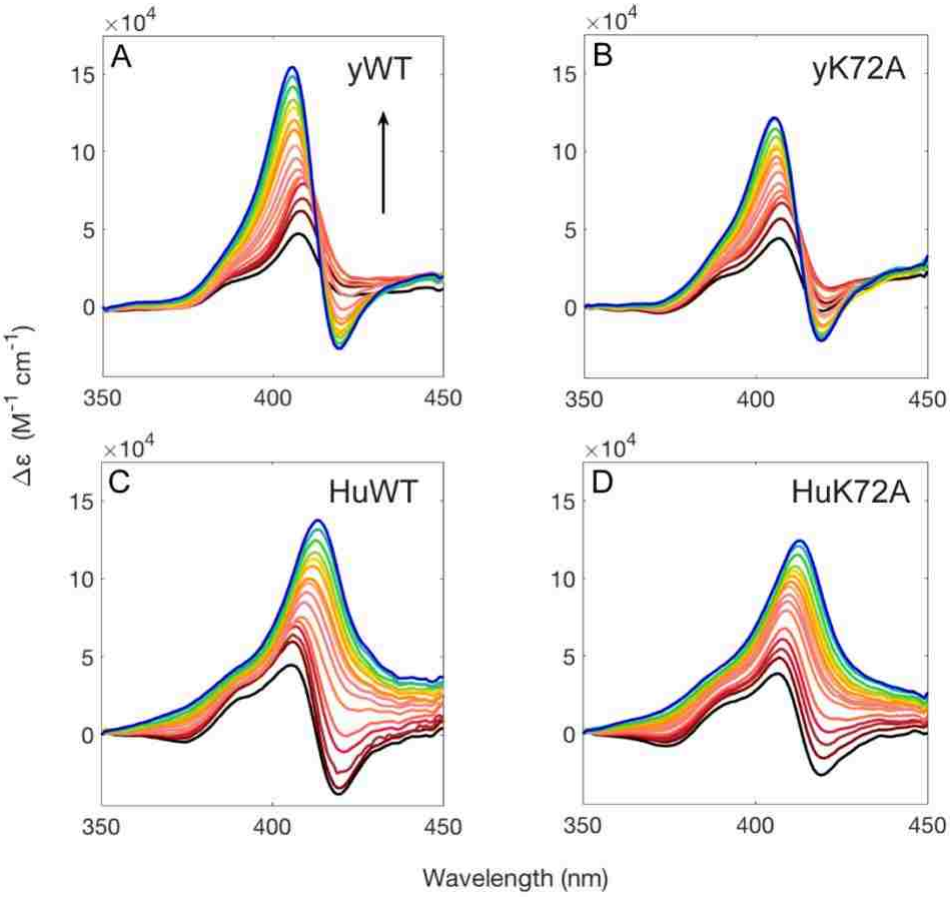

Figure 3.6. CD spectra as a function of the concentration of 100 nm CL vesicles for (A) yWT and (B) yK72A iso-1-Cyt*c* and (C) HuWT and (D) HuK72A Cyt*c*. Protein concentration was 10 μM. Black arrow denotes direction of signal shift of the positive peak during titrations. 0 M exposed lipid concentration corresponds to the black curve for each mutant. Maximum exposed (outer leaflet) lipid concentration was 200 μM and corresponds to the blue spectrum for each protein.

For human Cyt*c*, the magnitude of the Soret CD at the wavelength of the positive maximum in the 0 M CL spectrum was used to track CL binding. Because of the re-emergence of the negative trough in the Soret CD peak for yeast iso-1-Cyt*c*, the response of the Soret CD signal versus exposed LPR was quantified by subtracting the magnitude of the Soret CD at the wavelength of the negative trough from the magnitude of the Soret CD at the wavelength of the positive peak in 0 M CL.

Figure 3.7 shows binding isotherms monitored by Soret CD for yWT and yK72A iso-1-Cyt*c* (Figure 3.7A) and for HuWT and HuK72A Cyt*c* (Figure 3.7B) plotted versus exposed LPR. The mutations affect the amplitude of the change in the Soret CD as observed for CL binding of Lys→Asn variants of horse Cyt*c*.[26] We fit the data to the simplest possible model, a single site Langmuir-type binding isotherm allowing for cooperativity (eq 3.1, Experimental procedures).[16, 18] The resultant parameters (Table 3.1), K_d(app), and the cooperativity, n, were used to plot percent bound protein versus exposed LPR for each variant (Figure 3.8). It is evident from these plots and the parameters in Table 3.1 that the K72A mutation causes no significant change in the K_d(app) of CL for yeast iso-1-Cyt*c* and human Cyt*c* and perhaps a small decrease in the cooperativity.

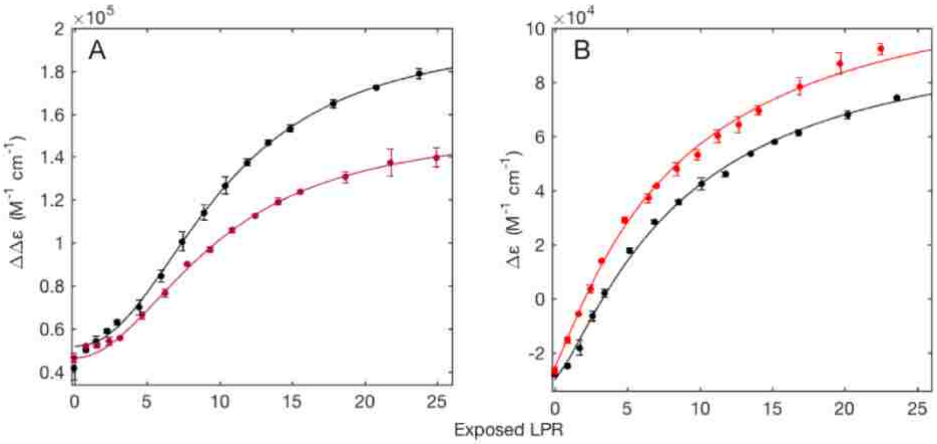

Figure 3.7. Yeast iso-1-Cyt*c* and human Cyt*c* Soret CD signal response to cardiolipin. (A) yWT (black) and yK72A (red) iso-1-Cyt*c* Soret CD signal as a function of exposed (outer leaflet) LPR. Data points at each LPR are the difference between the CD signal at the wavelength of the positive maximum and the wavelength of the negative minimum in the Soret region of the CD spectrum of iso-1-Cyt*c* in the absence of vesicles. (B) HuWT (black) and HuK72A (red) Cyt*c* Soret CD signal as a function of exposed LPR. Data points at each LPR are the CD signal at the wavelength of the positive maximum in the Soret region of the CD spectrum of human Cyt*c* in the absence of vesicles. All titrations were carried out at 25 °C and pH 8 using 100% CL vesicles extruded through a 100 nm membrane. Error bars are the standard deviations of the average values from three independent trials. Solid curves are fits to eq 3.1.

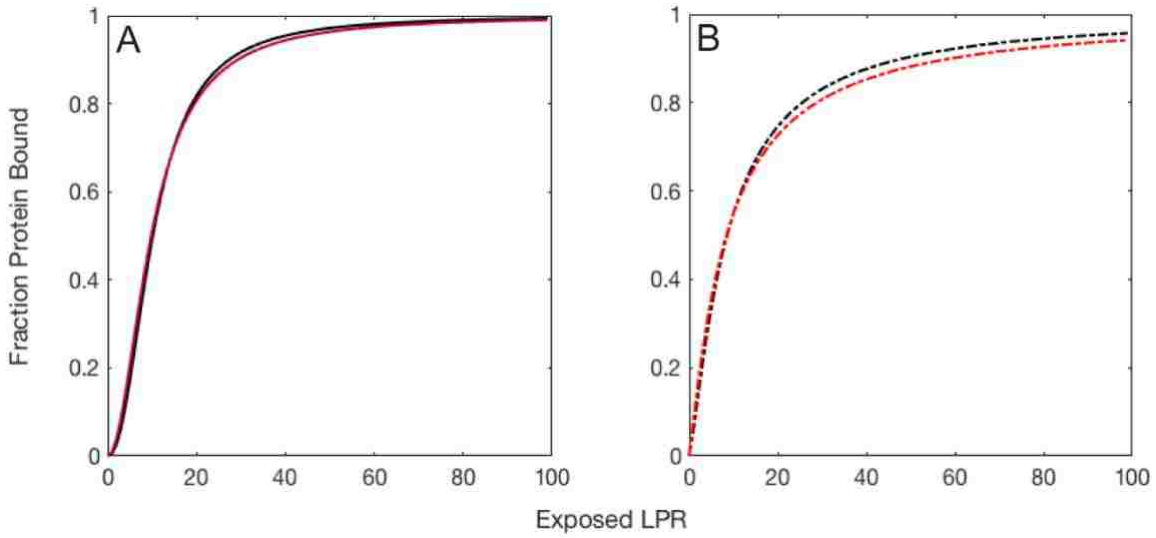

Figure 3.8. (A) Plots of fraction protein bound versus exposed (outer leaflet) lipid to protein ratio (LPR) for yWT (black) and yK72A (red) iso-1-Cyt*c* using the parameters extracted from a fit to eq 3.1. (B) Plots of fraction protein bound versus exposed LPR for HuWT (black) and Hu K72A (red) Cyt*c* using the parameters extracted from a fit to eq 3.1. Fraction bound = $(s(x)-s_0)/(s_1-s_0)$ in these plots.

Table 3.1. Thermodynamic Parameters for Cyt*c* Site A Binding to 100% CL Vesicles

	CD[a,b]		Fluorescence[a,c]	
variant	K_d(app) (LPR, μM)	n	K_d(app) (LPR, μM)	n
yWT	10.2 ± 0.3 (102 ± 3)	2.2 ± 0.1	23.4 ± 0.8 (117 ± 4)	2.3 ± 0.2
yK72A	9.8 ± 0.2 (98 ± 2)	2.01 ± 0.07	26.2 ± 0.8 (131 ± 4)	2.3 ± 0.1
HuWT	8.6± 0.7 (86 ± 7)	1.27 ± .09	36.0 ± 3.6 (180 ± 18)	2.2 ± 0.2
HuK72A	8.4 ± 1.2 (84 ± 12)	1.1 ± 0.1	40.5 ± 3.0 (203 ± 15)	1.9 ± 0.1

[a]Reported in exposed (outer leaflet) lipid to protein ratio (LPR) and in brackets in μM exposed lipid concentration. Error corresponds to the standard error in the fit of the parameter. [b]Cyt*c* concentration was 10 μM. [c]Cyt*c* concentration was 5 μM.

3.3.3. Site A Binding Monitored by Trp59 Fluorescence.

Trp59 fluorescence also was used to track binding for yWT and yK72A iso-1-Cyt*c* and for HuWT and HuK72A Cyt*c*. Trp59 fluorescence enhancement results from loss of Cyt*c* tertiary structure (unfolding) as Trp59 moves away from the heme.[48] Growth in the intensity of emission was seen for all four proteins in titrations of 5 μM solutions of each Cyt*c* (Figure 3.9). All variants show a shift in the peak emission wavelength from ~330 nm to ~340 (Figure 3.10), consistent with Trp59 moving from a buried to a surface-exposed site in contact with ordered but not bulk water.[49] The Trp59 environment is not as polar as for guanidine hydrochloride unfolded Cyt*c*, where the emission maximum shifts to ~350 nm (Figs. 3.11 – 3.13).

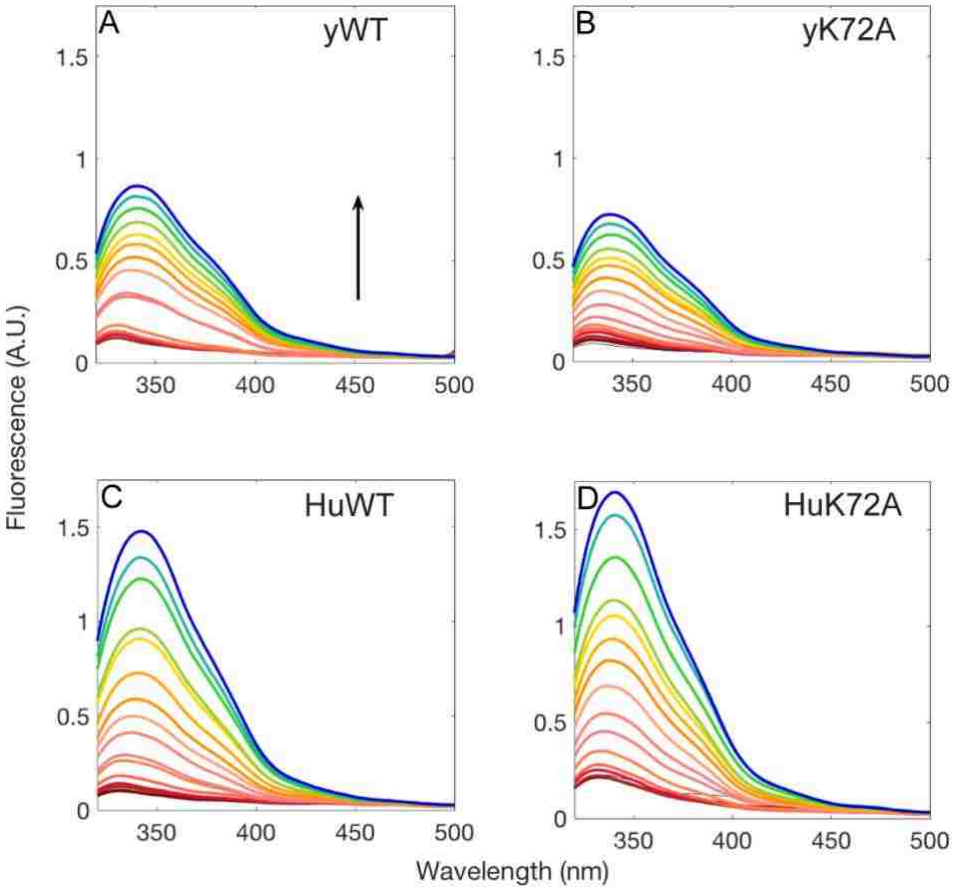

Figure 3.9. Fluorescence spectra as a function of the concentration of 100 nm CL vesicles for (A) yWT and (B) yK72A iso-1-Cyt*c* and (C) HuWT and (D) HuK72A Cyt*c*. Protein concentration was 5 μM. Black arrow denotes direction of signal shift during the titration. 0 M exposed lipid concentration corresponds to the dark red signal for each Cyt*c* variant. Maximum exposed lipid concentration (250 μM) corresponds to the blue spectrum for each variant.

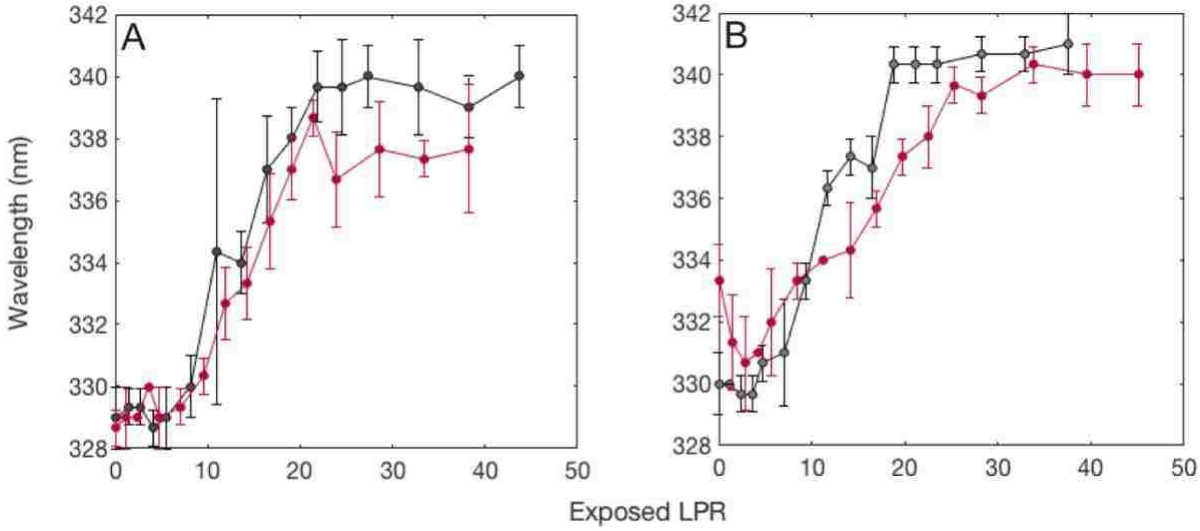

Figure 3.10. (A) yWT (black) and yK72A (red) iso-1-Cyt*c* fluorescence emission peak location versus exposed (outer leaflet) LPR. (B) HuWT (gray) and HuK72A (red) Cyt*c* fluorescence emission peak location versus exposed LPR.

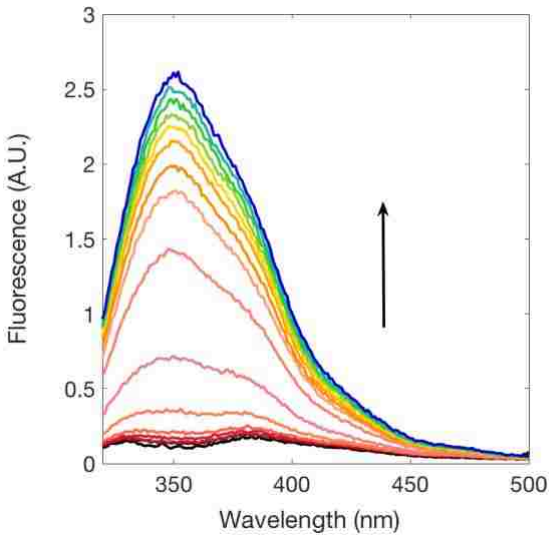

Figure 3.11. Trp59 fluorescence spectra of 10 μM yWT iso-1-Cyt*c* at pH 7, 25 ºC, in 20 mM Tris, 40 mM NaCl over a titration from 0 M (black) to 3 M (blue) GdnHCl concentration. Fluorescence measured in arbitrary units (A.U.). Black arrow indicates direction of increase in fluorescence intensity with increasing GdnHCl concentration.

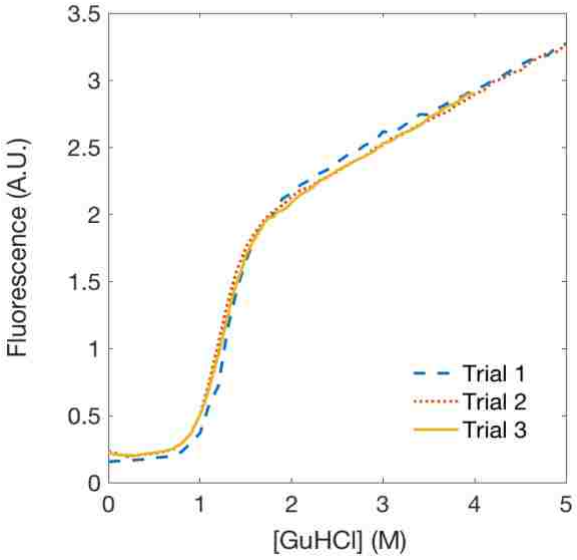

Figure 3.12. Trp59 fluorescence intensity (350 nm) progression of 10 μM yWT iso-1-Cyt*c* at pH 7, 25 °C, in 20 mM Tris, 40 mM NaCl over 3 independent GdnHCl titrations from 0 M to 5 M. Fluorescence measured in arbitrary units (A.U.).

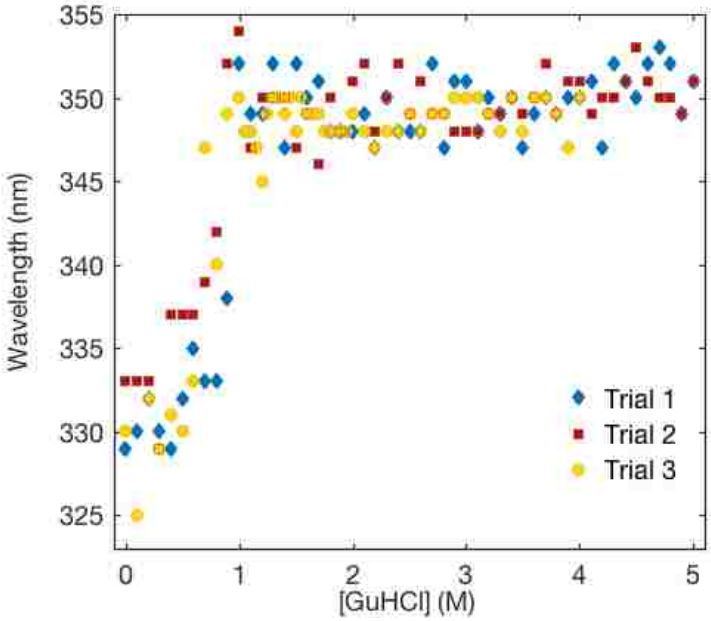

Figure 3.13. Trp59 fluorescence peak shift monitored for 3 trials over GdnHCl titrations from 0 M to 5 M GdnHCl for yWT iso-1-Cyt*c*.

Titrations were monitored at the wavelength corresponding to the emission peak at the highest CL vesicle concentration for each Cyt*c* variant studied. Figure 3.14 shows the increase in Trp59 fluorescence for both yeast iso-1-Cyt*c* and human Cyt*c* variants as exposed LPR increases, consistent with significant disruption of tertiary structure. Previous work on horse Cyt*c* has shown similar effects on Trp59 fluorescence during titrations with CL-containing vesicles.[16, 17] The overall increase in fluorescence is larger for human Cyt*c* than for yeast iso-1-Cyt*c*. Human Cyt*c* also requires higher LPR to complete the CL titration. The fluorescence-monitored titration data were fit to a single-site Langmuir-type binding model allowing for cooperativity (eq 3.1, Experimental procedures). Parameters from these fits (Table 3.1) were used to plot fraction of bound protein versus exposed LPR (Figure 3.15). Attenuation of apparent binding by the K72A mutation is more evident when monitored by fluorescence versus Soret CD. For both human and yeast iso-1-Cyt*c*, K_d(app) in terms of exposed LPR is significantly larger than observed when titrations with CL vesicles are monitored by Soret CD (Table 3.1).

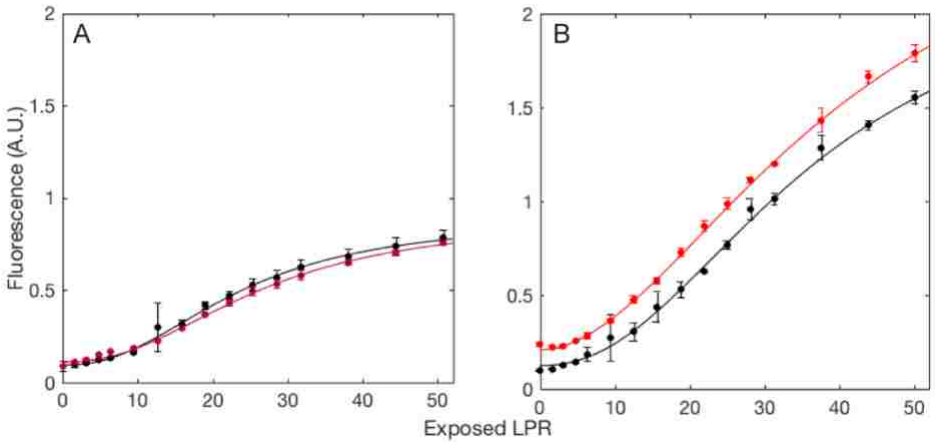

Figure 3.14. (A) yWT (black) and yK72A (red) iso-1-Cyt*c* fluorescence intensity as a function of exposed LPR. (B) HuWT (black) and K72A (red) Cyt*c* fluorescence intensity as a function of exposed LPR. All titrations were carried out at 5 μM protein concentration using 100 nm 100% CL lipid vesicles at pH 8 and 25 °C. Fluorescence intensity was followed at the wavelength of maximum intensity in the fluorescence emission spectrum of Cyt*c* at the highest lipid concentration. Solid curves are fits to eq 3.1.

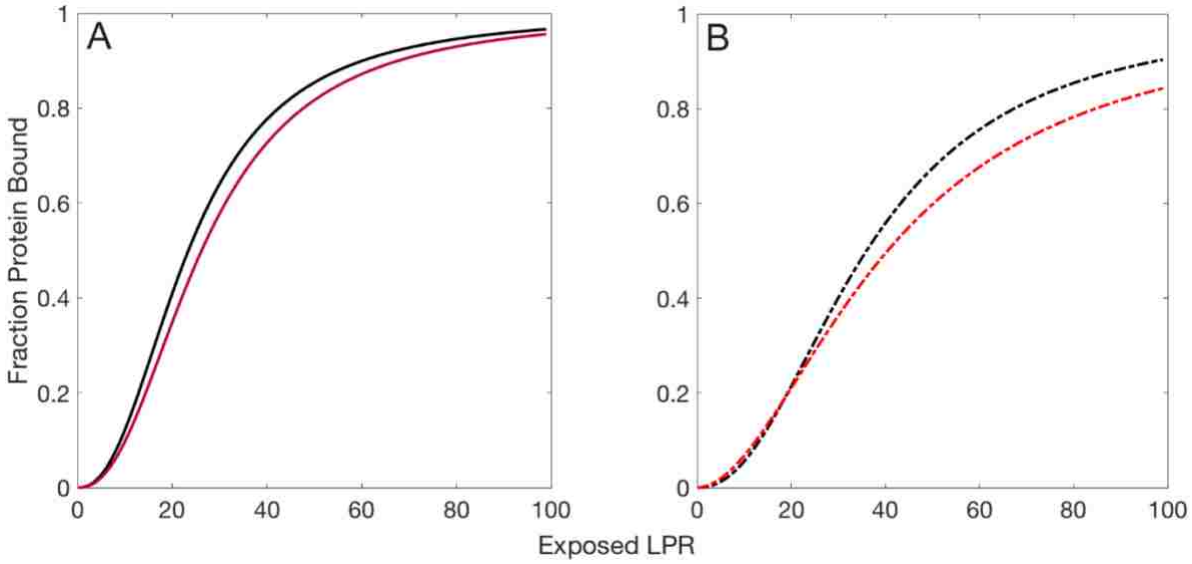

Figure 3.15. (A) Fraction protein bound versus exposed (outer leaflet) LPR for yK72 (black) and yK72A (red) iso-1-Cyt*c* using parameters in Table 3.1. (B) Fraction protein bound versus exposed LPR for HuK72 (black) and HuK72A (red) Cyt*c* using parameters in Table 3.1. Fraction bound = $(s(x)-s_0)/(s_1-s_0)$.

3.4. DISCUSSION

3.4.1. Similarities and Differences between Site A Binding to CL Vesicles for Yeast Iso-1-Cyt*c* and Human Cyt*c*.

The primary similarity between the interaction of yeast iso-1-Cyt*c* and human Cyt*c* with CL vesicles is that both proteins show two binding phases. Based on the initial low amplitude phase that occurs prior to formation of the isodichroic point with the yeast protein, we assume that both binding phases are intramolecular structural rearrangements of Cyt*c* on the membrane surface. The first phase, which occurs at lower exposed LPR, is

observable with Soret CD and thus involves rearrangement of the local heme environment. The presence of a positive/negative couplet in the Soret CD spectrum of the native state of Cyt*c* has been attributed to the presence of Met80 ligation to the heme[50] and of Phe82 near the heme,[51] although the exact nature of the interaction that produces the couplet may be more complex.[52] The loss of this couplet is observed when human Cyt*c* binds to CL and initially for iso-1-Cyt*c* binding to CL (Fig. 3.6). Loss of the couplet is also observed for the alkaline conformer,[47] providing some insight into the possible nature of the small structural rearrangement that occurs at lower LPR when Cyt*c* binds to CL. Structural studies of the alkaline conformer of iso-1-Cyt*c* show that it is compact with a rearrangement of Ω-loop D.[53, 54] However, structural studies on a K72A variant of iso-1-Cyt*c* show that loss of Met80 ligation is possible with a very small structural rearrangement.[37] The second binding phase occurs at significantly higher exposed LPR and leads to an increase in the Trp59 fluorescence. The increase in Trp59 fluorescence is attributable to reduced quenching of the fluorescence by the heme due to increased Trp59 to heme distance, indicating a significant loss of tertiary structure.[48] These observations are qualitatively consistent with previous work on horse Cyt*c*, which supports an equilibrium between compact and extended conformers, with the extended conformer favored at higher LPR.[8, 16] While our data only inform on the heme-Trp59 distance, the increase in the Trp59 to heme distance at higher LPR is consistent with the fluorescence resonance energy transfer studies of Pletneva and coworkers,[8] which indicate that the 60's and C-terminal helices move away from the heme in the extended conformer.

The second similarity for yeast iso-1-Cyt*c* and human Cyt*c* interactions with CL is that site A binding is not strongly affected by the K72A mutation. This result indicates

that the other lysines (73, 86, 87) in site A can compensate for the loss of Lys72 for Cyt*c*/CL binding at pH 8.

Fitting data to eq 3.1 reveals differences in variant response to CL binding. For the first phase, K_d(app), is similar for yWT, yK72A, HuWT and HuK72A (Table 3.1). However, the cooperativity parameter, n, for HuWT and HuK72A Cyt*c* is lower by ~0.9 units than for yWT and yK72A iso-1-Cyt*c*. Despite the similar K_d(app) values, the cooperativity suggests that site A for human Cyt*c* may only accommodate ~1 lipid, while yeast iso-1-Cyt*c* interacts with ~2 lipids. This difference might be attributed to population of the alkaline conformer for yeast iso-1-Cyt*c* at pH 8.0. However, the pK_{app} of the alkaline transition for yK72A is 8.6 (versus 8.0 for yWT)[36, 38] with no significant effect on K_d(app) or n (Table 3.1). Thus, the higher value of n for yeast iso-1-Cyt*c* does not appear to be specific to the degree of population of the alkaline conformer. The details of the structural rearrangement of the heme crevice also appear to differ between yeast and human Cyt*c*. Yeast iso-1-Cyt*c* shows a reemergence of the negative CD band near 420 nm, reminiscent of the shape of the native Soret CD spectrum, which is not observed with human Cyt*c*. This observation suggests that for iso-1-Cyt*c* the position of Phe82 could become more nativelike[51] or that Met80 ligation is partially restored[50] during this phase of binding to CL.

Comparison of K_d(app) from CD versus fluorescence data shows significant shifts in K_d(app) reported in terms of LPR for both yeast and human Cyt*c* (Table 3.1). The K_d(app) for the fluorescence detected site A interaction is 2-fold larger for yeast iso-1-Cyt*c* than for Soret CD detected site A interactions. A much larger 4-fold shift in K_d(app) is observed for human Cyt*c*. The cooperativity, n, differs for yeast versus human Cyt*c* for

the smaller structural rearrangement monitored by Soret CD, but is near 2 for both yeast and human Cyt*c* for the larger structural rearrangement monitored by fluorescence at higher LPR. The K_d(app) values for CD and fluorescence detected interactions of 100% CL vesicles with site A are close enough for the yeast protein that the cooperativity parameters for the two structural rearrangements may not be fully independent. Thus, it is possible that n for one of the phases for the yeast iso-1-Cyt*c* interaction with CL is inflated. The higher stability of human Cyt*c* versus yeast iso-1-Cyt*c*[44] may be a factor in the larger LPR needed to disrupt the tertiary structure of human versus yeast iso-1-Cyt*c* in the larger conformational rearrangement at higher LPR. The closer spacing of the stabilities of the substructures of yeast iso-1-Cyt*c*[38] compared to mammalian Cyt*c*[55, 56] could be a factor, as well. The larger LPR for loss of tertiary structure of human Cyt*c* on the surface of a CL vesicle, as detected by Trp59 fluorescence, suggests that more membrane surface area may be required to unfold the more stable protein. Stability provides a compelling argument for the higher LPR required to partially unfold human Cyt*c* on CL vesicles. However, the surface charge pattern near site A, which differs for human Cyt*c* versus yeast iso-1-Cyt*c* (see Figure 3.2), could also impact the partial unfolding phase of Cyt*c* on CL vesicles.

The larger increase in fluorescence for human Cyt*c* versus yeast iso-1-Cyt*c* (Figures 3.9 and 3.14) suggests a larger disruption of the structure of human Cyt*c* than for yeast iso-1-Cyt*c* in the large structural rearrangement at higher LPR. It is known that extended conformers of Cyt*c* have higher peroxidase activity.[8] While there is some debate about the physiological significance of extended conformers,[11] it is plausible that the higher LPR required to produce the more extended conformer of human Cyt*c* versus yeast iso-1-

Cyt*c*, combined with the larger extent of unfolding apparent for the human versus the yeast protein at higher LPR, demonstrate the evolution of both a more stringent and efficient switch for the peroxidase activity of Cyt*c* early in apoptosis.

For yeast iso-1-Cyt*c*, the K72A mutation leads to a small increase in the K_d(app) for the larger fluorescence-detected structural rearrangement (Table 3.1). For human Cyt*c*, the K72A mutation causes a small decrease in the cooperativity, n, for the larger fluorescence-detected structural rearrangement (Table 3.1). Thus, Lys72 affects the binding mode monitored by Trp59 fluorescence more significantly than the binding mode monitored by Soret CD. However, when site A is isolated at pH 8, Lys72 is not necessary for the structural rearrangements that occur when Cyt*c* interacts with 100% CL vesicles.

3.4.2. Comparison with Previous Data for Binding of CL to Cyt*c*.

It is of interest to compare our results to those obtained at lower pH where multiple binding sites contribute to the interaction of Cyt*c* with CL-containing vesicles. Previous work by Santucci and coworkers was carried out with 100% CL vesicles at pH 7 using yeast iso-1-Cyt*c*[22, 23] and horse Cyt*c*.[18, 26, 27] They observe biphasic binding curves with Soret CD measurements and similar binding curves for yeast iso-1-Cyt*c* and horse Cyt*c*.[18, 22] At pH 7, sites C, L and A will all contribute to Cyt*c* binding to CL vesicles. Thus, more complex binding curves are expected. The observed binding affinities,[18] when corrected to exposed lipid concentrations, are ~1x10^5 M^{-1} (K_d = 10 μM, n = 2) and ~5x10^4 M^{-1} (K_d = 20 μM, n =4). Two binding constants of similar magnitude were also observed with horse Cyt*c* by Pandiscia and Schweitzer-Stenner using 20% CL (80% DOPC) vesicles at pH 7.4, when their data are analyzed in terms of CL concentration exposed on the outer

leaflet of the vesicle.[16] Multiple binding sites should be available at pH 7.4, too. For purposes of comparison, we provide K_d(app) in μM units in Table 3.1. The K_d values reported at pH 7 – 7.4 are ~5-fold smaller than what we observe (K_d(app) ~ 85-100 μM), suggesting that the availability of multiple binding sites leads to significantly higher overall CL binding affinity. Studies by Pandiscia and Schweitzer-Stenner with 100% CL vesicles at pH 7.4 are more difficult to compare with our data because they were analyzed with a more complex model.[17] However, the binding curves are also consistent with considerably higher affinities than we observe under our binding conditions.

A K72N variant of horse Cyt*c* appears not to bind to 100% CL vesicles,[26] in contrast to our results with K72A variants of human Cyt*c* and yeast iso-1-Cyt*c*. Alanine versus asparagine variants may behave differently. GdnHCl titration data for Lys→Asn variants of horse Cyt*c* yield unusual biphasic unfolding curves, whereas the K72A variants of yeast iso-1-Cyt*c*[57] and human Cyt*c*[35] have monophasic unfolding curves like the wild type proteins. Thus, the Lys→Asn variants may perturb the stability of Cyt*c* in a manner that also affects binding to cardiolipin.

3.4.3. Conservation of Lysine at position 72 of Cyt*c*.

Lysine at position 72 of mitochondrial Cyt*c* is strongly, but not absolutely conserved in all known cytochromes *c*.[58] It is important,[59] although not absolutely essential,[60] for interaction with redox partners in the electron transport chain. It is important for formation of a strong complex with Apaf-1,[32, 34, 40] although mutation to other residues does not completely abrogate activation of caspases by the apoptosome.[40, 60, 61] Truncation of Lys72 to alanine enhances the intrinsic peroxidase activity of both yeast iso-1-Cyt*c*[37]

and human Cyt*c*.[35] Thus, Lys72 also plays some role in the peroxidase activity of Cyt*c*, which acts as a signaling switch in the early stages of apoptosis. Lys72 also affects the binding of Cyt*c* to CL-containing vesicles. However, the results presented here indicate that, while it may be important for binding at some CL binding sites,[26, 27] it is not essential for interactions at site A. Thus, the strong conservation of Lys at position 72 of Cyt*c* does not appear to be because it is essential for any one function, but because it is an important contributor to most of the functions of Cyt*c*.

3.5. CONCLUSION

In summary, at pH 8, we are able to isolate the site A binding site. In the absence of the C and L binding sites, the interaction of Cyt*c* with CL vesicles is significantly weaker. The K_d(app) values obtained by Soret CD, in terms of exposed LPR, are similar for human Cyt*c* and yeast iso-1-Cyt*c*, indicating that the initial small structural rearrangement requires a comparable amount of space on the surface of CL vesicles. The second and larger structural rearrangement monitored by Trp59 fluorescence occurs at significantly higher LPR for human Cyt*c* than for yeast iso-1-Cyt*c*, indicating that more surface area on CL vesicles is required to unfold the more stable human Cyt*c*. Based on the larger increase in Trp fluorescence for the human versus the yeast protein, the degree of unfolding is larger, indicating a more extended conformer for the human versus the yeast protein. This more extended conformer may yield higher peroxidase activity.[8] Thus, the signaling switch which controls peroxidase activity early in apoptosis may have evolved to be a more stringent, but more effective, switch. Neither phase of the interaction with

CL vesicles through site A is strongly affected by the K72A mutation indicating that other lysines can compensate for Lys72 at site A.

.

3.6. REFERENCES

(1) Dickerson, R. E., and Timkovich, R. (1975) Cytochromes *c*, In *The Enzymes, 3rd ed.* (Boyer, P. D., Ed.) 3rd ed., pp 397-547, Academic Press, New York.

(2) Liu, X., Kim, C. N., Yang, J., Jemmerson, R., and Wang, X. (1996) Induction of apoptotic program in cell-free extracts: requirement for dATP and cytochrome *c*, *Cell 86*, 147-157.

(3) Jiang, X., and Wang, X. (2004) Cytochrome *c*-mediated apoptosis, *Annu. Rev. Biochem. 73*, 87-106.

(4) Orrenius, S., and Zhivotovsky, B. (2005) Cardiolipin oxidation sets cytochrome *c* free, *Nat. Chem. Biol. 1*, 188-189.

(5) Kagan, V. E., Tyurin, V. A., Jiang, J., Tyurina, Y. Y., Ritov, V. B., Amoscato, A. A., Osipov, A. N., Belikova, N. A., Kapralov, A. A., Kini, V., Vlasova, I. I., Zhao, Q., Zou, M., Di, P., Svistunenko, D. A., Kurnikov, I. V., and Borisenko, G. G. (2005) Cytochrome *c* acts as a cardiolipin oxygenase required for release of proapoptotic factors, *Nat. Chem. Biol. 1*, 223-232.

(6) Muenzner, J., and Pletneva, E. V. (2014) Structural transformations of cytochrome *c* upon interaction with cardiolipin, *Chem. Phys. Lipids 179*, 57-63.

(7) Kagan, V. E., Bayir, H. A., Belikova, N. A., Kapralov, O., Tyurina, Y. Y., Tyurin, V. A., Jiang, J., Stoyanovsky, D. A., Wipf, P., Kochanek, P. M., Greenberger, J. S., Pitt, B., Shvedova, A. A., and Borisenko, G. (2009) Cytochrome *c*/cardiolipin relations in mitochondria: a kiss of death, *Free Radical Biol. Med. 46*, 1439-1453.

(8) Hanske, J., Toffey, J. R., Morenz, A. M., Bonilla, A. J., Schiavoni, K. H., and Pletneva, E. V. (2012) Conformational properties of cardiolipin-bound cytochrome *c*, *Proc. Natl. Acad. Sci. U.S.A. 109*, 125-130.

(9) Hong, Y., Muenzner, J., Grimm, S. K., and Pletneva, E. V. (2012) Origin of the conformational heterogeneity of cardiolipin-bound cytochrome *c*, *J. Am. Chem. Soc. 134*, 18713-18723.

(10) Muenzner, J., Toffey, J. R., Hong, Y., and Pletneva, E. V. (2013) Becoming a peroxidase: cardiolipin-induced unfolding of cytochrome *c*, *J. Phys. Chem. B 112*, 12878-12886.

(11) Mandal, A., Hoop, C. L., DeLucia, M., Kodali, R., Kagan, V. E., Ahn, J., and van der Wel, P. C. A. (2015) Structural changes and proapoptotic peroxidase activity of cardiolipin-bound mitochondrial cytochrome *c*, *Biophys. J. 109*, 1873-1884.

(12) Rytömaa, M., Mustonen, P., and Kinnunen, P. K. J. (1992) Reversible, nonionic, and pH-dependent association of cytochrome *c* with cardiolipin-phosphatidylcholine liposomes, *J. Biol. Chem. 267*, 22243–22248.

(13) Rytömaa, M., and Kinnunen, P. K. J. (1995) Reversibility of the binding of cytochrome *c* to liposomes, *J. Biol. Chem. 270*, 3197-3202.

(14) Rytömaa, M., and Kinnunen, P. K. J. (1994) Evidence for two distinct acidic phospholipid-binding sites in cytochrome *c*, *J. Biol. Chem. 269*, 1770-1774.

(15) Pandiscia, L. A., and Schweitzer-Stenner, R. (2014) Salt as a catalyst in the mitochondria: returning cytochrome *c* to its native state after it misfolds on the surface of cardiolipin containing membranes, *Chem. Commun. 50*, 3674-3676.

(16) Pandiscia, L. A., and Schweitzer-Stenner, R. (2015) Coexistence of native-like and non-native partially unfolded ferricytochrome *c* on the surface of cardiolipin-containing liposomes, *J. Phys. Chem. B 119*, 1334-1349.

(17) Pandiscia, L. A., and Schweitzer-Stenner, R. (2015) Coexistence of native-like and non-native cytochrome *c* on anionic liposomes with different cardiolipin content, *J. Phys. Chem. B 119*, 12846-12859.

(18) Sinibaldi, F., Fiorucci, L., Patriarca, A., Lauceri, R., Ferri, T., Coletta, M., and Santucci, R. (2008) Insights into the cytochrome *c*-cardiolipin interaction. Role played by ionic strength, *Biochemistry 47*, 6928-6935.

(19) Tuominen, A. K. J., Wallace, C. J. A., and Kinnunen, P. K. J. (2002) Phospholipid-cytochrome *c* interaction: evidence for the extended lipid anchorage, *J. Biol. Chem. 277*, 8822-8826.

(20) Heimburg, T., and Marsh, D. (1993) Investigation of secondary and tertiary structural-changes of cytochrome-*c* in complexes with anionic lipids using amide hydrogen-exchange measurements - an FTIR study, *Biophys. J. 65*, 2408-2417.

(21) Kostrzewa, A., Páli, T., Wojciech, F., and Marsh, D. (2000) Membrane location of spin-labeled cytochrome *c* determined by paramagnetic relaxation reagents, *Biochemistry 39*, 6066-6074.

(22) Sinibaldi, F., Howes, B. D., Piro, M. C., Polticelli, F., Bombelli, C., Ferri, T., Coletta, M., Smulevich, G., and Santucci, R. (2010) Extended cardiolipin anchorage to cytochrome *c*: a model for protein-mitochondrial membrane binding, *J. Biol. Inorg. Chem. 15*, 689-700.

(23) Sinibaldi, F., Droghetti, E., Polticelli, F., Piro, M. C., Pierro, D. D., Ferri, T., Smulevich, G., and Santucci, R. (2011) The effects of ATP and sodium chloride on the cytochrome *c*–cardiolipin interaction: The contrasting behavior of the horse heart and yeast proteins, *J. Inorg. Biochem. 105*, 1365-1372.

(24) Kawai, C., Prado, F. M., Nunes, G. L. C., Di Mascio, P., Carmona-Ribeiro, A. M., and Nantes, I. L. (2005) pH-dependent interaction of cytochrome *c* with mitochondrial mimetic

membranes: the role of an array of positively charges amino acids, *J. Biol. Chem. 280*, 34709-34717.

(25) O'Brien, E. S., Nucci, N. V., Fuglestad, B., Tommos, C., and Wand, A. J. (2015) Defining the apoptotic trigger: the interaction of cytochrome *c* and cardiolipin, *J. Biol. Chem. 290*, 30879-30887.

(26) Sinibaldi, F., Howes, B. D., Droghetti, E., Polticelli, F., Piro, M. C., Pierro, D. D., Fiorucci, L., Coletta, M., Smulevich, G., and Santucci, R. (2013) Role of lysines in cytochrome *c*−cardiolipin interaction, *Biochemistry 52*, 4578−4588.

(27) Sinibaldi, F., Milazzo, L., Howes, B. D., Piro, M. C., Fiorucci, L., Polticelli, F., Ascenzi, P., Coletta, M., Smulevich, G., and Santucci, R. (2017) The key role played by charge in the interaction of cytochrome *c* with cardiolipin, *J. Biol. Inorg. Chem. 22*, 19–29.

(28) Laun, P., Buettner, S., Rinnerthaler, M., Burhans, W. C., and Breitenbach, M. (2012) Yeast Aging and Apoptosis, In *Subcellular Biochemistry: Aging Research in Yeast* (Breitenbach, M., Jazwinski, S. M., and Laun, P., Eds.), pp 207-232, Springer, Netherlands.

(29) Berghuis, A. M., and Brayer, G. D. (1992) Oxidation state-dependent conformational changes in cytochrome *c*, *J. Mol. Biol. 223*, 959-976.

(30) Rajagopal, B. S., Edzuma, A. N., Hough, M. A., Blundell, K. L. I. M., Kagan, V. E., Kapralov, A. A., Fraser, L. A., Butt, J. N., Silkstone, G. G., Wilson, M. T., Svistunenko, D. A., and Worrall, J. A. R. (2013) The hydrogen-peroxide-induced radical behaviour in human cytochrome *c*–phospholipid complexes: implications for the enhanced pro-apoptotic activity of the G41S mutant, *Biochem. J. 456*, 441-452.

(31) DeLano, W. L. (2002) The PyMOL molecular graphics system, *DeLano Scientific, San Carlos, CA, USA*.

(32) Kluck, R. M., Ellerby, L. M., Ellerby, H. M., Naiem, S., Yaffe, M. P., Margoliash, E., Bredesen, D., Mauk, A. G., Sherman, F., and Newmeyer, D. D. (2000) Determinants of cytochrome *c* pro-apoptotic activity. The role of lysine 72 trimethylation, *J. Biol. Chem. 275*, 16127-16133.

(33) Kluck, R. M., Martin, S. J., Hoffman, B. M., Zhou, J. S., Green, D. R., and Newmeyer, D. D. (1997) Cytochrome *c* activation of CPP32-like proteolysis plays a critical role in a *Xenopus* cell-free apoptosis system, *EMBO J. 16*, 4639-4649.

(34) Yu, T., Wang, X., Purring-Koch, C., Wei, Y., and McLendon, G. L. (2001) A mutational epitope for cytochrome *c* binding to the apoptosis protease activation factor-1, *J. Biol. Chem. 276*, 13034-13038.

(35) Nold, S. M., Lei, H., Mou, T.-C., and Bowler, B. E. (2017) Effect of a K72A Mutation on the Structure, Stability, Dynamics and Peroxidase Activity of Human Cytochrome *c*, *Biochemistry 56*, 3358−3368.

(36) Pollock, W. B., Rosell, F. I., Twitchett, M. B., Dumont, M. E., and Mauk, A. G. (1998) Bacterial expression of a mitochondrial cytochrome *c*. Trimethylation of Lys72 in yeast iso-1-cytochrome *c* and the alkaline conformational transition, *Biochemistry 37*, 6124-6131.

(37) McClelland, L. J., Mou, T.-C., Jeakins-Cooley, M. E., Sprang, S. R., and Bowler, B. E. (2014) Structure of a mitochondrial cytochrome *c* conformer competent for peroxidase activity, *Proc. Natl. Acad. Sci. U.S.A. 111*, 6648-6653.

(38) Duncan, M. G., Williams, M. D., and Bowler, B. E. (2009) Compressing the free energy range of substructure stabilities in iso-1-cytochrome *c*, *Protein Sci. 18*, 1155-1164.

(39) Rosell, F. I., and Mauk, A. G. (2002) Spectroscopic properties of a mitochondrial cytochrome *c* with a single thioether bond to the heme prosthetic group, *Biochemistry 41*, 7811-7818.

(40) Olteanu, A., Patel, C. N., Dedmon, M. M., Kennedy, S., Linhoff, M. W., Minder, C. M., Potts, P. R., Deshmukh, M., and Pielak, G. J. (2003) Stability and apoptotic activity of recombinant human cytochrome *c*, *Biochem. Biophys. Res. Commun. 312*, 733-740.

(41) Cherney, M. M., Junior, C., and Bowler, B. E. (2013) Mutation of trimethyllysine-72 to alanine enhances His79-heme mediated dynamics of iso-1-cytochrome *c*, *Biochemistry 52*, 837-846.

(42) Redzic, J. S., and Bowler, B. E. (2005) Role of hydrogen bond networks and dynamics in positive and negative cooperative stabilization of a protein, *Biochemistry 44*, 2900-2908.

(43) Wandschneider, E., Hammack, B. N., and Bowler, B. E. (2003) Evaluation of cooperative interactions between substructures of iso-1-cytochrome *c* using double mutant cycles, *Biochemistry 42*, 10659-10666.

(44) Goldes, M. E., Jeakins-Cooley, M. E., McClelland, L. J., Mou, T.-C., and Bowler, B. E. (2016) Disruption of a hydrogen bond network in human versus spider monkey cytochrome *c* affects heme crevice stability, *J. Inorg. Biochem. 158*, 62-69.

(45) Margoliash, E., and Frohwirt, N. (1959) Spectrum of horse-heart cytochrome *c*, *Biochem. J. 71*, 570-572.

(46) Elmer-Dixon, M. M., and Bowler, B. E. (2017) Rapid quantification of cardiolipin and DOPC lipid and vesicle concentration, *Anal. Biochem. 520*, 58-61.

(47) Verbaro, D., Hagarman, A., Soffer, J., and Schweitzer-Stenner, R. (2009) The pH dependence of the 695 nm charge transfer band reveals the population of an intermediate

state of the alkaline transition of ferricytochrome *c* at low ion concentrations, *Biochemistry 48*, 2990-2996.

(48) Tsong, T. Y. (1974) The Trp-59 fluorescence of ferricytochrome *c* as a sensitive measure of the over-all protein conformation, *J. Biol. Chem. 249*, 1988-1990.

(49) Burstein, E. A., Vedenkina, N. S., and Ivkova, M. N. (1973) Fluorescence and the location of tryptophan residues in protein molecules, *Photochem. Photobiol. 18*, 263-279.

(50) Santucci, R., and Ascoli, F. (1997) The Soret circular dichroism spectrum as a probe for the heme Fe(III)-Met(80) axial bond in horse cytochrome *c*, *J. Inorg. Biochem. 68*, 211–214.

(51) Pielak, G. J., Oikawa, K., Mauk, A. G., Smith, M., and Kay, C. M. (1986) Elimination of the native Soret Cotton effect of cytochrome *c* by replacement of the invariant phenylalanine using site-directed mutagenesis, *J. Am. Chem. Soc. 108*, 2724-2727.

(52) Hagarman, A., Duitch, L., and Schweitzer-Stenner, R. (2008) The conformational manifold of ferricytochrome *c* explored by visible and far-UV electronic circular dichroism spectroscopy, *Biochemistry 47*, 9667-9677.

(53) Amacher, J. F., Zhong, F., Lisi, G. P., Zhu, M. Q., Alden, S. L., Hoke, K. R., Madden, D. R., and Pletneva, E. V. (2015) A compact structure of cytochrome *c* trapped in a lysine-ligated state: loop refolding and functional implications of a conformational switch, *J. Am. Chem. Soc. 137*, 8435-8449.

(54) Assfalg, M., Bertini, I., Dolfi, A., Turano, P., Mauk, A. G., Rosell, F. I., and Gray, H. B. (2003) Structural model for an alkaline form of ferricytochrome *c*, *J. Am. Chem. Soc. 125*, 2913-2922.

(55) Bai, Y., Sosnick, T. R., Mayne, L., and Englander, S. W. (1995) Protein folding intermediates: native-state hydrogen exchange, *Science 269*, 192-197.

(56) Krishna, M. M., Lin, Y., Rumbley, J. N., and Englander, S. W. (2003) Cooperative omega loops in cytochrome *c*: role in folding and function, *J. Mol. Biol. 331*, 29-36.

(57) McClelland, L. J., Seagraves, S. M., Khan, M. K. A., Cherney, M. M., Bandi, S., Culbertson, J. E., and Bowler, B. E. (2015) The response of Ω-loop D dynamics to truncation of trimethyllysine 72 of yeast iso-1-cytochrome *c* depends on the nature of loop deformation, *J. Biol. Inorg. Chem. 20*, 805-819.

(58) Zaidi, S., Hassan, M. I., Islam, A., and Ahmad, F. (2014) The role of key residues in structure, function, and stability of cytochrome-*c*, *Cell. Mol. Life Sci. 71*, 229-255.

(59) Margoliash, E., and Schejter, A. (1996) How does a small protein become so popular?: A succinct account of the developement of our understanding of cytochrome *c*, In *Cytochrome*

c: A Multidisciplinary Approach (Scott, R. A., and Mauk, A. G., Eds.), pp 3-31, University Science Books, Sausalito, CA.

(60) Abdullaev, Z. K., Bodrova, M. E., Chernyak, B. V., Dolgikh, D. A., Kluck, R. M., Pereverzev, M. O., Arseniev, A. S., Efremov, R. G., Kirpichnikov, M. P., Mokhova, E. N., Newmeyer, D. D., Roder, H., and Skulachev, V. P. (2002) A cytochrome *c* mutant with high electron transfer and antioxidant activities but devoid of apoptogenic effect, *Biochem. J. 362*, 749-754.

(61) Zhou, M., Li, Y., Hu, Q., Bai, X.-c., Huang, W., Yan, C., Scheres, S. H. W., and Shi, Y. Atomic structure of the apoptosome: mechanism of cytochrome *c*- and dATP-mediated activation of Apaf-1, *Genes Dev. 29*, 2349-2361.

CHAPTER 4: Electrostatic Constituents of Cardiolipin binding to site A of Cytochrome *c*

4.1. INTRODUCTION

Cytochrome *c* is a well-used model system for studies on protein folding,[1, 2] conformational dynamics[3] and long distance electron transfer in proteins and protein complexes.[4] With regard to studies on its biological function, the emphasis of recent research has shifted from its role in the electron transport chain[5, 6] to understanding its role during apoptosis.[7-9] Cytochrome *c* (Cyt*c*) abandons its function as an electron transporter in the electron transport chain during apoptosis, oxidizes cardiolipin and is released from the inner mitochondrial membrane followed by passage through the outer mitochondrial membrane into the cytoplasm.[10] Upon its release from the mitochondria, Cyt*c* binds apoptotic protease activating factor 1 (Apaf-1)[11] and, in the presence of dATP, forms the apoptosome which in turn, initiates the apoptotic pathway.[12, 13] Work has shown that Cyt*c* undergoes a conformational rearrangement upon binding to cardiolipin (CL). Various model systems incorporating CL-containing membranes have been used to elucidate the true nature of the protein-lipid interaction[10, 14-28] for Cyt*c* in the mitochondria. Several binding modes have been proposed to describe the interactions of Cyt*c* with these membrane mimetic systems. However, the nature of both the structural rearrangement and the constituents of the binding sites remain a matter of considerable debate.[14-24] Thus, further characterization of the Cyt*c*-CL interaction is important.

Four regions of Cyt*c* have been postulated to interact with CL. The anionic site (site A) sits on the flexible Ω-loop D and is thought to electrostatically interact with CL.[14] Lys72 and, to a lesser extent, Lys73 have been identified as primary constituents of site A.[14, 17, 29, 30] Lysines 86 and 87 have also been proposed to be constituents of site A.[31] The cardiolipin binding site, site C,

is believed to involve hydrogen bonding of protonated cardiolipin to Asn52.[14] Site C is also believed to involve a hydrophobic component. The L site is comprised of lysines at residues 22, 25, 27 and histidines at residues 26 and 33 that interact with CL via electrostatic and hydrogen bonding interactions at low pH.[32] This site is opposite site A, allowing Cyt*c* to bridge two membrane surfaces, thus, promoting membrane fusion. The N site containing residues F36, G37, T58, W59 and K60 may be yet another interaction site for CL.[33]

Two major protein conformations have been proposed to characterize Cyt*c* structure upon interaction with CL on lipid bilayer surfaces. Some results suggest a native-like folded structure binds to the lipid membrane.[15, 23, 33, 34] Site C is believed to involve insertion of one or more of the hydrocarbon chains of the CL lipid into the hydrophobic core of Cytc.[15, 35-37] This interaction, which has been referred to as an extended lipid anchorage,[15, 35] would seem to require a well-defined binding that would best be provided by a compact structure. The ability of Cytc to form a well-defined binding pocket for hydrocarbons has recently been shown through a set of X-ray structures, which show the hydrocarbon chain of detergents bind within a well-defined pocket in domain-swapped dimers of yeast iso-1-cytochrome *c* (iso1-Cyt*c*).[38] However, there is also good evidence for an equilibrium between compact and partially unfolded structures on CL-containing membrane surfaces, with the partially unfolded structures favored when the lipid to protein ratio (LPR) is higher.[17-19, 26, 27] Peroxidase activity data indicate that this partially unfolded conformer has higher catalytic activity.[18]

Previous mutagenesis studies on the constituents of site A using horse Cyt*c* have been carried out with 100% CL vesicles at pH 7.[29, 30] Under these conditions, both sites A and C contribute to binding.[28] Recent crystallographic studies on detergents bound to a domain-swapped dimer of yeast iso-1-Cyt*c* show that the head group of CL may interact with the hydrophobic site C with

acyl chain emerging near Lys73. Thus, it is possible that binding studies at pH 7 on variants with mutate surface lysines may report on both binding at sites A and C.

We have recently shown that binding of CL to site A of both human Cyt*c* and yeast iso-1-Cyt*c* can be accomplished without interference from other binding sites at pH 8.[39] At pH 8, Lys72 was not essential for the binding of either the yeast or the human protein to 100% CL liposomes.[39] The work presented here aims to further clarify the relative importance of lysines 72, 73 86 and 87 to the site A binding site of Cyt*c* for CL. Using the Soret band region of the circular dichroism (CD) spectrum of Cyt*c* (350-450 nm) and fluorescence from Trp59 (emission from 320-500 nm), we have investigated A site binding. We show that charge neutralization at residues 72, 73, 86 and 87 (Figure 4.1) in site A by alanine-scanning attenuates binding. Further, double charge neutralization substitutions at residues 72 and 73 and at residues 86 and 87 do not completely prevent binding. All binding titrations monitored by Soret CD demonstrate a strong binding at an exposed (outer leaflet) lipid to protein ratio (LPR) of <12. An electrostatic binding event at an exposed LPR of ~20 is detected by fluorescence-monitored titration data. The binding event involves partial unfolding of the protein structure. The apparent degree of unfolding is strongly effected by which lysines constitute site A.

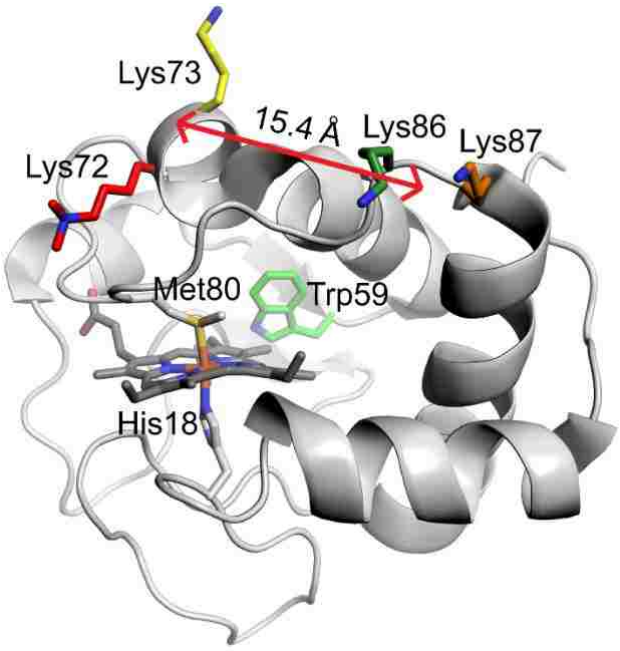

Figure 4.1. Structure of yeast iso-1-Cyt*c* (PDB ID 2YCC)[40] with Lys72 (red), Lys73 (yellow), Lys86 (dark green), Lys87 (orange) and Trp59 (light green) shown behind heme (black) and its ligands Met80 and His18. Red arrow measures width of postulated A site.

4.2. EXPERIMENTAL PROCEDURES

4.2.1. Preparation of Yeast Cyt*c* Variants.

Iso-1 Cyt*c* variants were prepared in the pRbs_BTR1 plasmid[41] carrying the yeast iso-1-cytochrome *c* gene, *CYC1*, with a C102S substitution to prevent disulfide dimerization. The plasmid also carries the *CYC3* gene (yeast heme lyase) permitting covalent attachment of heme in the cytoplasm. The PCR-based QuikChange Lightning method (Agilent) was used to prepare all variants. The starting point for mutagenesis were the previously described WT[39] and K72A[42] variants of iso-1-Cyt*c*. Primer sequences for the following mutations: K73A, K72|73A (Lys→Ala at positions 72 and 73), K86A, K87A, K86|87A (Lys→Ala at positions 86 and 87),

K72|73|86|87A (Lys→Ala at positions 72, 72, 86 and 87), can be found in Table A.6. For the K72|73|86|87A variant, pRbs_BTR1 DNA carrying the K72|73A variant was used as template and the K86|87A primer (Table A.6) was used to introduce the required mutations. Mutagenesis reaction mixtures were transformed into in *Escherichia coli* XL10 Gold competent cells (Agilent). DNA was extracted from single colonies, following overnight cultures, using the Wizard MiniPrep DNA Purification Kit (Promega Inc). Mutated plasmids were sequenced (Eurofins, Louisville, KY) to verify the mutations conferring the Lys→Ala substitutions.

4.2.2. Protein Expression of Yeast Iso-1-Cytochrome *c* Variants.

All variants were expressed and purified using previously reported methods.[43, 44] HPLC cation exchange (Uno S6 column, BioRad) was used to purify iso-1-Cyt*c* variants in the reduced state.[44] Immediately prior to experiments, iso-1-Cyt*c* variants were oxidized using 5 mg of ferricyanide per mg of protein followed by size exclusion chromatography using Sephadex G-25 resin (GE Life Sciences) equilibrated to and run with buffer appropriate to the experiment. Protein concentration and the degree of oxidation was measured with a Beckman Coulter DU 800 spectrophotometer using previously reported extinction coefficients for Cyt*c* at 339, 526.5, 541.75 and 550 nm.[45]

4.2.3. Alkaline Transition Detected by pH Titration.

The alkaline conformational transition of Cyt*c* variants K73A, K72|73A, K86A, K87A, K86|87A and K72|73|86|87A was measured using a Beckman Coulter DU 800 UV-Vis spectrophotometer with a 10 mm pathlength Beckman Coulter MICRO CELL. Absorbance was measured from 600 to 750 nm in 1 nm increments at a scan rate of 400 nm/min with a bandwidth

of 1 nm. The absorbance at 695 nm was used as a probe for the Met80-heme ligation of the native state of Cyt*c*.[46] Absorbance at 750 nm was used as a baseline to correct for spectrometer drift during the titration yielding $A_{695corr}$ ($A_{695corr} = A_{695}-A_{750}$). Titrations were performed at room temperature (20 ± 1 °C) with 400 μM protein in 0.1 M NaCl. Protein samples were initially prepared in solution at low pH (approximately pH 5 – 6) and titrations were performed by adding equal amounts of 800 μM protein in 0.2 M NaCl and varying concentrations of NaOH (0.03 to 0.3 M) to increase the solution pH by 0.05 – 0.1 pH units. $A_{695corr}$ absorbance values were plotted versus pH and fit to a modified Henderson-Hasselbalch equation incorporating both proton linkage number, n, and the apparent pK_a, pK_{app}, for formation of the alkaline conformer as previously described.[43]

4.2.4. Global Unfolding Measured using Guanidine Hydrochloride Titration.

An Applied Photophysics (Leatherhead, UK) Chirascan circular dichroism (CD) spectrophotometer interfaced with a Hamilton Microlab 500 series auto-titrator was used to perform guanidine hydrochloride (GdnHCl) titrations, as previously described.[47] All titrations were carried out at 10 μM protein concentration in 20 mM Tris Buffer, 40 mM NaCl, at pH 7 and 25 °C. Three independent trials were acquired for Cyt*c* variants K73A, K72|73A, K86A, K87A, K86|87A, K72|73|86|87A. A corrected ellipiticity at 222 nm, $\theta_{222corr}$, was calculated by subtracting ellipticity at 250 nm, θ_{250}, as baseline from ellipticity at 222 nm, θ_{222}, to evaluate loss of helicity during the GdnHCl titration. $\theta_{222corr}$ plotted versus GdnHCl were fit assuming a linear free energy relationship between protein stability and GdnHCl concentration[48] as previously reported.[49, 50]

4.2.5. Preparation of Cardiolipin vesicles.

Cardiolipin [1′,3′-bis(1,2-dioleoyl-sn-glycero-3-phospho)-sn-glycerol (TOCL)] from Avanti Polar Lipids, Inc. (Alabaster, AL) was used to prepare pure (100%) CL vesicles by extrusion through 100 nm membranes using an Avanti mini-extruder, as previously described.[39] Vesicle and lipid concentration were evaluated by Mie scattering using a Beckman Coulter DU 800 UV-Vis spectrometer, as previously described.[39, 51] Vesicles were used immediately after preparation.

4.2.6. Iso-1-Cyt*c*-CL Binding Titrations.

Cardiolipin binding experiments were performed in 20 mM TES, 0.1 mM EDTA buffer at pH 8 using a batch procedure as previously described.[39] Briefly, freshly prepared 100% CL vesicles were mixed by hand in a 1:1 ratio with stock protein 30 minutes prior to spectroscopic measurements. Samples were prepared independently for each concentration of lipid for each trial. A set of vesicle solutions at twice the desired final concentration was prepared for 1:1 mixing with stock solutions of the iso-1-Cyt*c* variants to produce the set of solutions at the desired exposed LPR for the binding curves. Titrations were monitored by Soret CD or Trp fluorescence using an Applied Photophysics Chirascan CD Spectrometer with the sample holder temperature set to 25 ^{o}C. For Soret CD, spectra were measured from 350 – 450 nm using the 4 mm pathlength of a Hellma 4x10 mm quartz cuvette. Spectra were acquired using a 1 nm descending step, 1.8 nm bandwidth, at a scan rate of 3 s/nm. Three independent titrations were carried out for each variant. For Trp59 fluorescence, excitation was at 295 nm (5 nm bandwidth). A Hellma 5x5 mm fluorescence cuvette was used. Excitation bleed-through was filtered using a 305 nm cutoff filter (Newport Corporation, Irvine, CA) in front of the emission monochromator. Emission spectra were measured from 320 - 500 nm using a 1 nm step and a 2.5 nm bandwidth

with an acquisition time of 0.5 sec per step using a scanning emission monochromator provided by Applied Photophysics. A minimum of three independent trials were acquired for each Cyt*c* variant. All Soret CD and fluorescence spectra were smoothed using a 6th order Savitsky-Golay smoothing technique before averaging data points from the three independent trials.

4.2.7. Near UV Circular Dichroism Spectroscopy.

CD spectra in the aromatic region were acquired with an Applied Photophysics Chirascan CD Spectrophotometer set to scan from 350 – 250 nm in 1 nm steps (1.8 nm bandwidth) at a scan rate of 3.0 s/nm. Spectra were acquired at 25 ^{o}C in a 10x4 mm Hellma Quartz cuvette utilizing the 4 mm path length. Stock solutions of each variant were prepared at 100 μM in 20 mM TES buffer, 0.1 mM EDTA, pH 8. Stock solutions were then mixed 1:1 with the same buffer to produce protein at 50 μM for data collection. Samples of protein in GdnHCl were prepared by mixing the protein stock solutions 1:1 with 6 M GdnHCl buffered with 20 mM TES buffer, 0.1 mM EDTA, pH 8 resulting in a 50 μM protein solution in 3 M GdnHCl. Samples of protein in the presence of CL vesicles were prepared by mixing protein stock solutions with vesicles at 1 mM CL concentration in 20 mM TES buffer, 0.1 mM EDTA, pH 8 giving a final solution of 50 μM protein in the presence of 500 μM CL (exposed LPR = 5). CL containing samples were equilibrated for 30 minutes prior to acquiring spectra. Spectra of solutions of CL vesicles were also prepared by mixing 20 mM TES buffer, 0.1 mM EDTA, pH 8 and the stock 1 mM CL in a 1:1 ratio to demonstrate that light scattering off of the vesicles did not affect the near UV CD spectra of iso-1-Cytc bound to the CL vesicles.

4.3. RESULTS

4.3.1. Variants of Iso-1-Cyt*c* Used to Probe Binding of CL vesicles to Site A.

We have previously reported the effect of a K72A variant on the binding of iso-1-Cyt*c* through site A to CL vesicles at pH 8. Two binding phases were observed for WT (Lys72 is not trimethylated because of expression from *E. coli*[52]) iso-1-Cyt*c* and the K72A variant. At lower exposed (outer leaflet) lipid to protein ratio (LPR) a CD monitored binding event occurred, which we attributed to a local conformational rearrangement and yielded an apparent dissociation constant, K_d(app) near 10 in units of exposed LPR. This binding phase was unaffected by the K72A substitution. The second phase, monitored by Trp59 fluorescence, yielded an apparent dissociation constant, K_d(app) near 23 in units of exposed LPR, which increased modestly to an exposed LPR near 26 in the presence of the K72A substitution. These results indicated that binding through site A at pH 8 did not depend strongly on a single lysine.

Site A binding has been attributed to electrostatic interactions with two subclusters of lysines, Lys72/Lys73[14, 17, 29, 30] and Lys86/Lys87[53] that are separated by 15.4 ± 2.5 Å (α-carbon to α -carbon distances, see Figure 4.1) with the closest distance being the 12.4 Å separating the α -carbons of Lys73 and Lys86. Thus, it is possible that elimination of a single Lys would simply adjust the orientation of iso-1-Cyt*c* on the membrane surface without strongly affecting K_d(app). To evaluate the role of this cluster on the interaction between iso-1-Cyt*c* with 100 nm pure (100%) CL vesicles, we have prepared single substitution variants with each lysine replaced with alanine. To probe the role of the two lysine subclusters, we have prepared Lys72|73Ala and Lys86|87Ala double substitution variants. Finally, to determine whether or not site A mediated binding is limited to this cluster of four lysines we have prepared the quadruple substitution variant, Lys72|73|86|87Ala. We note that all variants were expressed from *E. coli*. Thus, for

variants that contain Lys72, it will not be trimethylated[52] as is the case when expression of iso-1-Cyt*c* is from the native host, *Saccharomyces cerevisiae*.

4.3.2. Local and Global Protein Unfolding.

Iso-1-Cyt*c* undergoes a conformational change at mildly alkaline pH, typical of mitochondrial cytochromes *c*,[3, 46] from the native conformer with Met80 ligated to the sixth coordination site of the heme iron (See Figure 4.1) to a conformer with a lysine replacing Met80. The conformational switch for yeast iso-1-Cyt*c* involves a change from heme ligation to Met80 to ligation by Lys72, Lys73 or Lys79.[50, 52] For iso-1-Cyt*c* expressed from *S. cerevisiae*, the apparent pK_a, pK_{app} of the alkaline transition is 8.6.[54, 55] pK_{app} decreases to near 8.0 when Lys72 is not trimethylated.[41, 52] Because we are measuring the binding of iso-1-Cyt*c* variants to CL vesicles at pH 8, to selectively monitor binding to site A, it is important to determine the effect of the Lys→Ala mutation on pK_{app}, so we know the degree to which the alkaline conformer is populated under our iso-1-Cyt*c*-CL binding conditions.

Figure 4.2 shows individual pH titrations of K73A, K72|73A, K86A, K87A, K86|87A, K72|73|86|87A variants as well as WT Cyt*c*. pH titrations were performed in triplicate for each mutant and individual trials were fit to a modified Henderson-Hasselbalch as outlined in Experimental Procedures. Figure 4.2. shows that the titrations cluster into two distinct groups. The group that has a higher pK_{app}, comprises the variants that lack Lys72. The resultant thermodynamic parameters are reported in Table 4.1. The single mutant variants K73A, K86A, K87A and double mutant K86|87A show modest shifts in pK_{app} to more basic pH relative to the pK_{app} of WT iso-1-Cyt*c* expressed from *E. coli*. The K72|73A and K72|73|86|87A variants show a more pronounced basic shift in the pK_{app} of the alkaline transition to values near 8.7. The pK_{app}

observed from yeast-expressed K73A iso-1-Cyt*c*, where the alkaline state ligand is Lys79 is 8.82 ± 0.02,[56] consistent with Lys79 being the alkaline state ligand for the K72|73A and K72|73|86|87A variants, as expected.

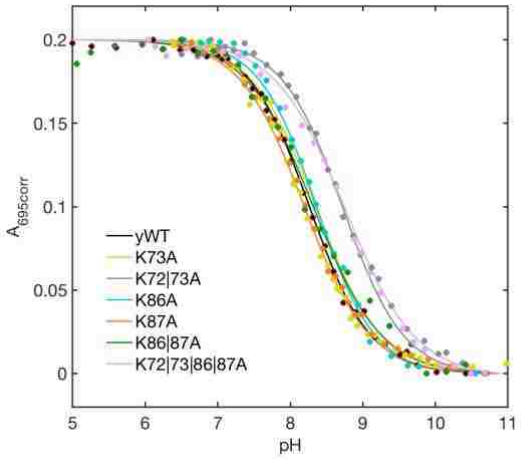

Figure 4.2. Corrected absorbance at 695 nm ($A_{695corr} = A_{695nm} - A_{750nm}$) versus pH for WT (black), K73A (yellow), K72|73A (grey), K86A (cyan), K87A (orange), K86|87A (green) and K72|73|86|87A (lavender) iso-1-Cyt*c*. Data were collected at 20 ± 1 ^{o}C in 0.1 M NaCl with a protein concentration of 400 μM. Solid lines are fits to a modified Henderson-Hasselbalch as described in Experimental Procedures in the main text.

Table 4.1. Thermodynamic parameters for local and global unfolding of iso-1-Cyt*c* variants by pH GdnHCl titrations, respectively.

Variant	pH Titration		GdnHCl Denaturation		
	pK_{app}	n	$\Delta G_u^{o'}(H_2O)$, kcal/mol	*m*, kcal/mol•M	C_m, M
WT[a]	8.00 ± 0.05	0.98 ± 0.01	5.05 ± 0.30	4.24 ± 0.13	1.19 ± 0.04
K72A[b]	8.65 ± 0.01	1.15 ± 0.01	5.31 ± 0.08	4.39 ± 0.09	1.21 ± 0.01
K73A	8.16 ± 0.01	0.99 ± 0.00	4.87 ± 0.08	3.79 ± 0.10	1.29 ± 0.03
K72|73A	8.71 ± 0.01	1.02 ± 0.04	5.48 ± 0.04	4.05 ± 0.05	1.32 ± 0.04
K86A	8.37 ± 0.02	1.02 ± 0.06	4.87 ± 0.07	4.40 ± 0.03	1.11 ± 0.01
K87A	8.12 ± 0.04	1.04 ± 0.09	4.79 ± 0.06	4.04 ± 0.11	1.19 ± 0.02
K86|87A	8.37 ± 0.56	1.07 ± 0.02	4.60 ± 0.09	3.77 ± 0.14	1.22 ± 0.06
K72|73|86|87A	8.75 ± 0.02	0.86 ± 0.01	5.09 ± 0.07	4.12 ± 0.06	1.24 ± 0.01

[a]Data from ref. [41]
[b]Data from ref. [49]

Global protein unfolding was investigated using GdnHCl unfolding monitored by CD. Figure 4.3 shows individual GdnHCl unfolding titrations for the K73A, K72|73A, K86A, and K87A variants. The thermodynamic parameters for all variants are provided in Table 4.1. Table 4.1 shows modest changes in Gibb's free energy indicating these substitutions have small effects on the global stability for these variants. Single Lys→Ala substitutions have very modest effects on global stability. The double and quadruple substitution variants demonstrate compensatory and largely additive behavior between lysines. Most notably, the K86|87A double substitution variant decreases global stability by ~0.4 kcal/mol while the K72|73A substitution variant increases global stability by ~0.5 kcal/mol. The compensatory effect of combining these substitution variants to form the quadruple substitution variant K72|73|86|87A results in an additive effect on global stability with the ΔΔG relative to WT iso-1-Cyt*c* being only 0.1 kcal/mol.

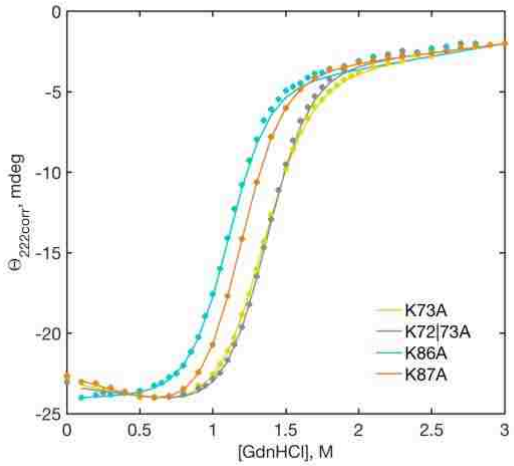

Figure 4.3. GdnHCl unfolding shown as corrected ellipiticity, $\theta_{222corr}$, versus GdnHCl concentration for K73A (yellow), K72|73A (grey), K86A (cyan), K87A (orange) iso-1-Cyt*c*. Data were collected at 25 ^{o}C, 10 μM protein, 20 mM Tris Buffer, 40 mM NaCl, at pH 7. Solid lines show fits of the data to a two-state model assuming a linear dependence of the free energy of unfolding on GdnHCl concentration.

4.3.3. Cardiolipin Binding Monitored by CD.

The Soret region of the CD spectrum, from 350-450 nm, was used to investigate conformational changes in iso-1-Cyt*c* corresponding the heme environment during CL titrations.[57, 58] Iso-1-Cyt*c* site A variants at 10 μM protein concentration were titrated with 100 nm cardiolipin vesicles from 0-250 μM exposed lipid concentration (0-25 exposed LPR). Figure 4.4 shows Soret CD spectra for the K73A and K87A variants of iso-1-Cyt*c* from the averaged data of 3 independent trials where each spectrum corresponds to data averaged at a specific lipid concentration.

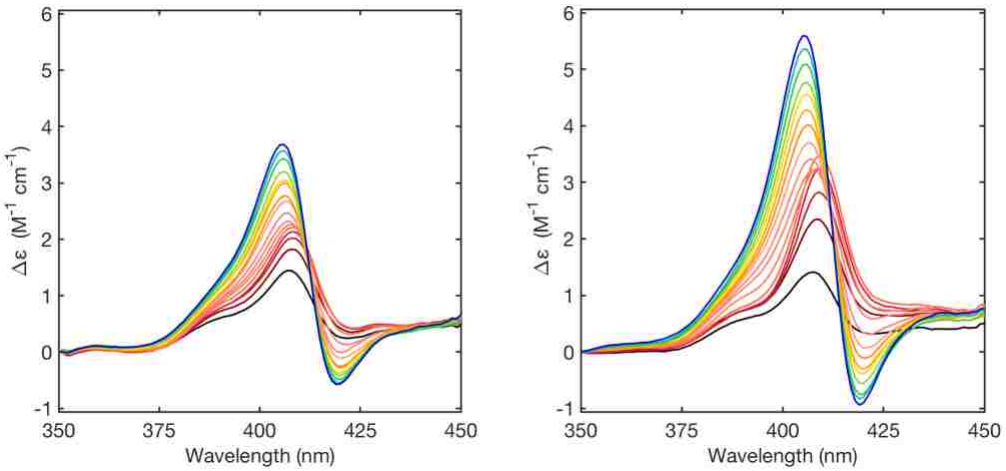

Figure 4.4. Soret CD spectra of 10 μM the K73A (left) and K87A (right) variants of yeast iso-1-Cyt*c* with 100 nm TOCL vesicles in 20 mM TES buffer, 0.1 mM EDTA at pH 8 and 25 °C. Lipid concentration increases from 0 μM to 250 μM exposed (outer leaflet) lipid (black→red→blue).

For WT iso-1-Cyt*c* and many of the variants, the negative CD band near 420 nm is missing, although this is not universally true (Figure 4.5, Figure 4.6). Lack of this band likely results from the fact that WT and many of these variants have pK_{app} values near 8 (see Table 4.1). Interestingly, this negative band re-emerges at high exposed LPR (Figure 4.4). After the three lowest exposed LPR data points, an isodichroic point is established indicating that a two state process is occurring for the remainder of the titration (Figure 4.4). The same isodichoric point is observed for all variants investigated (Figure 4.6).

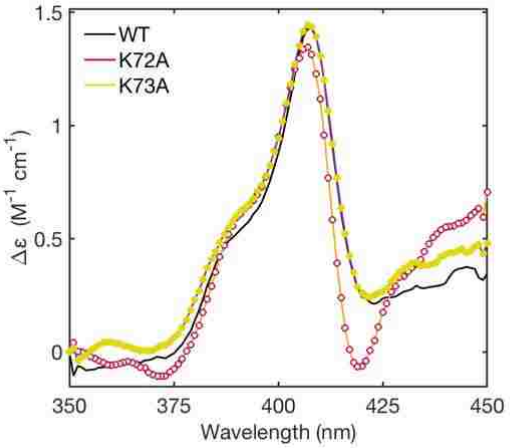

Figure 4.5. Soret CD spectra of WT yeast iso-1-Cyt*c* (black), and the K72A (red) and K73A (yellow) variants in 20 mM TES buffer, 0.1 mM EDTA at pH 8 and 25 ^{o}C.

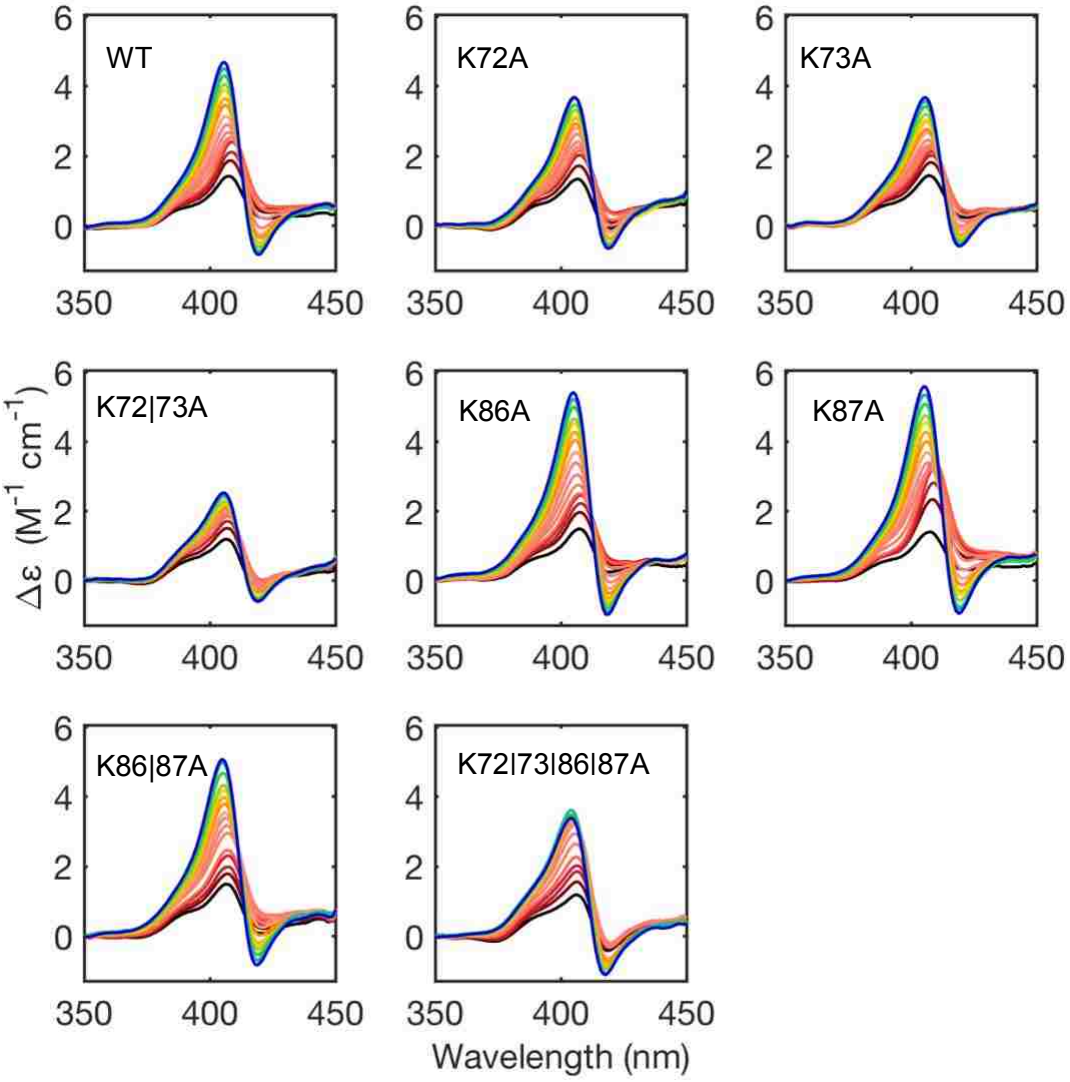

Figure 4.6. Soret CD spectra of 10 μM yeast iso-1-Cyt*c* variants titrated with 100 nm CL vesicles in 20 mM TES, 0.1 mM EDTA buffer at pH 8 and at 25 °C. Exposed (outer leaflet) CL concentration ranges from 0→200 μM (black→red→blue).

The Soret CD spectrum of WT iso-1-Cyt*c* expressed from *S. cerevisiae* has a characteristic positive peak at 406 nm and negative trough at 420 nm.[59, 60] For WT iso-1-Cyt*c* expressed from *E. coli*, the negative trough near 420 nm is essentially eliminated (Figure 4.6). For the K73A the perturbation to the Soret CD spectrum is similar to WT iso-1-Cyt*c*. However, the negative through near 420 nm is more prominent for the K72A variant. Based on the pK_{app} values in Table 4.1, the population of the alkaline conformer will be near 50% for WT iso-1-Cytc and the K73A variant at pH 8. The higher pK_{app} of the K72A variant will lead to <20% population of the alkaline conformer at pH 8. Thus, the diminished negative trough in buffer at pH 8 appears to be linked to population of the alkaline conformer.

Pandiscia et al.[27] showed a shift in the peak location in the Soret CD during titration with CL-containing vesicles. They used a peak to trough amplitude defined by the initial, unbound protein signal to characterize lipid-protein interactions. Peak wavelength shifts were observed (blue shifted) during the titration of each variant with CL vesicles (Figures 4.4 and 4.6). Following Pandiscia et al, relative amplitude was defined for each variant as the peak minus the trough of the unbound protein. The peak and trough wavelength for the unbound state were used to define amplitude throughout the titration (Figure 4.7). Monitoring the peak-trough amplitude in the Soret region of each variant effectively tracks changes in the heme environment as the exposed LPR increases.

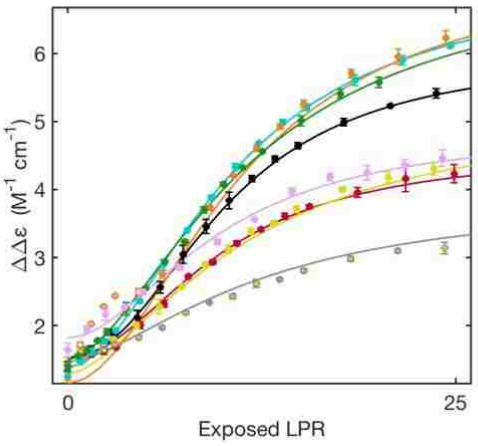

Figure 4.7. The difference in the CD signal at the peak and the trough wavelengths of the unbound iso-1-Cyt*c* variants, $\Delta\Delta\varepsilon = \Delta\varepsilon_{max} - \Delta\varepsilon_{min}$, as 100 nm TOCL vesicles are titrated into 10 μM solutions of yeast iso-1-Cyt*c* variants in 20 mM TES, 0.1 M EDTA buffer at pH 8 and 25 °C. The titrations are reported in exposed LPR. WT (black), K72A (red), K73A (yellow), K72|73A (gray), K86A (cyan), K87A (orange), and K86|87A (green) data points are fit to a one-site cooperative binding model (eq 4.1, solid curves). The K72|73|86|87A (lavender) variant data points are simply connected with a dashed line.

4.3.4. Fits of Soret CD Amplitudes to a One-site Cooperative Binding Model.

The amplitude, $\Delta\Delta\varepsilon$, due to protein binding to CL liposomes varies from variant to variant with the largest amplitude observed for the K87A, K86A and K86|87A variants and the smallest change in amplitude over the titration demonstrated by the K72|73A variant (Figure 4.7). Averaged Soret CD amplitude data as a function of exposed LPR for each variant were fit to a one-site cooperative Hill equation (eq 4.1)[26] to elucidate A-site specific CL binding,

$$s(x) = \frac{s_o + s_1\left(\frac{x}{K_d(app)}\right)^n}{1+\left(\frac{x}{K_d(app)}\right)^n} \qquad (4.1)$$

where the spectroscopic value, s(x) corresponds to the amplitude measured at the exposed LPR, x, in the titration, s_o is the value of spectroscopic parameter for the initial state, s_1 is the value of spectroscopic parameter for the final state, K_d(app) is the apparent dissociation

Table 4.2. Thermodynamic parameters for binding of site A of Cyt*c* to 100% CL vesicles.

	CD[a,b]		Fluorescence[a,c]	
Variant	K_d(app) (LPR, μM)	*n*	K_d(app) (LPR, μM)	*n*
WT	10.2 ± 0.2 (102 ± 2)	2.2 ± 0.1	23.4 ± 0.8 (117 ± 4)	2.3 ± 0.2
K72A	9.8 ± 0.2 (98 ± 2)	2.01 ± 0.07	26.2 ± 0.8 (131 ± 4)	2.31 ± 0.10
K73A	11.5 ± 0.8 (115 ± 8)	1.6 ± 0.1	29.8 ± 1.7 (139 ± 6)	2.07 ± 0.15
K72|73A	12.4 ± 1.2 (124 ± 12)	1.6 ± 0.1	34.0 ± 2.7 (195 ± 23)	1.77 ± 0.13
K86A	10.6 ± 0.4 (106 ± 4)	1.85 ± 0.08	22.9 ± 0.7 (114 ± 4)	1.93 ± 0.08
K87A	11.2 ± 0.3 (112 ± 3)	1.92 ± 0.06	22.0 ± 0.9 (107 ± 4)	1.97 ± 0.13
K86|87A	11.6 ± 0.8 (116 ± 8)	1.7 ± 0.1	22.2 ± 0.7 (109 ± 3.7)	2.88 ± 0.15

[a]Reported in exposed (outer leaflet) lipid to protein ratio (LPR) and in brackets μM exposed lipid concentration. Error corresponds to the standard error in the fit of the parameter. [b]Cyt*c* concentration was 10 μM. [c]Cyt*c* concentration was 5 μM.

constant for the iso-1-Cyt*c*-CL interaction at the membrane surface, and *n* is the associated Hill coefficient and can be interpreted as the number of lipids binding to site A. Figure 4.7 shows the fit to eq 4.1 overlaid with the amplitude data for each mutant. Parameters for the fits to eq 4.1 are reported in Table 4.2.

The values of K_d(app) for the K72A and K86A variants are within error the same as for WT, whereas there are small increases in K_d(app) for the K73A and K87A variants. Within error the double-substitution variants, K72|73A and K86|87A, have K_d(app) values that are identical to

those observed for the K73A and K87A variants. The modest effect on K_d(app) for the binding event monitored by Soret CD indicates that the variation in the degree of population of the alkaline conformer for these variants does not significantly affect the binding event observed by Soret CD,

All variants show a decrease in their Hill coefficient, *n*, relative to WT, suggesting that loss of lysines decreases the average number of lipids interacting with site A. Loss in lipid binding is modest for both K72A and K87A (~0.2 and ~0.3 lipids). K73A and K86A demonstrate a more pronounced loss in lipid binding through their Lys→Ala substitutions (~0.6 and ~0.35 lipids, respectively). The double mutant, K72|73A has the same decrease in *n* as the K73A variant in (~0.6 lipids), whereas the K86|87A exhibits a further decrease in lipid binding (~0.5 lipids) indicating that both lysines of this subcluster contribute to the CL interaction.

4.3.5. Cardiolipin Binding Monitored using Trp59 Fluorescence.

Tryptophan fluorescence was used as a secondary probe to investigate environmental changes indicative of protein structural rearrangement (partial to full unfolding) in and around the heme crevice as a result of the iso-1-Cyt*c*-CL interaction. Cyt*c* has one tryptophan at position 59 in the heme crevice (Figure 4.1) that is quenched by heme when the protein is folded. The increase in Trp59 fluorescence when Trp59 moves away from the heme has been used to monitor loss of tertiary structure when Cyt*c* unfolds.[61] Exposure of WT and variant forms of iso-1-Cyt*c* to 100% CL vesicles leads to increased tryptophan fluorescence, corresponding to a distance increase of Trp59 from the heme, which is indicative of partial or full unfolding of the protein (Figure 4.8, Figure 4.9). A red shift of fluorescence peak location is observed for WT and all variants (Figure 4.10), consistent with an increase in the solvent exposure of Trp59.

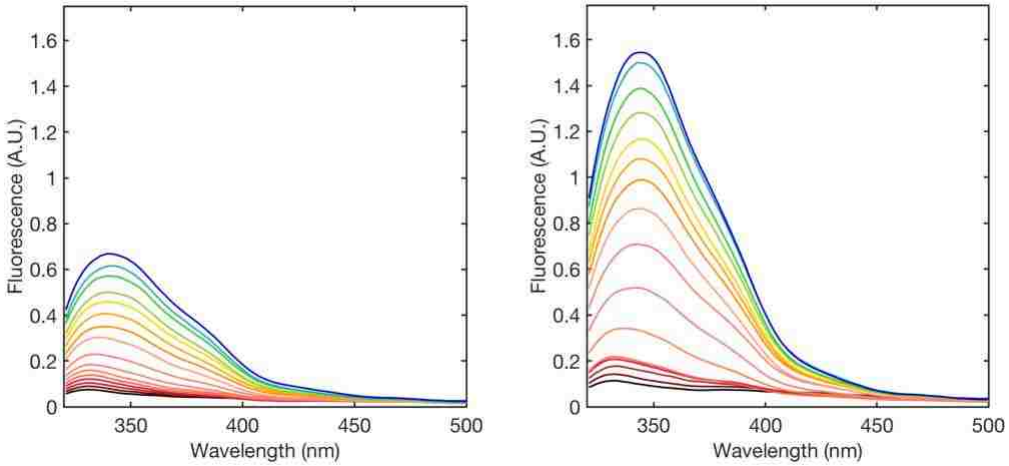

Figure 4.8. Trp59 Fluorescence emission spectra of 5 μM K73A (left) and K87A (right) iso-1-Cyt*c* titrated with 100 nm TOCL vesicles in 20 mM TES, 0.1 mM EDTA buffer at pH 8 and 25 ^{o}C. Lipid concentration increases from 0 μM to ~250 μM (outer leaflet) lipid concentration (black→red→blue). Fluorescence is in arbitrary units (A.U).

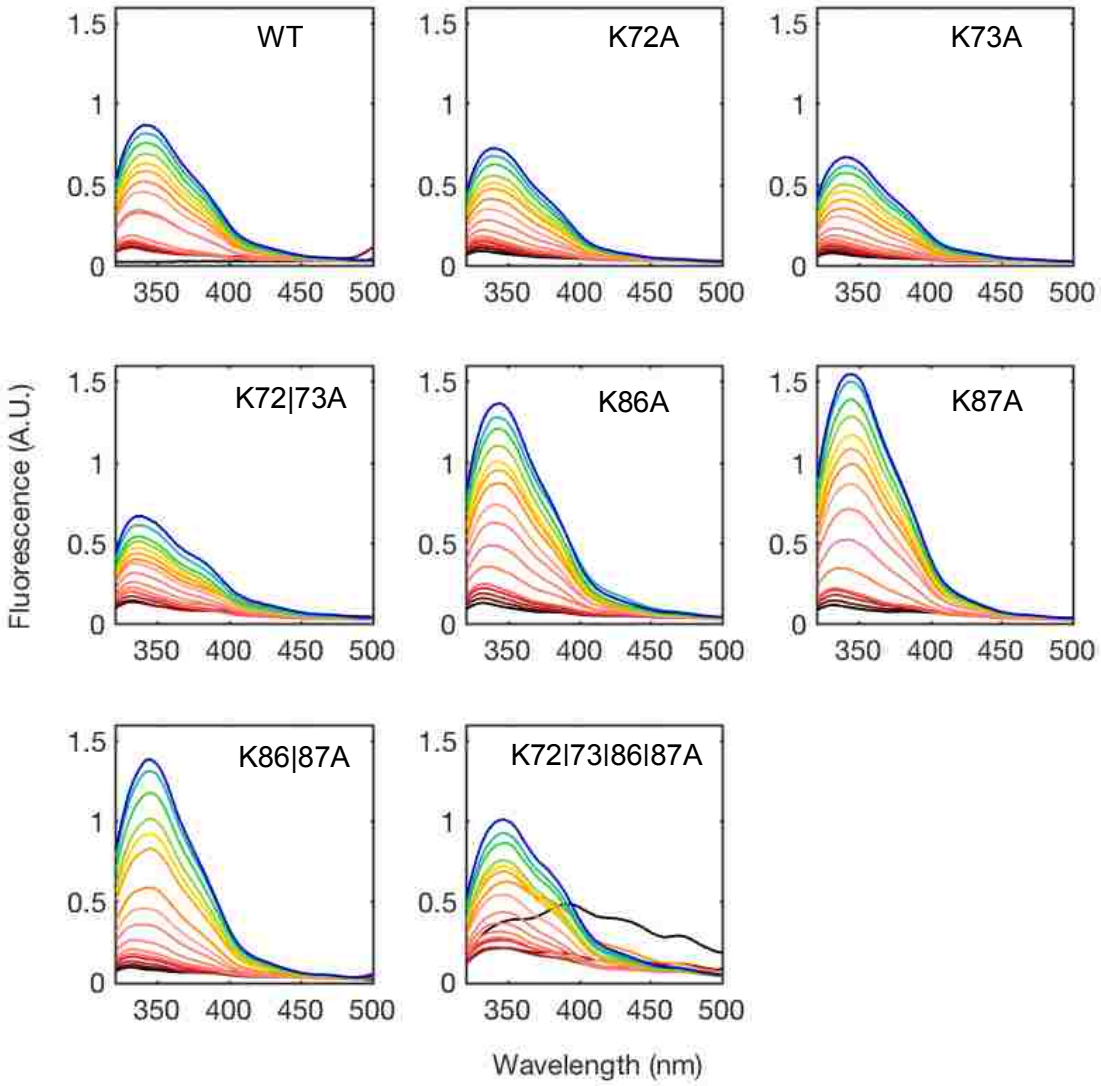

Figure 4.9. Trp59 fluorescence emission spectra of 5 μM yeast iso-1-cyt*c* variants titrated with 100 nm CL vesicles in 20 mM TES. 0.1 mM EDTA buffer at pH 8 and at 25 ºC. Exposed (outer leaflet) CL concentration ranges from 0→250 μM (black→red→blue).

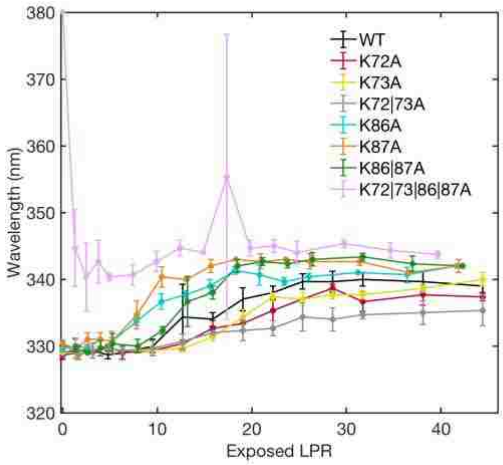

Figure 4.10. Trp59 spectral peak location (in nm) from 100 nm CL vesicles titrated into 5 μM WT(black), K72A (red), K73A (yellow), K72|73A (gray), K86A (cyan), K87A (orange), and K86|87A (green) iso-1-Cyt*c* in 20 mM TES. 0.1 mM EDTA buffer at pH 8 and at 25 ^{o}C. Titrations are reported in exposed LPR.

To track progression of the iso-1-Cyt*c*-CL interaction by fluorescence, the peak wavelength location in the final titration spectrum of each variant (see Figure 4.10) was used. The increase in fluorescence intensity versus exposed LPR for each variant is shown in Figure 4.11. Peak shift and center of mass shift were also tracked over the course of the titration (Figure 4.10, Figure 4.12). Both peak shift and center of mass shift demonstrate the impact of lysine removal on solvent exposure of Trp59. K86|87A and K87A demonstrate the greatest red shift in peak location while K72|73A has the smallest peak shift relative to the folded protein (Figure 4.10). K86|87A and K87A also have the largest shift in center of mass location while K72|73A center of mass shift is minimal (Figure 4.12).

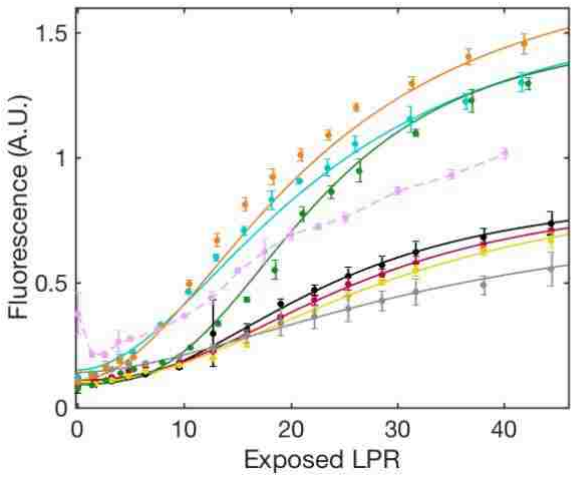

Figure 4.11. Increase in Trp59 emission during titration of iso-1-cyt*c* variants with 100 nm CL vesicles in 20 mM TES, 0.1 mM EDTA buffer at pH 8 and 25 ºC. The concentration of iso-1-Cyt*c* was 5 µM in all titrations. A single-site cooperative binding model is fit to titration data (solid curves). Error bar are one standard deviation from multiple independent trials, WT(black), K72A (red), K73A (yellow), K72|73A (gray), K86A (cyan), K87A (orange), and K8|687A (green). The K72|73|86|87A variant (lavender data points connected by a dashed line) is shown without a fit. Fluorescence measured in arbitrary units.

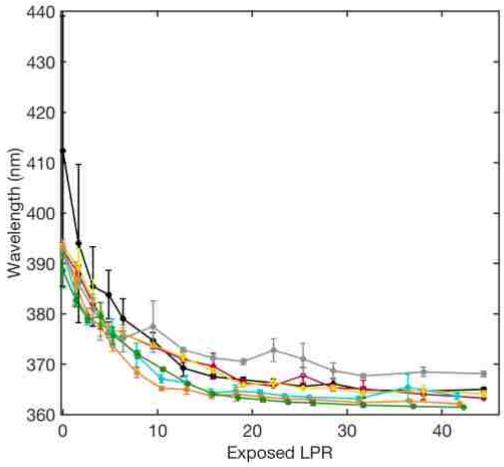

Figure 4.12. Trp59 spectral center of mass location (in nm) for 100 nm CL vesicles titrated into 5 μM WT(black), K72A (red), K73A (yellow), K72|73A (gray), K86A (cyan), K87A (orange), and K86|87A (green) iso-1-Cyt*c* in 20 mM TES, 0.1 mM EDTA buffer at pH 8 and at 25 °C. Titrations are reported in exposed LPR.

The fluorescence binding curves for each variant were fit using eq 1 (Figure 4.11). The K_d(app) with respect to exposed LPR obtained from fluorescence data for each variant is 2- to 3-fold larger than K_d(app) obtained from the Soret CD-monitored titration data. This observation indicates that the iso-1-Cyt*c*-CL interaction is biphasic (Figure 4.13). The magnitude of the change in K_d(app) obtained from fluorescence data also depends on which subcluster of site A contains the Lys→Ala substitution(s). Substitution of one or both of the lysines in the Lys86/Lys87 subcluster of site A has minimal impact on K_d(app). By contrast, substitution of the lysines in the Lys72/73 subcluster leads to significant increases in K_d(app), with the K72|73A double-substitution variant increasing K_d(app) by 45%. It is also noteworthy that variants with

substitutions in the Lys86/Lys87 subcluster all lead to significant increases in Trp59 fluorescence relative to WT iso-1-Cyt*c* (Figures 4.8, 4.9 and 4.11) when bound to CL at high exposed LPR.

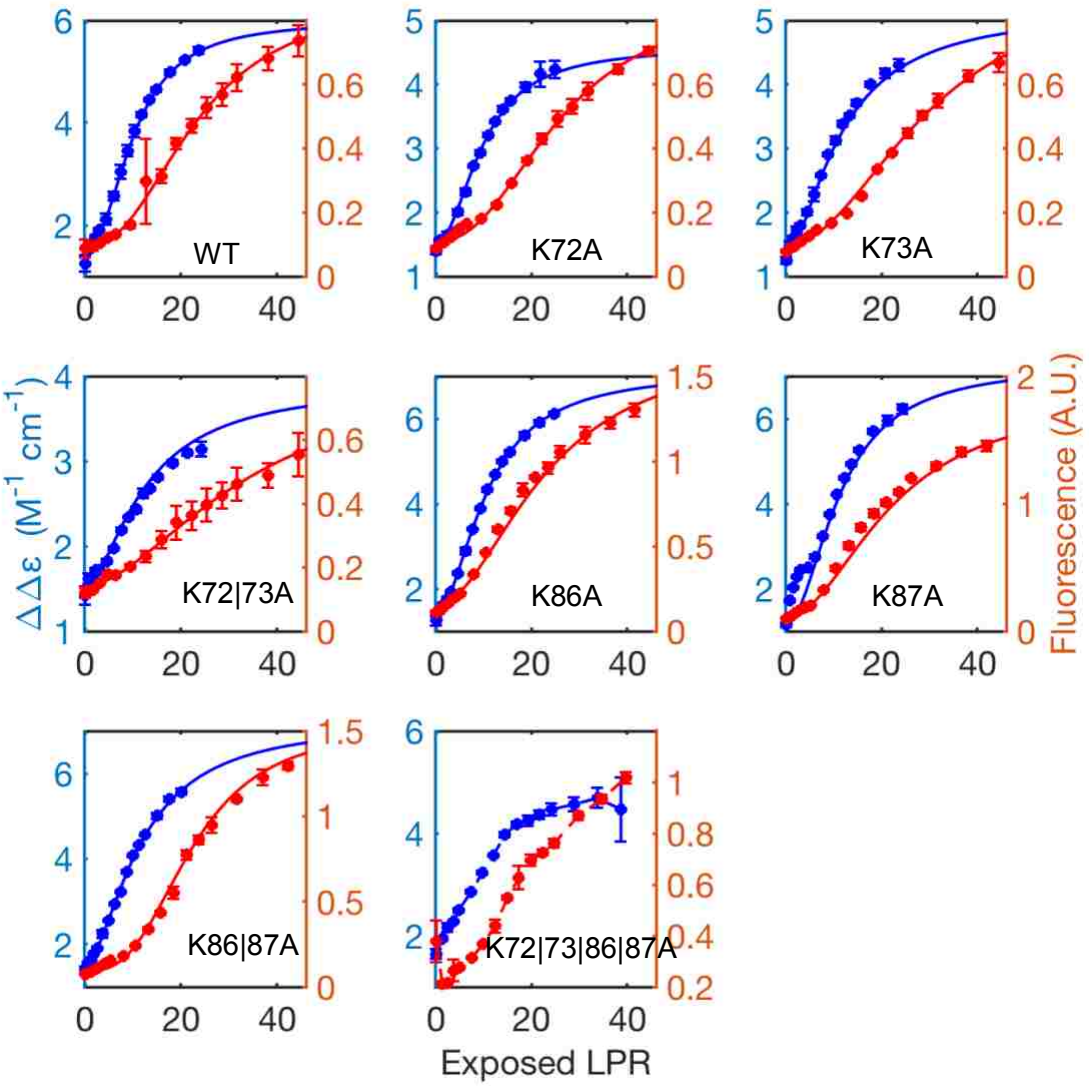

Figure 4.13. Soret CD signal change ($\Delta\Delta\varepsilon = \Delta\varepsilon_{max} - \Delta\varepsilon_{min}$) for 100 nm CL vesicles titrated into 10 µM yeast iso-1-Cyt*c* variants in 20 mM TES, 0.1 mM EDTA buffer at pH 8 (**blue**) overlaid with Trp59 emission amplitudes for 100 nm CL vesicles titrated into 5 µM yeast iso-1-Cyt*c* variants in 20 mM TES, 0.1 mM EDTA buffer at pH 8 (**red**). Titration reported as a function of exposed LPR. A one-site cooperative binding model is fit to the titration data (solid lines). Data were acquired at 25 ºC.

The magnitude of K_d(app) for the K86A, K87A, and K86|87A variants shows minimal perturbation from the WT K_d(app) (decrease of 0.5 – 1.5 in units of exposed LPR, see Table 4.2). This minimal response suggests that lysines at residues 86 and 87 do not strongly impact the large scale structural rearrangement that occurs at high exposed LPR and causes Trp59 to move away from the heme. Conversely, the K_d(app) for the K72A, K73A and K72|73A variants increases more significantly relative to WT iso-1-Cyt*c* (3 – 11 in units of exposed LPR). The increase in required exposed lipids to induce partial unfolding indicates that Lys72 and Lys73 are both important for partial unfolding of iso-1-Cyt*c* on CL liposomes.

For fluorescence monitored binding phase, all variants, except K72A, demonstrate changes in the number of lipids bound, *n*. The K73A diminishes *n* by 0.2 units and the K72|73A variants decreases *n* by ~0.5 units. Thus, removal of both lysines, K72|73A, has a combined cooperativity loss greater than expected based on the values of *n* for the individual variants. K86A and K87A show decreases in *n* of ~0.35 and ~0.30 lipids. However, the K86|87A variants show an additive increase in *n* of approximately ~0.55 lipids.

4.3.6. Trp59 Environment Monitored using Circular Dichroism.

The CD region reporting Trp59 rearrangement was investigated to determine the role of CL in local rearrangement around the amino acid following the work of Pinheiro et al.[62] Figure 4.14. shows near UV CD in the absence (folded protein) and presence (unfolded protein) of 3 M GdnHCl as well as in the presence of CL vesicles at a concentration corresponding to an exposed LPR of 5 for each variant. Each variant demonstrates minimal perturbation of the near UV CD signal in the presence of CL under crowded conditions on the membrane surface. The sharp minima at 282 and 289 nm are characteristic of Trp59 in the native state structure of iso-1-

Cyt*c*.[63] This finding shows that in the region of the binding curve where the surface density of iso-1-Cyt*c* is expected to be high (low exposed LPR), the perturbation to the near UV CD, and thus to the Trp59 environment, is minimal. By contrast, large changes in the near UV CD are observed in 3 M GdnHCl where all variants are expected to fully unfolded (see Figure 4.3). These results indicate that at low exposed LPR the environment of Trp59 is only modestly perturbed. Previous work on horse Cyt*c* binding to phosphatidylserine (DOPS) vesicles at a high exposed LPR of 125 show complete loss of the near UV signal due to Trp59.[62]

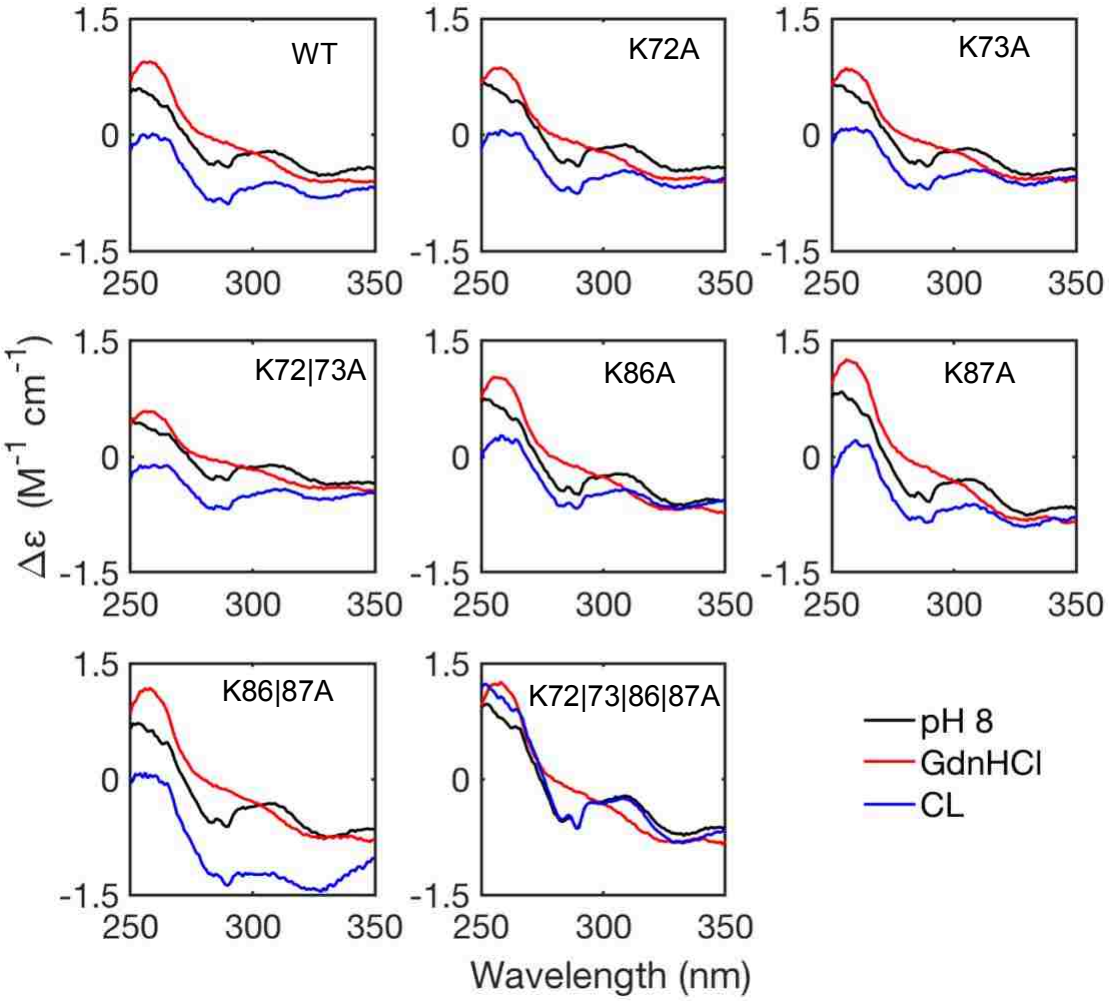

Figure 4.14. Near UV CD of 50 µM yeast iso-1-Cyt*c* variants in 20 mM TES, 0.1 mM EDTA buffer at pH 8 (**black**) overlaid with 50 µM yeast iso-1-Cyt*c* variants mixed with 500 µM 100 nm CL vesicles in 20 mM TES, 0.1 mM EDTA buffer at pH 8 (exposed LPR = 5; **blue**) and with 50 µM yeast iso-1-Cyt*c* variants in 3 M GdnHCl in 20 mM TES, 0.1 mM EDTA buffer at pH 8 (**red**). All spectra were recorded at 25 °C.

4.4. DISCUSSION

4.4.1. General Features of Cardiolipin Binding to Site A at pH 8.

In previous work, we established that we can isolate binding to site A at pH 8.[39] Under these conditions, we no longer observe an increase in light scattering in the UV-Vis absorbance spectrum that is typical of binding to site L.[32] We are also above the pH regime where binding to site C is expected to occur.[14] In our previous report, we observed that an isodichroic point in the Soret CD spectra of WT yeast iso-1-Cyt*c* and a K72A variant begins to form at an exposed LPR near 3.[39] This result indicates that initial intermolecular binding occurs below an exposed LPR of ~3 with the remainder of the titration representing a conformational rearrangement of iso-1-Cyt*c* on the surface of 100% CL vesicles. A similar behavior is observed here for all of the site A Lys→Ala variants. However, the isodichroic point does not establish until a somewhat higher exposed LPR for the K87A (see Figure 4.4) and the K86|87A variant (Figure 4.6), suggesting that these substitutions weaken the initial intermolecular binding to the CL vesicles. In the case of the quadruple substitution variant, K72|73|86|87A, a separate intermolecular binding phase is apparent in the binding isotherm (Figure 4.7), indicating that intermolecular binding is significantly weakened for this variant.

In our previous report,[39] and for all variants studied here, the majority of the amplitude signal propagation of the Soret CD-monitored binding titration occurs after the initial intermolecular association. The minimal effect of intermolecular association on the Soret CD at small values of exposed LPR indicates that when the membrane surface is crowded, the structure of iso-1-Cyt*c* is minimally effected by binding to 100% CL vesicles. Consistent with this observation, the largest change in the Soret CD signal occurs during the initial intermolecular association of the

K72|73|86|87A variant for which intermolecular association is not complete until larger values of exposed LPR. Because we are observing intramolecular rearrangements of membrane bound iso-1-Cyt*c*, which appear to be dependent on available space on the membrane surface, we report all apparent dissociation constants, K_d(app), in terms of exposed LPR.

In our previous work, binding monitored by Trp59 fluorescence occurs at larger values of exposed LPR than binding monitored by Soret CD.[39] This observation is consistent with two sequential structural rearrangements on the surface of the CL vesicles. The same behavior is observed here for all site A Lys→Ala variants (Figure 4.13 and Table 4.2). The characteristic positive/negative couplet observed for the Soret CD of the native state of Cyt*c* has been attributed to the presence of the heme-Met80 bond[64] and is believed to report on the orientation of Ph82 relative to the heme,[59] although exact structural determinants of the splitting of the couplet are likely more complex.[65] An X-ray structure of the K72A variant of iso-1-Cyt*c* at pH 8.8 shows that a modest structural rearrangement of iso-1-Cyt*c* is sufficient to permit replacement of the Met80 heme ligand by water. Quenching of Trp59 fluorescence is used to monitor loss of tertiary structure as Trp59 moves away from the heme (see Figure 4.1).[61] For most of the site A Lys→Ala variants, the increase in Trp59 fluorescence is small during the CD-monitored transition (Figure 4.13). Thus, the first structural rearrangement is likely a small conformational rearrangement that alters the heme environment. The modest effect of CL binding on the near UV CD spectrum of iso-1-Cyt<u>c</u> at low exposed LPR (Figure 4.14) is also consistent with this conclusion. The second conformational change, which leads to a large increase in Trp fluorescence, is consistent with significant unfolding of iso-1-Cyt*c*. The existence of an equilibrium between compact and extended conformers has previously been demonstrated for the binding of horse Cyt*c* to CL vesicles.[18, 26] These features of CL binding to site A of yeast

iso-1-Cyt*c* qualitatively remain unaltered even by complete elimination of the four lysines (K72|73|86|87A variant) most commonly considered to define the boundaries of site A (Figure 4.13). This observation indicates that site A may be a more extensive binding site than previously thought.

4.4.2. Effect of Lys→Ala Substitutions in Site A on the Structure of Iso-1-Cyt*c* bound to CL Vesicles.

For CL vesicle binding to the cluster of positive charges that comprise site A, the degree of perturbation to the structure of iso-1-Cyt*c*, as detected by either Soret CD or Trp59 fluorescence, depends on whether the substitution is in the Lys72/73 or the Lys86/87 charge subcluster. The K86A, K87A and K86|87A variants all show a larger change in both the Soret CD signal (Figures 4.4, 4.6 and 4.7) and a greater increase in the Trp59 fluorescence (Figures 4.8, 4.9 and 4.11) compared to the binding of WT iso-1-Cyt*c* to CL vesicles. Thus, elimination of the Lys86 and/or Lys87 charges leads to a larger perturbation of the heme environment for binding to CL vesicles at low exposed LPR (crowded vesicle surface) and a larger degree of loss of tertiary structure for binding to CL vesicles at high exposed LPR (uncrowded vesicle surface). By contrast, the K72A, K73A and K72|73A variants all cause a smaller change in both the Soret CD signal (Figures 4.4, 4.6 and 4.7) and a smaller increase in the Trp59 fluorescence (Figures 4.8, 4.9 and 4.11) compared to the binding of WT iso-1-Cyt*c* to CL vesicles. Therefore, elimination of the Lys72 and/or Lys73 charges leads to a smaller perturbation of the heme environment at low exposed LPR (crowded vesicle surface) and a larger degree of loss of tertiary structure at high exposed LPR (uncrowded vesicle surface).

The shift in the emission maximum of Trp59 upon binding to CL vesicles (Figure 4.10) is also consistent with the relative degree of unfolding indicated by the increase in Trp59 fluorescence observed for the different site A Lys→Ala variants (Figures 4.8, 4.9 and 4.11). For WT iso-1-Cyt*c*, the wavelength of maximum emission from the Trp59 shifts from ~330 nm for the native state of iso-1-Cyt*c* to near 340 nm when bound to CL vesicles through site A at high exposed LPR.[39] This shift in emission maximum indicates that Trp59 moves from a buried to a surface-exposed site in contact with ordered water when bound to CL vesicles.[66] Exposure to bulk water typically leads to an emission maximum near 350 nm for tryptophan.[66] For the K86A, K87A and K86|87A variants the emission maximum shifts to ~342 nm indicating greater exposure to bulk water for these variants when bound through site A to CL vesicles at high exposed LPR (Figure 4.10). The greater exposure to bulk water for these variants relative to WT iso-1-Cyt*c* is consistent with the higher degree of unfolding relative to WT iso-1-Cyt*c* indicated by their higher emission intensity when bound to CL vesicles at high exposed LPR (Figures 4.8, 4.9 and 4.11). For the K72A, K73A and K72|73A variants the emission maximum shift is smaller than for WT iso-1-Cytc, shifting only to ~335 nm for the K72|73A variant at high exposed LPR (Figure 4.10). The smaller shift in emission maximum for these variants indicates that Trp59 is more buried for these variants when bound through site A to CL vesicles at high exposed LPR. A more buried Trp59 for these variants relative to WT iso-1-Cyt*c* is consistent with the lesser degree of unfolding relative to WT iso-1-Cyt*c* indicated by their lower emission intensity when bound to CL vesicles at high exposed LPR (Figures 4.8, 4.9 and 4.11).

These observations indicate that binding through the Lys72/Lys73 charge subcluster of site A is necessary for larger conformational rearrangements both at low exposed LPR (crowded vesicle surface) and high exposed LPR when bound to CL vesicles through site A. By contrast, the

Lys86/Lys87 charge subcluster of site A appears to inhibit larger scale conformational rearrangements at both at low exposed LPR (crowded vesicle surface) and high exposed LPR when bound to CL vesicles through site A. When lysines 86 and 87 are substituted by alanine, binding to CL vesicles through site A leads to larger conformational rearrangements. The K72|73|86|87A variant, which eliminates both site A charge subclusters shows conformational rearrangements upon binding to CL vesicles that are intermediate between the effects of the two subclusters (Figures 4.6-4.9) indicating that the effects of the two charge subclusters on binding to CL vesicles through site A are compensatory.

4.4.3. Effect of Lys→Ala Substitutions in Site A on K_d(app) and the cooperativity of binding of Iso-1-Cyt*c* to CL Vesicles.

In our comparative study on yeast iso-1-Cyt*c* versus human Cyt*c* binding to CL vesicles via site A,[39] we noted that our K_d(app) values are higher (weaker apparent binding) that in previous studies carried out at pH 7 and 7.4.[26, 28-30, 36, 67] This difference likely reflects the involvement of site C and site L in these studies of binding at lower pH. Lys→Asn and Lys→Arg substitutions in Ω-loop-D (residues 70 – 85) also indicated that Lys73 and Lys79 were critical for binding at pH 7. We see no such specificity in our data at pH 8. This difference likely reflects participation of site C and/or site L at pH 7. Site C is believed to involve direct insertion of one or more of the hydrocarbon chains of CL into the hydrophobic core of Cyt*c*.[15, 35, 36] Insertion of a hydrocarbon chain undoubtedly introduces restrictions not present for binding only through site A, the anionic site.

As discussed above, our data for the binding of iso-1-Cytc variants to CL vesicles via site A are consistent with the thermodynamic parameters in Table 4.2 reporting on conformational

rearrangements of iso-1-Cyt*c* already bound on the surface of the CL vesicles. That said, it is evident for the K87A and K86|87A variants and most particularly the K72|73|86|87A variant (Figure 4.6 and 4.7) that the isodichroic point for binding monitored by Soret CD does not form until further into the binding titration. This observation suggests that these variants have qualitatively weaker intermolecular association with CL vesicles than WT iso-1-Cyt*c*. Because of the low amplitude of this pre-isodichroic point phase, we were unable to fit the data for these variants to a more complex model.

The most noteworthy observation in Table 4.2 is that K_d(app) is not strongly sensitive to the site A Lys→Ala substitutions. Once bound to the membrane, two stages of conformational rearrangement occur, a first phase under crowded conditions (low exposed LPR) involving perturbation of the heme environment and a second phase involving partial unfolding of Cyt*c* that requires more space on the membrane surface (high exposed LPR). The relative insensitivity of K_d(app) to site A Lys→Ala substitutions suggests that site A is fairly malleable, with the loss of one or more lysines relatively easily replaced by nearby lysines. We were unable to obtain a reliable fit of the Soret CD or the Trp59 emission versus exposed LPR data to the simple one site cooperative binding model for the K72|73|86|87A variant which has all lysines commonly attributed to site A replaced with alanine. It is evident that two separable conformational rearrangements still occur (Figures 4.7, 4.11 and 4.13). Thus, in the absence of the "site A" lysines other nearby positively charged groups, (Arg13, Arg91 and Lys88 for the Lys86/Lys87 charge subcluster and Lys54, Lys55 and Lys79 for the Lys72/Lys73 subcluster) appear to be able to cause similar structural rearrangements at similar degrees of crowding (exposed LPR) on the membrane surface.

The K_d(app) for the first phase monitored by Soret CD is only modestly sensitive to exposed LPR. The K73A and K86A variants yield K_d(app) within error of the WT value of 10.2 ± 0.2, with maximal increases of 15 – 20% for the K72|73A and K86|87A variants. The cooperativity, *n*, which provides an estimate of the number of CL involved in this phase, decreases for all variants. Thus, elimination of lysines appears to decrease the number of lipids that interact with iso-1-Cyt*c* in the first conformational rearrangement. For the Lys72/Lys73 subcluster, Lys73 is the dominant contributor to the cooperativity, whereas in the Lys86/Lys87 subcluster the two lysines appear to contribute equally to the cooperativity of the conformational rearrangement when the surface of the membrane is crowded.

The behavior of K_d(app) for the second phase monitored by Trp59 fluorescence depends strongly on the subcluster of site A, which has had its charges neutralized. Substitution of either Lys72 or Lys73 increases K_d(app) and the increase is roughly additive in the K72|73A variant with the K72|73A variant showing a 45% increase in K_d(app). For the Lys86/Lys87 charge subcluster, Lys→Ala substitutions do not affect K_d(app). The effect of substitutions in the Lys86/Lys87 subcluster on the emission maximum and on the degree of increase in Trp59 emission intensity upon binding to CL vesicles suggest a higher degree of unfolding than for WT iso-1-Cyt*c*. More extensive unfolding might be expected to lead to a higher K_d(app) in terms of exposed LPR (less crowded membrane surface needed). Based on the smaller red shift in the Trp59 emission maximum and the decrease in Trp59 emission intensity for Lys→Ala subsitutions in the Lys72/Lys73 charge subcluster, the space needed on the membrane is expected to be less for these variants to partially unfold. Thus, changes in K_d(app) do not correlate well with degree of unfolding assessed by Trp59 fluorescence (Trp59-heme distance). It can be speculated that neutralization of the Lys86/87 charge subcluster shifts the site A

interaction toward partial unfolding centered around Lys54/Lys55 and Lys72/Lys73, increasing the Trp59-heme distance but not requiring a large increase in the space needed on the membrane relative to WT iso-1-Cyt*c*. In the absence of the Lys72/Lys73 charge subcluster, partial unfolding may be dominated by the Lys86/Lys87 charge subcluster with concomitant unfolding of the C-terminal helix. This possibility would require more space on the membrane, but might lead to a smaller increase in the Trp59-heme distance for iso-1-Cyt*c* bound to CL vesicles at high exposed LPR if Ω-loop-C (residues 40 – 57) is less disrupted in the absence of Lys72/Lys73. Fluorescence resonance energy transfer studies on horse Cyt*c* binding to CL vesicles are consistent with both the 60s helix and the C-terminal helix moving away from the heme.[18] Substitutions in the Lys72/73 versus the Lys86/87 charge subcluster may shift the ensemble of iso-1-Cyt*c* structures on the membrane surface from ones involving partial unfolding near the 60s helix versus the C-terminal helix.

In all cases, the cooperativity, *n*, in Table 4.2 for the second phase of structural rearrangement when iso-1-Cyt*c* is bound to CL vesicles is near 2, indicating that no matter the composition of site A interactions, direct interaction with ~2 CL lipids is needed for partial unfolding of iso-1-Cyt*c*. The cause of the increase in *n* for the K86|87A variant is unclear based on the current data.

4.4.4. Implications for the Peroxidase Activity Signaling Switch in Apoptosis.

Studies on horse Cyt*c* bound to CL vesicles indicate that the degree of structural rearrangement that occurs on CL vesicles correlates with the peroxidase activity of the bound Cyt*c*.[18] The effects of neutralizing the different subclusters of iso-1-Cytc show that the distribution of positively charged amino acids on the surface of Cyt*c* can be used to control the

magnitude of the structural rearrangement that occurs when Cyt*c* binds to CL on the inner mitochondrial membrane. Thus, it is possible that the distribution of charges on the surface of Cyt*c* has evolved to maximize the increase in peroxidase activity of Cyt*c* and thus the effectiveness of the signaling switch when it is bound to CL in the early stages of apoptosis. Our previous comparative study of the binding of yeast iso-1-Cyt*c* and human Cyt*c* to 100% CL vesicles is consistent with the hypothesis. The magnitude of the enhancement in Trp59 emission for WT human Cyt*c* relative to WT iso-1-Cyt*c* is similar to the effect of elimination of the Lys86/Lys87 charge subcluster for iso-1-Cyt*c*. Thus, the distribution of charges on the surface of human Cyt*c* (see Figure 2 in ref. [39]) appears to have evolved to allow for a larger structural rearrangement when human Cyt*c* binds to CL. Recent studies on the G41S and Y48H disease-causing variants of human Cyt*c* indicate a linkage between increased dynamics at the interface of Ω-loops C (residues 40 – 57) and D (residues 70 – 85) and enhanced peroxidase activity.[68, 69] The similarity of the behavior of the Lys86/87 iso-1-Cyt*c* charge subcluster variants and human Cyt*c* may reflect evolution of Cyt*c* toward a distribution of charges on the surface of human Cyt*c* that favors opening at the interface of Ω-loops C and D when bound to CL vesicles. Such evolution of the charge distribution could optimize the peroxidase signaling switch in the early stages of apoptosis.

4.5. CONCLUSIONS

We show that binding of iso-1-Cyt*c* to 100% CL vesicles specifically through site A at pH 8, is not strongly dependent on any one of the four lysines commonly attribute to site A. Our results indicate that the specific complement of positively charged residues comprising site A is fairly malleable. These results contrast with previous work at pH 7 which suggest that lysines 72 and

79 are critical for binding to CL.[29, 30] The difference is likely because binding at pH 7 includes contributions from other binding sites such as site C. Our data also show that the details of both the small structural rearrangement at low exposed LPR (crowded membrane surface) and the larger structural rearrangement at high exposed LPR (uncrowded membrane surface) are significantly dependent on the site A lysines available for interaction with CL. These results suggest that site A may have evolved to optimize the structural switch that turns on peroxidase activity in the early stages of apoptosis.

4.6. REFERENCES

(1) Englander, S. W. (2000) Protein folding intermediates and pathways studied by hydrogen exchange, *Annu. Rev. Biophys. Biomol. Struct. 29*, 213-238.

(2) Colón, W., and Roder, H. (1997) Kinetic role of early intermediates in protein folding, *Curr. Opin. Struct. Biol. 7*, 15-28.

(3) Cherney, M. M., and Bowler, B. E. (2011) Protein dynamics and function: making new strides with an old warhorse, the alkaline conformational transition of cytochrome *c*, *Coord. Chem. Rev. 255*, 664-677.

(4) Gray, H. B., and Winkler, J. R. (2005) Long-range electron transfer, *Proc. Natl. Acad. Sci. U.S.A. 102*, 3534-3539.

(5) Dickerson, R. E., and Timkovich, R. (1975) Cytochromes *c*, In *The Enzymes, 3rd ed.* (Boyer, P. D., Ed.) 3rd ed., pp 397-547, Academic Press, New York.

(6) Pettigrew, G. W., and Moore, G. R. (1987) *Cytochromes c: Biological Aspects*, Springer-Verlag, New York.

(7) Hannibal, L., Tomasina, F., Capdevila, D. A., Demicheli, V., Tórtora, V., Alvarez-Paggi, D., Jemmerson, R., Murgida, D. H., and Radi, R. (2016) Alternative conformations of cytochrome *c*: structure, function and detection, *Biochemistry 55*, 407-428.

(8) Alvarez-Paggi, D., Hannibal, L., Castro, M. A., Oviedo-Rouco, S., Demicheli, V., Tórtora, V., Tomasina, F., Radi, R., and Murgida, D. H. (2017) Multifunctional cytochrome *c*: learning new tricks from an old dog, *Chem. Rev. 117*, 13382−13460.

(9) Kagan, V. E., Bayir, H. A., Belikova, N. A., Kapralov, O., Tyurina, Y. Y., Tyurin, V. A., Jiang, J., Stoyanovsky, D. A., Wipf, P., Kochanek, P. M., Greenberger, J. S., Pitt, B., Shvedova, A. A., and Borisenko, G. (2009) Cytochrome *c*/cardiolipin relations in mitochondria: a kiss of death, *Free Radical Biol. Med. 46*, 1439-1453.

(10) Kagan, V. E., Tyurin, V. A., Jiang, J., Tyurina, Y. Y., Ritov, V. B., Amoscato, A. A., Osipov, A. N., Belikova, N. A., Kapralov, A. A., Kini, V., Vlasova, I. I., Zhao, Q., Zou, M., Di, P., Svistunenko, D. A., Kurnikov, I. V., and Borisenko, G. G. (2005) Cytochrome *c* acts as a cardiolipin oxygenase required for release of proapoptotic factors, *Nat. Chem. Biol. 1*, 223-232.

(11) Purring-Koch, C., and McLendon, G. (2000) Cytochrome *c* binding to Apaf-1: The effects of dATP and ionic strength, *Proc. Natl. Acad. Sci. U.S.A. 97*, 11928-11931.

(12) Liu, X., Kim, C. N., Yang, J., Jemmerson, R., and Wang, X. (1996) Induction of apoptotic program in cell-free extracts: requirement for dATP and cytochrome *c*, *Cell 86*, 147-157.

(13) Jiang, X., and Wang, X. (2004) Cytochrome *c*-mediated apoptosis, *Annu. Rev. Biochem. 73*, 87-106.

(14) Rytömaa, M., and Kinnunen, P. K. J. (1994) Evidence for two distinct acidic phospholipid-binding sites in cytochrome *c*, *J. Biol. Chem. 269*, 1770-1774.

(15) Rytömaa, M., and Kinnunen, P. K. J. (1995) Reversibility of the binding of cytochrome *c* to liposomes, *J. Biol. Chem. 270*, 3197-3202.

(16) Tuominen, E. K. J., Zhu, K., Wallace, C. J. A., Clark-Lewis, I., Craig, D. B., Rytömaa, M., and Kinnunen, P. K. J. (2001) ATP Induces a conformational change in lipid-bound cytochrome *c*, *J. Biol. Chem. 276*, 19356–19362.

(17) Muenzner, J., and Pletneva, E. V. (2014) Structural transformations of cytochrome *c* upon interaction with cardiolipin, *Chem. Phys. Lipids 179*, 57-63.

(18) Hanske, J., Toffey, J. R., Morenz, A. M., Bonilla, A. J., Schiavoni, K. H., and Pletneva, E. V. (2012) Conformational properties of cardiolipin-bound cytochrome *c*, *Proc. Natl. Acad. Sci. U.S.A. 109*, 125-130.

(19) Hong, Y., Muenzner, J., Grimm, S. K., and Pletneva, E. V. (2012) Origin of the conformational heterogeneity of cardiolipin-bound cytochrome *c*, *J. Am. Chem. Soc. 134*, 18713-18723.

(20) Amacher, J. F., Zhong, F., Lisi, G. P., Zhu, M. Q., Alden, S. L., Hoke, K. R., Madden, D. R., and Pletneva, E. V. (2015) A compact structure of cytochrome *c* trapped in a lysine-ligated state: loop refolding and functional implications of a conformational switch, *J. Am. Chem. Soc. 137*, 8435-8449.

(21) Muenzner, J., Toffey, J. R., Hong, Y., and Pletneva, E. V. (2013) Becoming a peroxidase: cardiolipin-induced unfolding of cytochrome *c*, *J. Phys. Chem. B 112*, 12878-12886.

(22) Nantes, I. L., Zucchi, M. R., Nascimento, O. R., and Faljoni-Alario, A. (2001) Effect of heme iron valence state on the conformation of cytochrome *c* and its association with membrane interfaces - A CD and EPR investigation, *J. Biol. Chem. 276*, 153-158.

(23) Mandal, A., Hoop, C. L., DeLucia, M., Kodali, R., Kagan, V. E., Ahn, J., and van der Wel, P. C. A. (2015) Structural changes and proapoptotic peroxidase activity of cardiolipin-bound mitochondrial cytochrome *c*, *Biophys. J. 109*, 1873-1884.

(24) Heimburg, T., and Marsh, D. (1993) Investigation of secondary and tertiary structural-changes of cytochrome-*c* in complexes with anionic lipids using amide hydrogen-exchange measurements - an FTIR study, *Biophys. J. 65*, 2408-2417.

(25) Gorbenko, G. P., Molotkovsky, J. G., and Kinnunen, P. K. J. (2006) Cytochrome *c* interaction with cardiolipin/phosphatidylcholine model membranes: effect of cardiolipin protonation, *Biophys. J. 90*, 4093–4103.

(26) Pandiscia, L. A., and Schweitzer-Stenner, R. (2015) Coexistence of native-like and non-native partially unfolded ferricytochrome *c* on the surface of cardiolipin-containing liposomes, *J. Phys. Chem. B 119*, 1334-1349.

(27) Pandiscia, L. A., and Schweitzer-Stenner, R. (2015) Coexistence of native-like and non-native cytochrome *c* on anionic liposomes with different cardiolipin content, *J. Phys. Chem. B 119*, 12846-12859.

(28) Sinibaldi, F., Fiorucci, L., Patriarca, A., Lauceri, R., Ferri, T., Coletta, M., and Santucci, R. (2008) Insights into the cytochrome *c*-cardiolipin interaction. Role played by ionic strength, *Biochemistry 47*, 6928-6935.

(29) Sinibaldi, F., Howes, B. D., Droghetti, E., Polticelli, F., Piro, M. C., Di Pierro, D., Fiorucci, L., Coletta, M., Smulevich, G., and Santucci, R. (2013) Role of lysines in cytochrome *c*−cardiolipin interaction, *Biochemistry 52*, 4578−4588.

(30) Sinibaldi, F., Milazzo, L., Howes, B. D., Piro, M. C., Fiorucci, L., Polticelli, F., Ascenzi, P., Coletta, M., Smulevich, G., and Santucci, R. (2017) The key role played by charge in the interaction of cytochrome *c* with cardiolipin, *J. Biol. Inorg. Chem. 22*, 19–29.

(31) Kostrzewa, A., Páli, T., Froncisz, W., and Marsh, D. (2000) Membrane location of spin-labeled cytochrome *c* determined by paramagnetic relaxation reagents, *Biochemistry 39*, 6066-6074.

(32) Kawai, C., Prado, F. M., Nunes, G. L. C., Di Mascio, P., Carmona-Ribeiro, A. M., and Nantes, I. L. (2005) pH-dependent interaction of cytochrome *c* with mitochondrial mimetic membranes: the role of an array of positively charges amino acids, *J. Biol. Chem. 280*, 34709-34717.

(33) O'Brien, E. S., Nucci, N. V., Fuglestad, B., Tommos, C., and Wand, A. J. (2015) Defining the apoptotic trigger: the interaction of cytochrome *c* and cardiolipin, *J. Biol. Chem. 290*, 30879-30887.

(34) Rytömaa, M., Mustonen, P., and Kinnunen, P. K. J. (1992) Reversible, nonionic, and pH-dependent association of cytochrome *c* with cardiolipin-phosphatidylcholine liposomes, *J. Biol. Chem. 267*, 22243–22248.

(35) Tuominen, A. K. J., Wallace, C. J. A., and Kinnunen, P. K. J. (2002) Phospholipid-cytochrome *c* interaction: evidence for the extended lipid anchorage, *J. Biol. Chem. 277*, 8822-8826.

(36) Sinibaldi, F., Howes, B. D., Piro, M. C., Polticelli, F., Bombelli, C., Ferri, T., Coletta, M., Smulevich, G., and Santucci, R. (2010) Extended cardiolipin anchorage to cytochrome *c*: a model for protein-mitochondrial membrane binding, *J. Biol. Inorg. Chem. 15*, 689-700.

(37) Ascenzi, P., Polticelli, F., Marino, M., Santucci, R., and Coletta, M. (2011) Cardiolipin drives cytochrome *c* proapoptotic and antiapoptotic actions, *IUBMB Life 63*, 160-165.

(38) McClelland, L. J., Steele, H. B. B., Whitby, F. G., Mou, T.-C., Holley, D., Ross, J. B. A., Sprang, S. R., and Bowler, B. E. (2016) Cytochrome *c* can form a well-defined binding pocket for hydrocarbons, *J. Am. Chem. Soc. 138*, 16770–16778.

(39) Elmer-Dixon, M. M., and Bowler, B. E. (2017) Site A-mediated partial unfolding of cytochrome *c* on cardiolipin vesicles is species-dependent and does not require Lys72, *Biochemistry 56*, 4830−4839.

(40) Berghuis, A. M., and Brayer, G. D. (1992) Oxidation state-dependent conformational changes in cytochrome *c*, *J. Mol. Biol. 223*, 959-976.

(41) Duncan, M. G., Williams, M. D., and Bowler, B. E. (2009) Compressing the free energy range of substructure stabilities in iso-1-cytochrome *c*, *Protein Science 18*, 1155-1164.

(42) McClelland, L. J., Mou, T.-C., Jeakins-Cooley, M. E., Sprang, S. R., and Bowler, B. E. (2014) Structure of a mitochondrial cytochrome *c* conformer competent for peroxidase activity, *Proc. Natl. Acad. Sci. U.S.A. 111*, 6648-6653.

(43) McClelland, L. J., Seagraves, S. M., Khan, M. K. A., Cherney, M. M., Bandi, S., Culbertson, J. E., and Bowler, B. E. (2015) The response of Ω-loop D dynamics to truncation of trimethyllysine 72 of yeast iso-1-cytochrome *c* depends on the nature of loop deformation, *J. Biol. Inorg. Chem. 20*, 805-819.

(44) Cherney, M. M., Junior, C., and Bowler, B. E. (2013) Mutation of trimethyllysine-72 to alanine enhances His79-heme mediated dynamics of iso-1-cytochrome *c*, *Biochemistry 52*, 837-846.

(45) Margoliash, E., and Frohwirt, N. (1959) Spectrum of horse-heart cytochrome *c*, *Biochem. J. 71*, 570-572.

(46) Moore, G. R., and Pettigrew, G. W. (1990) *Cytochromes c: Evolutionary, Structural and Physicochemical Aspects*, Springer-Verlag, New York.

(47) Kristinsson, R., and Bowler, B. E. (2005) Communication of stabilizing energy between substructures of a protein, *Biochemistry 44*, 2349-2359.

(48) Pace, C. N., and Vanderburg, K. E. (1979) Determining globular protein stability: guanidine hydrochloride denaturation of myoglobin, *Biochemistry 18*, 288-292.

(49) McClelland, L. J., Seagraves, S. M., Khan, M. K. A., Cherney, M. M., Bandi, S., Culbertson, J. E., and Bowler, B. E. (2015) The response of Ω-loop D dynamics to truncation of trimethyllysine 72 of yeast iso-1-cytochrome c depends on the nature of loop deformation, *JBIC Journal of Biological Inorganic Chemistry 20*, 805-819.

(50) Cherney, M. M., Junior, C. C., Bergquist, B. B., and Bowler, B. E. (2013) Dynamics of the His79- heme alkaline transition of yeast iso- 1- cytochrome c probed by conformationally gated electron transfer with Co(II) bis(terpyridine), *Journal of the American Chemical Society 135*, 12772.

(51) Elmer-Dixon, M. M., and Bowler, B. E. (2017) Rapid quantification of cardiolipin and DOPC lipid and vesicle concentration, *Anal. Biochem. 520*, 58-61.

(52) Pollock, W. B., Rosell, F. I., Twitchett, M. B., Dumont, M. E., and Mauk, A. G. (1998) Bacterial expression of a mitochondrial cytochrome *c*. Trimethylation of Lys72 in yeast iso-1-cytochrome *c* and the alkaline conformational transition, *Biochemistry 37*, 6124-6131.

(53) Kostrzewa, A., Páli, T., Wojciech, F., and Marsh, D. (2000) Membrane location of spin-labeled cytochrome *c* determined by paramagnetic relaxation reagents, *Biochemistry 39*, 6066-6074.

(54) Rosell, F. I., Ferrer, J. C., and Mauk, A. G. (1998) Proton-linked protein conformational switching: definition of the alkaline conformational transition of yeast iso-1-ferricytochrome *c*, *J. Am. Chem. Soc. 120*, 11234-11245.

(55) Nelson, C. J., and Bowler, B. E. (2000) pH dependence of formation of a partially unfolded state of a Lys 73 -> His variant of iso-1-cytochrome *c*: implications for the alkaline conformational transition of cytochrome *c*, *Biochemistry 39*, 13584-13594.

(56) Rosell, F. I., Ferrer, J. C., and Mauk, A. G. (1998) Proton- linked protein conformational switching: definition of the alkaline conformational transition of yeast iso- 1-ferricytochrome c, *Journal of the American Chemical Society 120*, 11234.

(57) Santucci, R., Bongiovanni, C., Mei, G., Ferri, T., Polizio, F., and Desideri, A. (2000) Anion size modulates the structure of the a state of cytochrome c, *Biochemistry 39*, 12632-12638.

(58) Soffer, J. B., Fradkin, E., Pandiscia, L. A., and Schweitzer-Stenner, R. (2013) The (not completely irreversible) population of a misfolded state of cytochrome c under folding conditions, *Biochemistry 52*, 1397.

(59) Pielak, G. J., Oikawa, K., Mauk, A. G., Smith, M., and Kay, C. M. (1986) Elimination of the native Soret Cotton effect of cytochrome *c* by replacement of the invariant phenylalanine using site-directed mutagenesis, *J. Am. Chem. Soc. 108*, 2724-2727.

(60) Dragomir, I., Hagarman, A., Wallace, C., and Schweitzer-Stenner, R. (2007) Optical band splitting in cytochrome *c* at room temperature probed by visible electronic circular dichroism spectroscopy, *Biophys. J. 92*, 989-998.

(61) Tsong, T. Y. (1974) The Trp-59 fluorescence of ferricytochrome *c* as a sensitive measure of the over-all protein conformation, *J. Biol. Chem. 249*, 1988-1990.

(62) Pinheiro, T. J. T., Elöve, G. A., Watts, A., and Roder, H. (1997) Structural and kinetic description of cytochrome *c* unfolding induced by the interaction with lipid vesicles, *Biochemistry 36*, 13122-13132.

(63) Davies, A. M., Guillemette, J. G., Smith, M., Greenwood, C., Thurgood, A. G., Mauk, A. G., and Moore, G. R. (1993) Redesign of the interior hydrophilic region of mitochondrial cytochrome c by site-directed mutagenesis, *Biochemistry 32*, 5431-5435.

(64) Santucci, R., and Ascoli, F. (1997) The Soret circular dichroism spectrum as a probe for the heme Fe(III)-Met(80) axial bond in horse cytochrome *c*, *J. Inorg. Biochem. 68*, 211–214.

(65) Hagarman, A., Duitch, L., and Schweitzer-Stenner, R. (2008) The conformational manifold of ferricytochrome *c* explored by visible and far-UV electronic circular dichroism spectroscopy, *Biochemistry 47*, 9667-9677.

(66) Burstein, E. A., Vedenkina, N. S., and Ivkova, M. N. (1973) Fluorescence and the location of tryptophan residues in protein molecules, *Photochem. Photobiol. 18*, 263-279.

(67) Sinibaldi, F., Droghetti, E., Polticelli, F., Piro, M. C., Di Pierro, D., Ferri, T., Smulevich, G., and Santucci, R. (2011) The effects of ATP and sodium chloride on the cytochrome *c*–cardiolipin interaction: The contrasting behavior of the horse heart and yeast proteins, *J. Inorg. Biochem. 105*, 1365-1372.

(68) Karsisiotis, A. I., Deacon, O. M., Wilson, M. T., Macdonald, C., Blumenschein, T. M. A., Moore, G. R., and Worrall, J. A. R. (2016) Increased dynamics in the 40–57 Ω-loop of the G41S variant of human cytochrome *c* promote its pro-apoptotic conformation, *Sci. Rep. 6*, 30447.

(69) Deacon, O. M., Karsisiotis, A. I., Moreno-Chicano, T., Hough, M. A., Macdonald, C., Blumenschein, T. M. A., Wilson, M. T., Moore, G. R., and Worrall, J. A. R. (2017) Heightened dynamics of the oxidized Y48H variant of human cytochrome *c* increases its peroxidatic activity, *Biochemistry 56*, 6111-6124.

CHAPTER 5: Consequences of Cardiolipin Lipid Partitioning in Mixed Membrane Systems

5.1. INTRODUCTION

Lipid bilayers provide both a barrier for containment and exclusion of cellular components as well as a platform for protein interactions required for cell signaling. Not all bilayers are created equal and their composition varies greatly based on cellular location and functionality.[1] Membrane lipid composition is responsible for a host of lipid-protein interactions with both local and far reaching consequences.[2] Understanding the dynamics of mixed lipid bilayers and their impact on lipid-protein binding is essential for understanding their role in regulatory processes.

Cardiolipin (CL) is a structurally unique phospholipid that plays a pivotal role in the initial stages of apoptosis,[3,4] CL's structural characteristics could have a dramatic impact on its function in the mitochondria with overarching consequences that affect the entire cell. Most studies on the properties of CL and its interactions with proteins are carried out with 1',3'-bis[1,2-dioleoyl-*sn*-glyvero-3-phospho]-*sn*-glycerol (TOCL). With four mono-unsaturated acyl chains and two phosphate groups comprising its headgroup, TOCL has a classic inverted cone or type-2 lipid structure typical for lipids that tend to pack on concave surfaces.[1]

CL is synthesized in the matrix and is inserted into the concave surface of the inner leaflet of the inner mitochondrial membrane.[3,5,6] Here, it has many important roles from facilitating an ion gradient and tethering electron transport constituents to functioning as an apoptotic trigger.[5] Recent work shows that the electron transport chain electron shuttle, cytochrome *c* (Cyt*c*), oxidizes CL, causing dissociation of the Cyt*c*-CL complex, and thus facilitating the exit of Cyt*c* from mitochondria into the cytoplasm.[6] In the cytoplasm, Cyt*c* binds to apoptotic protease activating factor 1 (Apaf-1) causing the formation of the apoptosome, which initiates

apoptosis.[3,6] Both before and since the discovery of the role of Cyt*c* as a peroxidase that oxygenates CL in the earliest stages of apoptosis, considerable efforts has been directed at characterizing Cyt*c*-CL binding. A vast array of techniques and mimetic membrane systems has been employed to investigate Cyt*c*-CL binding in vitro. Both pure CL[7–9] and mixed lipid systems[6,10,19–22,11–18] modeling the content of CL in the IMM have been used extensively to characterize how Cyt*c* docks to CL producing a conformer of Cytc that can oxidize CL.

Four potential lipid binding sites on the surface of Cyt*c* have been described in the literature, the anionic (A-site),[10,13,23] the hydrophobic cardiolipin binding site which may involve hydrogen bonding to Asn52 (C-site),[10,13] the histidine rich, hydrogen bonding L-site[24] and the novel site (N site).[25] These four sites may work independently or in concert to dock CL and facilitate its oxidation at the peroxidase active site of a non-native conformer of Cyt*c*.[3,4,26–32,6,7,9,11,12,14,18,20] Mixed lipid systems using liposomes comprised of 20-50% CL have often been employed to study this interaction.[6,10,33,11,14,16,18–22] Lipid binding in these experiments has been investigated solely on the exterior of the liposomes. CL composition is generally offset with the neutral cylindrically shaped lipid 1,2-dioleoyl-*sn*-glycero-3-phosphocholine (DOPC) in these systems.[1] Given that the results of the various binding studies do not agree quantitatively, it is important to understand if partitioning of CL to the inner versus the outer leaflet of liposomes could be affecting the differing results observed with different model systems and different methods of vesicle preparation.

This paper elucidates the nature of two mixed membrane systems commonly used to characterize Cyt*c* binding to membranes by (1) evaluating the leaflet-dependent distribution of CL and DOPG in mixed lipid vesicles, (2) assessing potential anionic, headgroup-governed,

partitioning and (3) applying our findings on inner versus out leaflet CL distribution to Cyt*c* binding studies to evaluate the effect of CL partitioning on Cyt*c*-CL binding.

5.2. EXPERIMENTAL METHODS

5.2.1. Materials.

Cardiolipin (1',3'-bis[1,2-dioleoyl-*sn*-glycero-3-phospho]-*sn*-glycerol, TOCL), DOPC (1,2-dioleoyl-*sn*-glycero-3-phosphocholine), and DOPG (1,2-dioleoyl-*sn*-glycero-3-phospho-(1'-*rac*-glycerol) were purchased from Avanti Polar Lipids, Inc., Alabaster AL and used in vesicle formation without additional purification.

5.2.2. Preparation of 1,1,2,2,-tetrakis[4-(2-trimethylammonioethoxy)phenyl]ethene (TTAPE-Me).

TTAPE-Me was synthesized following previously reported methods.[34,35] Briefly, 3.0 g of 4,4' dihydroxybenzophenone (Sigma Aldrich), 5.0 g potassium carbonate (Sigma Aldrich), 4 mL 1,2 dibromoethane and 50 mL acetone were combined in a round bottom flask and refluxed overnight. Thin layer chromatography (TLC, 75% ethyl acetate in hexanes) was used to verify quantitative conversion of benzophenone to 4,4′-bis(2-bromoethoxy) benzophenone (BBEBP). The identity of BBEBP was verified via gas chromatography coupled to mass spectroscopy. 0.56 g of BBEBP, 28 ml of tetrahydrofuran, 0.146 mL of titanium tetrachloride (Sigma) and 0.168 g of zinc dust were combined in a round bottom and refluxed overnight. Conversion of BBEBP to 1,1,2,2-tetrakis[4-(2-bromoethoxy)phenyl]ethene (TBEPE) was verified by thin layer chromatography. The ^{1}H NMR spectrum matched that reported previously for TBEPE.[34] 0.4 g TBEPE, 10 mL of tetrahydrofuran and 2.25 mL dimethyl amine were mixed for 45 minutes at

25˚C to form TTAPE-Me. Product was purified a silica gel column and then dried using rotovap. Successful production of TTAPE-Me was verified by ^{1}H and ^{13}C NMR. Observed spectra were consistent with previously reported NMR spectra.[34]

5.2.3. Vesicle Preparation.

Mixed lipid samples were prepared to the desired mole ratio by combining the appropriate volume of each lipid, based on the reported lipid concentration provided by the manufacturer (Avanti Polar Lipids, Inc, Alabaster AL), in a 1 dram vial, mixed and dried under nitrogen to remove chloroform. Samples were reconstituted to desired total lipid concentration using 20 mM TES buffer, 0.1 mM EDTA, pH 8. Lipids and buffer were gently mixed using a low speed vortexer for 1 minute and set in a warm bath at approximately 40˚C for 9 minutes; this mixing was repeated ten times. Samples were then subjected to a freeze/thaw/mixing (-60˚C/40˚C/25˚C) cycle five times to form vesicles. Vesicles were then extruded to 100 nm using an Avanti mini extruder outfitted with two 100 nm pore membranes. Samples were passed through the extruder 11 times to guarantee approximate vesicle size. Vesicle size was confirmed to be 100 ± 5 nm using dynamic light scattering measurements carried out in triplicate with a Malvern Zetasizer. When detecting-external lipid, TTAPE-Me was added to extruded vesicle samples in 40 – 80-fold molar excess. When detecting total lipid distribution, vesicles were formed in presence of fluorophore by reconstituting lipid with buffer containing 40 – 80-fold molar excess of TTAPE-Me relative to total lipid concentration. CL/DOPC samples were prepared to a total lipid concentration of 1.5 mM. DOPG/DOPC samples were prepared to a total lipid concentration of 3 mM. Mixed lipid samples at each mole fraction for both external TTAPE-Me exposure and total (inner and outer leaflet) TTAPE-Me exposure were prepared independently in triplicate.

5.2.4. TTAPE-Me Fluorescence Measurements.

A Perkin-Elmer LS55 Fluorescence Spectrometer was used to acquire fluorescence spectra. Samples were excited at 350 nm in a 4 mm x 4 mm Hellma fluorescence cuvette. Emitted light was passed through a 350 nm cutoff filter to eliminate excitation breakthrough. Sample emission was acquired from 370-600 nm with a 2.5 nm bandwidth and a scan rate of 100 nm/min.

5.2.5. TTAPE-Me and Vesicle Concentration Determination.

Using a Beckman-Coulter DU800 Spectrophotometer, UV-Visible spectra were acquired in triplicate from 300-450 nm for samples in a Hellma 10 mm microcuvette. TTAPE-Me concentration was approximated using absorbance at 350 nm (due to no reported extinction coefficient) to ensure that all samples had the same excess of fluorophore. Measurements at 400, 425, and 450 nm were used to evaluate lipid concentration by Mie scattering as TTAPE-Me has no appreciable absorbance in this region. DLS measurements (Malvern Zetasizer) and the UV-Visible measurements at 400, 425 and 450 nm were used to calculate the total lipid and vesicle concentration as well as the concentration of each constituent in the mixed lipid vesicle using previously reported methods based on Mie scattering.[36,37]

5.2.6. Protein Purification.

Wild type (WT) yeast iso-1-cytochrome *c* (iso-1-Cyt*c*) was expressed and purified from *Escherichia coli* BL21-DE3 cells following previously reported procedures[38,39]. Unlike, WT iso1-Cyt*c* expressed from its native host, *Saccharomyces cerevisiae*, the Lys72 of WT iso-1-Cyt*c* expressed from *E. coli* is not trimethylated.[40]

5.2.7. Cytochrome *c* cardiolipin/DOPC and DOPC vesicle titrations.

Cardiolipin/DOPC and DOPC binding titrations of WT iso-1-Cyt*c* were performed by a batch procedure. Vesicle samples were prepared and quantified immediately prior to the experiment, as described above. WT iso-1-Cyt*c* purified as described above was adjusted to twice the desired concentration. A set of vesicle samples was prepared at twice the desired lipid concentration for each step of the titration. WT iso-1-Cyt*c* and vesicle samples were mixed in 1:1 volume ratios generating a set of samples at the desired experimental concentration of protein and lipid for each step of the titration. Samples were gently mixed and incubated at room temperature for 30 minutes before spectroscopic measurements at 25 ^{o}C. Measurements at each lipid concentration were performed in triplicate with independently prepared samples.

5.2.8. Circular Dichroism Spectroscopy.

An Applied Photophysics Chirascan CD Spectrophotometer was used to acquire Soret CD measurements of iso-1-Cyt*c*/vesicle titration samples. The spectral region 450-350 nm was probed with samples in a Hellma 4x10mm Quartz cuvette, utilizing the 4 mm pathlength. Spectra were acquired at 25 ^{o}C in 1 nm step increments, with a 1.8 nm bandwidth, and a 3 s sampling time at each wavelength. Each spectrum was smoothed using a 6th order Savitsky-Golay filter smoothing technique. Spectra from three independent trials were averaged at each lipid concentration.

5.2.9. Cytochrome *c* Fluorescence Spectroscopy.

An Applied Photophysics Chirascan CD Spectrophotometer was adapted for scanning fluorescence measurements using a scanning emission monochromator (Applied Photophysics).

Samples were placed in a 5x5 mm Hellma fluorescence cuvette. Trp59 of iso-1-Cyt*c* was excited at 295 nm with a 5 nm bandwidth. Excitation bleed through was filtered out using a 305 nm cutoff filter (Newport Co.) placed in front of the detector. Emission spectra were acquired from 320-500 nm at 25°C with 1 nm step, a 2.5 nm bandwidth and a 0.5 sec acquisition time per step. Emission spectra from three independent trials were averaged at each lipid concentration.

5.2.10. Cytochrome *c* Absorbance Spectroscopy.

A Beckman-Coulter DU800 UV-Visible Spectrophotometer was used to acquire iso-1-Cyt*c* spectra in the presence of varying concentrations of lipid vesicles. Samples were placed in a 10 mm pathlength Hellma microcuvette and scanned from 200-800 nm with a 1 nm step, a 5 nm bandwidth and a scan rate of 400 nm/min.

5.2.11. Data Fitting.

Fits of CD and fluorescence data as a function of exposed (outer leaflet) lipid to protein ratio (LPR) were attempted using a one-site cooperative Langmuir-type equation (eqn. 5.1) where s(x) is the reported spectroscopic value at a given exposed (outer leaflet) LPR and

$$s(x) = \frac{s_o + s_1\left(\frac{x}{K_d(\text{app})}\right)^n}{1+\left(\frac{x}{K_d(\text{app})}\right)^n} \qquad \text{(eqn. 5.1.)}$$

s_o and s_1, represent the value of s(x) in the initial (no lipid) and final (lipid bound) states, respectively. The apparent dissociation constant K_d(app) corresponds to the requisite lipid to protein ratio to produce 50% bound protein and *n* is the corresponding Hill coefficient.

5.3. RESULTS AND DISCUSSION

5.3.1. TTAPE-Me Fluoresces in the Presence of both CL and DOPG.

To determine the role of the inverted cone structure of CL in mediating partitioning of CL to the inner versus the outer leaflet of vesicles studies, an important control is to evaluate whether DOPG, a negatively-charged cylindrical lipid, behaves differently. It is preferable to measure partitioning of the two lipids using the same method. In previous work, TTAPE-Me was shown to fluoresce strongly in the presence of CL-containing vesicles.[33] It was also shown that DOPC vesicles containing phosphatidylserine at levels found in the mitochondria (1%) did not produce a significant fluorescence in the presence of TTAPE-Me.[33] To be able to compare the partitioning of CL versus DOPG to the inner versus the outer leaflet of an extruded vesicle, we initially compared the relative enhancement of emission from TTAPE-Me in the presence of CL versus DOPG. As a control, we compared the effects of DOPC vesicles (headgroup has no net charge) on the fluorescence of TTAPE-Me. Because CL has approximately twice the headgroup surface area of DOPG, we carried out studies with DOPG (and DOPC) vesicles at twice the lipid concentration as for the CL vesicles to keep the available surface area of CL and DOPG available for TTAPE-Me binding the same as a function of mole fraction. Pure lipid vesicles at lipid concentrations of 1.5 mM for CL, 3 mM for DOPC and 3 mM for DOPG (Figure 5.1) were exposed to excess TTAPE-Me. With excitation at 350 nm, TTAPE-Me has minimal fluorescence in the absence of lipid (Figure 5.1). In the presence of DOPC, no appreciable enhancement of fluorescence is detected (Figure 5.1). TTAPE-Me, therefore, does not report on the presence of DOPC. When exposed to pure CL vesicles, the fluorescence emission of TTAPE-Me is strongly enhanced with peak fluorescence at approximately 468 nm and a slight shoulder between 370-

400 nm (Figure 1). These findings are congruent with Leung et. al[34] who reported on TTAPE-Me as a probe for detecting CL. A similar enhancement in emission is observed for TTAPE-Me in the presence of pure DOPG vesicles with peak fluorescence at approximately 472 nm and a less prominent shoulder appearing between 370-400 nm compared to pure CL vesicles. Thus, TTAPE-Me exhibits enhanced fluorescence of similar magnitude in the presence of the anionic lipids CL and DOPG, with only minor differences in the emission spectra. These findings show that TTAPE-Me is capable of detecting the presence of anionic lipid but not does distinguish appreciably between different anionic lipid headgroups, at least for CL and DOPG.

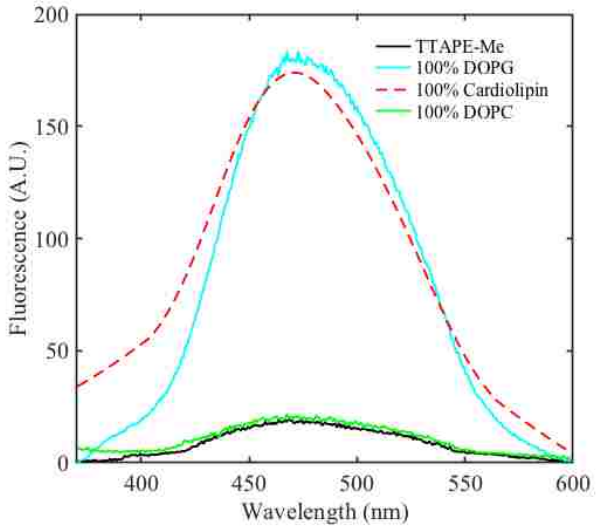

Figure 5.1. Emission spectra for free TTAPE-Me (black) added externally at 40 mM excess to vesicles in the presence of 100 nm pure vesicles of either 1.5 mM CL (red), 3 mM DOPC (green) and 3 mM DOPG (cyan) in 20 mM TES buffer, 0.1 mM EDTA at pH 8 and 25°C. Samples were excited at 350 nm with a bandwidth of 5 nm and emission was detected at 90° after passage through a 350 nm cutoff filter.

5.3.2. TTAPE-Me Detects DOPG on the Inner and Outer Leaflet of Vesicles.

The outer leaflets of vesicles at a constant concentration, but composed of varying mole fractions of DOPG and DOPC were exposed to excess TTAPE-Me and the fluorescence associated with the presence of DOPG was measured (Figure 5.2). Both the intensity at the peak of fluorescence and total fluorescence (area under the emission spectrum) increase linearly with respect to an increase in the mole fraction of DOPG (Figure 5.3,Left) demonstrating the ability of TTAPE-Me to quantitatively report the presence of DOPG. When DOPG/DOPC vesicles were formed in the presence of TTAPE-Me, exposing both leaflets to the fluorophore, the fluorescence also scaled linearly with the mole fraction of DOPG. However, the fluorescence was double that observed when only the outer leaflet was exposed to TTAPE-Me. This finding verifies that TTAPE-Me acts as a quantitative anionic lipid reporter for anionic lipid residing on both surfaces. Furthermore, this verifies that vesicle formation in the presence of TTAPE-Me permits detection of anionic lipid inside the vesicle. Black and gray trend lines have been added to figure 5.3 to demonstrate the approximate fluorescence reporter response expected for homogeneous lipid mixing with no preferential lipid partitioning to either the inner or outer leaflet of the vesicle. DOPG fluorescence reported using both peak fluorescence intensity at 460 nm and total fluorescence follow this trend closely strongly suggesting that DOPG has no preferential partitioning on the vesicle surface. This observation is congruent with the expected behavior of DOPG, which is a cylindrical lipid with no preference for leaflet curvature. These findings also suggest that there is no headgroup governed partitioning to a preferred curved surface for this system.

When reported fluorescence from outer leaflet exposure is compared to reported fluorescence for total vesicle exposure for each mole fraction of DOPG, it is evident that approximately 50%

of the total fluorescence is generated by the outer leaflet throughout the titration (Figure 5.3, Right). Half of the DOPG population is consistently reported on the outer leaflet leading to the conclusion that there is no preferential localization of DOPG on one specific leaflet.

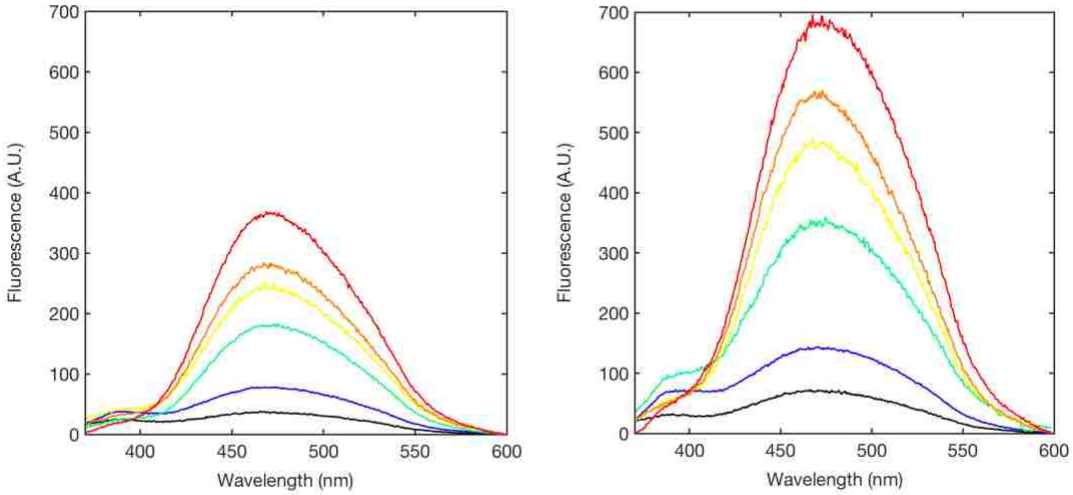

Figure 5.2. Raw TTAPE-Me fluorescence data corresponding to exposure to 100 nm DOPG/DOPC vesicles at 3 mM total lipid concentration composed of varying mole percent of DOPG (10%(Black), 20%(Dark Blue), 40%(Teal), 50%(Cyan), 70%(Yellow), 80%(Orange), and 100% (Red)). Data were acquired in 20 mM TES, 0.1 mM EDTA, at pH 8 and 25 ^{o}C. Left panel: only outer leaflet is exposed to excess TTAPE-Me. Right panel: both leaflets are exposed to excess TTAPE-Me.

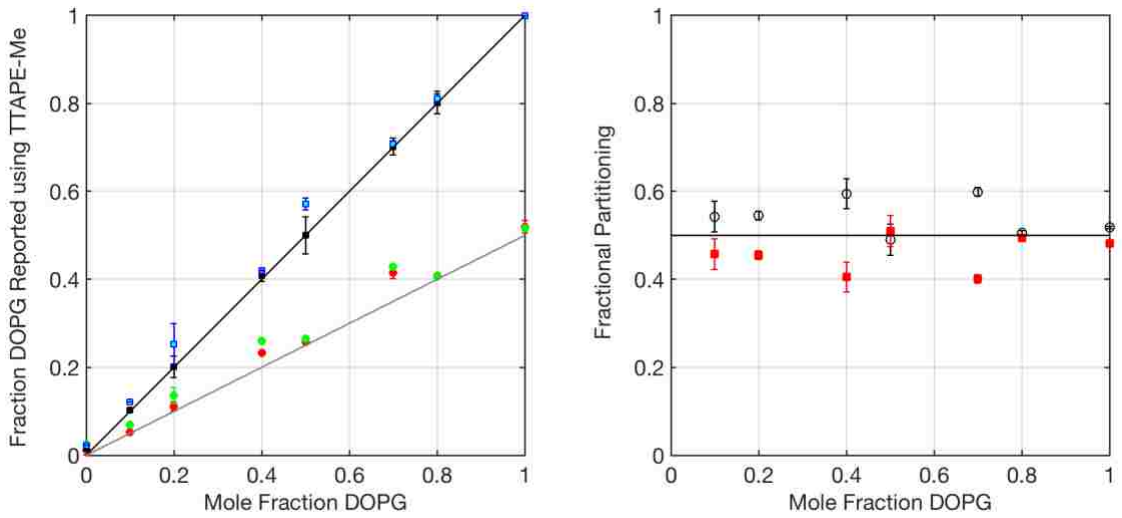

Figure 5.3. LEFT: Fraction of total DOPG reported by TTAPE-Me fluorescence at various mole fractions of DOPG, using the pure DOPG vesicles exposed to TTAPE-Me on both leaflets as the reference state. For samples exposed to TTAPE-Me on the outer leaflet, fluorescence peak intensity is shown with solid green circles and total integrated fluorescence emission with solid red circles. For samples exposed to TTAPE-Me on both the inner and outer leaflets, fluorescence peak intensity is shown with solid black squares and total integrated fluorescence emission with solid cyan squares. The solid black line shows the predicted linear dependence of fluorescence of homogeneously mixed DOPG/DOPC vesicles as a function of DOPG mole fraction when exposed to TTAPE-Me on both the inner and outer leaflets. The dashed gray line shows the predicted linear dependence of fluorescence of homogeneously mixed DOPG/DOPC vesicle as a function of DOPG mole fraction when exposed to TTAPE-Me on outer leaflet only. Error bars are the standard deviation derived from data for peak intensity or total fluorescence from 3 independent trials. **RIGHT:** Fraction of DOPG detected on the outer leaflet with respect to total DOPG detected on both the inner and outer leaflets by TTAPE-Me fluorescence as a function of DOPG mole fraction for DOPG/DOPC vesicles. Solid red squares use peak fluorescence

intensity of TTAPE-Me and empty black squares use total fluorescence emission of TTAPE-Me. The solid black line represents the ratio of 0.5 expected at all mole fractions for homogeneously mixed DOPG/DOPC vesicles with no preferential partitioning of the DOPG. Error bars are the standard deviation derived from data for peak intensity or total fluorescence from 3 independent trials.

5.3.3. TTAPE-Me Detects Cardiolipin on the Inner and Outer Leaflet of Vesicles.

The inner and outer leaflets of vesicles composed of varying mole fractions of CL and DOPC were exposed to excess TTAPE-Me and fluorescence associated with the presence of CL was measured (Figure 5.4). Both peak fluorescence intensity and total fluorescence increase linearly with respect to an increase in the mole fraction of CL in the vesicles when excess TTAPE-Me is present both inside and outside the vesicles (Figure 5.5, Left). A solid black line illustrates the expected linear dependence of fluorescence on the mole fraction of CL in the CL/DOPC vesicles. The close adherence of the observed data to the expected linear dependence on mole fraction of CL illustrates the ability of TTAPE-Me to report on total CL concentration, similar to its ability to quantify mitochondria based on its binding to CL.[33] By contrast, the fluorescence corresponding to external CL (Figure 5.5,Left) systematically falls below the theoretical trend line (gray dashed line) representing predicted external fluorescence for a homogeneously mixed lipid with no preferential partitioning to the inner concave surface of the vesicle. This observation is more clearly illustrated when the fluorescence of CL/DOPC vesicles only exposed to TTAPE-Me on the outer leaflet is compared to the fluorescence of CL/DOPC vesicle with excess TTAPE-Me available both inside and outside the vesicles (Figure 5.5, Right). When TTAPE-Me is only available on the outer leaflet of the vesicles, the amount of CL reported by TTAPE-Me is always considerably less than 50% of the TTAPE-Me fluorescence when TTAPE-Me is available to both the inner and outer leaflets of the vesicles, except when the mole fraction of CL is 1. Such deviations could result if the CL containing vesicles are not unilamellar. Transmission electron microscopy confirms that CL vesicles prepared by extrusion are unilamellar (Figure 5.6). Thus, our data show that for mixed lipid systems when CL is doped into DOPC bilayers, CL preferentially localizes on the concave inner leaflet of the vesicles. For

mixed CL/DOPC vesicles with a CL mole fraction of 0.5 or less, the fraction of the total CL that partition to the outer leaflet is ~0.2 (Figure 5.5, Right). This fractional partitioning indicates a 5:1 preference for the concave inner leaflet because of the inverted conical structure of CL.

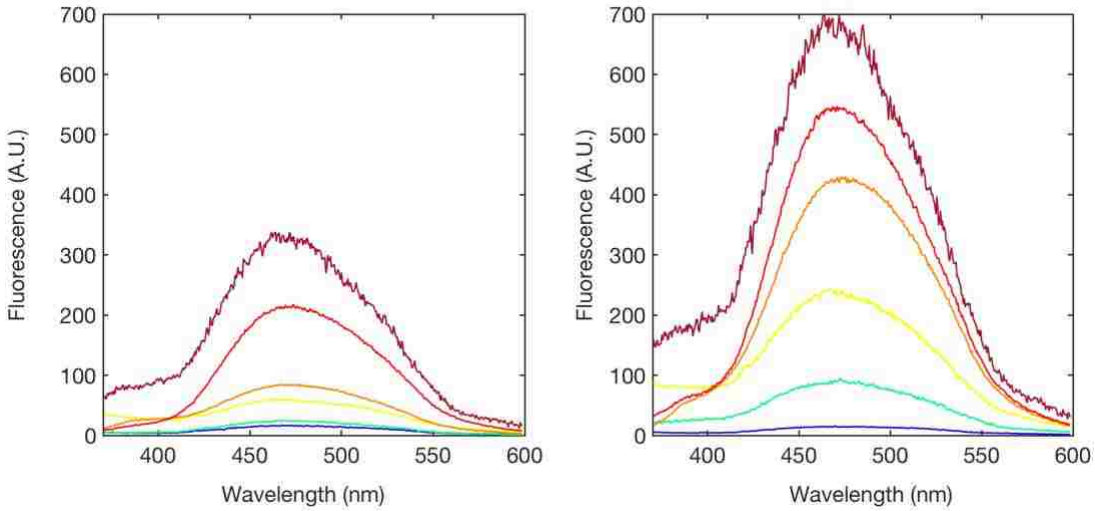

Figure 5.4. Raw TTAPE-Me fluorescence corresponding to exposure to 100 nm CL/DPOPC vesicles at 1.5 mM total lipid concentration composed of varying mole percent of CL (0% (Blue), 12%(Green), 34%(Yellow), 50%(Orange), 75%(Red), and 100%(Maroon)). Data were acquired in 20 mM TES, 0.1 mM EDTA, at pH 8 and 25 ^{o}C. Left panel: only outer leaflet is exposed to excess TTAPE-Me. Right panel: both leaflets are exposed to excess TTAPE-Me.

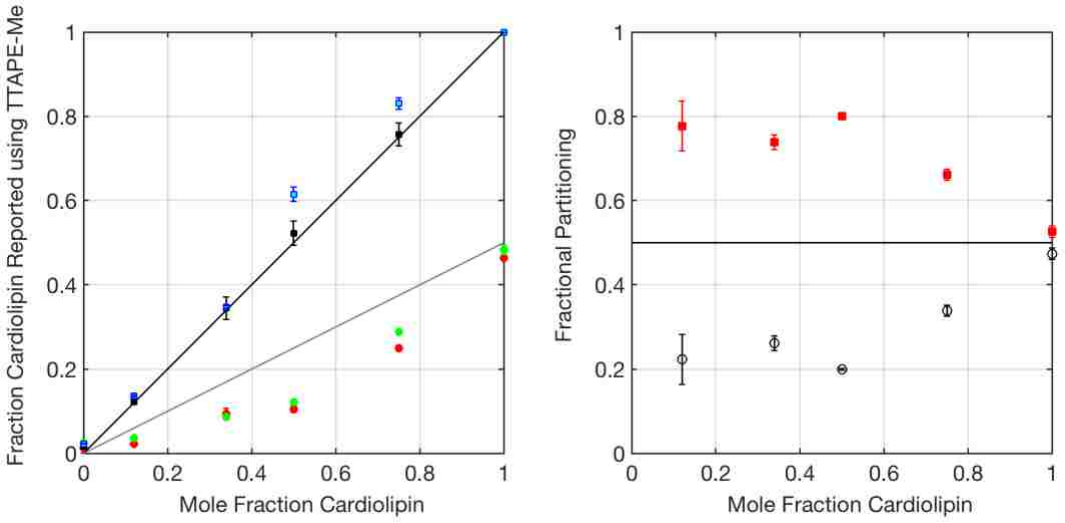

Figure 5.5. LEFT: Fraction of total CL reported at various mole fractions of CL by TTAPE-Me fluorescence, using the pure CL vesicles exposed to TTAPE-Me on both leaflets as the reference state. For samples exposed to TTAPE-Me on the outer leaflet, data fluorescence peak intensity are shown with solid green circles and data for total integrated fluorescence emission with solid red circles. For samples exposed to TTAPE-Me on both the inner and outer leaflets, fluorescence peak intensity data are shown with solid black circles and total integrated fluorescence emission data with solid cyan circles. The solid black line shows the predicted linear dependence of fluorescence of homogeneously mixed CL/DOPC vesicles as a function of CL mole fraction when exposed to TTAPE-Me on both the inner and outer leaflets. The dashed gray line shows the predicted linear dependence of fluorescence of homogeneously mixed CL/DOPC vesicle as a function of CL mole fraction when exposed to TTAPE-Me on the outer leaflet only. Error bars are the standard deviation derived from data for peak intensity or total fluorescence from 3 independent trials. **RIGHT:** Fraction of CL detected on the outer leaflet with respect to total CL detected on both the inner and outer leaflets by TTAPE-Me fluorescence as a function of CL mole fraction for CL/DOPC vesicles. Solid red squares use peak fluorescence intensity of

TTAPE-Me and empty black circles use total fluorescence emission of TTAPE-Me. The solid black line represents the ratio of 0.5 expected at all mole fractions for homogeneously mixed CL/DOPC vesicles with no preferential partitioning of the CL. Error bars are the standard deviation derived from data for peak intensity or total fluorescence from 3 independent trials.

Figure 5.6. Transmission electron microscopy image of 100% Cardiolipin vesicles extruded to 100 nm.

5.3.4. Cardiolipin Addition to DOPC Vesicles Induces Asymmetric Lipid Distribution but DOPG Does Not.

Measurement of TTAPE-Me fluorescence induced by DOPG in mixed DOPG/DOPC vesicles demonstrates that headgroup charge interactions per se do not cause asymmetric distribution of DOPG to the inner versus the outer leaflet when it is mixed with another cylindrically-shaped lipid. Roke and colleagues showed that vesicles containing phosphatidylserine and DOPC also do not generate asymmetric distributions of lipids between leaflets.[41] DOPG and DOPC have been shown to form charged domains laterally in a leaflet[42] but not between leaflets. Further, Tian and Baumgart showed that sorting of cylindrically-shaped lipids as a function of membrane curvature does not occur.[43] We also find no evidence of lipid partitioning between leaflets in our samples containing varying mole fractions of DOPG mixed with DOPC. DOPC appears to have no preferential localization, nor does it drive asymmetric lipid distribution. This is to be expected based on the findings of Roke and colleagues and Tian and Baumgart. Techniques employed here could not resolve phase separation in each leaflet.

Our studies on CL/DOPC show that CL preferentially partitions to the inner leaflet of a mixed lipid membrane. Neglecting potential headgroup interactions, CL's inverted cone shape alone predicts a preferred asymmetric distribution to concave surfaces.[44] Sorre et. al showed that DOPC can be sorted into a preferred bilayer as needed based on local environmental criteria.[45] Here, the structure of CL provides the needed packing instability required to drive DOPC to the outer leaflet while CL sorts preferentially onto the concave interior surface of the vesicle.

5.3.5. External Cytochrome *c* Binding to 100% DOPC Vesicles Demonstrates No Significant Protein-Lipid Binding.

Vesicles and liposomes are often prepared with varying concentrations of neutral DOPC when investigating Cyt*c* binding to CL.[6,10,20,22,11–14,16–19] To fully understand the role of lipid partitioning to binding of Cyt*c* in mixed lipid systems, wild type (WT) yeast iso-1-cytochrome *c* (iso-1-Cyt*c*) binding to DOPC was investigated. Because the headgroup of DOPC is neutral and the headgroup of CL carries two negative charge we use solution conditions that select for electrostatic binding to the A-site, namely a pH 8 buffer that suppresses binding at the L- and C-sites.[7] Specifically, electrostatic binding at the A-site of iso-1-Cyt*c* was investigated by titrating in varying concentrations of 100 nm pure DOPC vesicles in 20 mM TES buffer, 0.1 mM EDTA at pH 8. Binding was investigated using both the Soret CD and Trp59 fluorescence signals of iso-1-Cyt*c* during a DOPC vesicle titration (Figure 5.7). The Soret CD signal monitors the heme environment of iso-1-Cyt*c*. The heme is the known site of peroxidase activity in the protein and interactions at the heme have been directly linked to cardiolipin binding.[7,16,46] The Soret CD showed no appreciable change over the course of the titration implying that the structural rearrangement around the heme of iso-1-Cyt*c* that normally occurs when Cyt*c* binds to CL membranes does not occurs for extruded 20% CL/80% DOPC vesicles. A plot of the difference in the intensity of the positive maximum and negative minimum of the Soret CD spectrum, $\Delta\Delta\varepsilon$, also shows no significant change over the course of the titration further verifying a lack of lipid-induced heme rearrangement and thus binding of Cyt*c* to the DOPC vesicles (Figure 5.7).

Trp59 fluorescence has been used to investigate partial unfolding of the protein upon lipid interaction.[7,33] Lipid induced protein unfolding typically leads to an increase in Trp59 fluorescence. However, fluorescence did not increase when Cyt*c* was exposed to 100% DOPC

vesicles over a large range of exposed (outer leaflet) lipid to protein ration (LPR) (Figure 5.7). An analysis of the intensity of the peak of fluorescence over the range of the titration shows no significant change due to exposure to DOPC vesicles. Thus, DOPC vesicles do not induce partial unfolding of Cyt*c*, as detected by Trp59 fluorescence, a signature for binding of Cyt*c* to membrane surfaces. This finding is in accordance with previous studies that demonstrate Cyt*c*'s preferential binding to anionic lipid headgroups.[16]

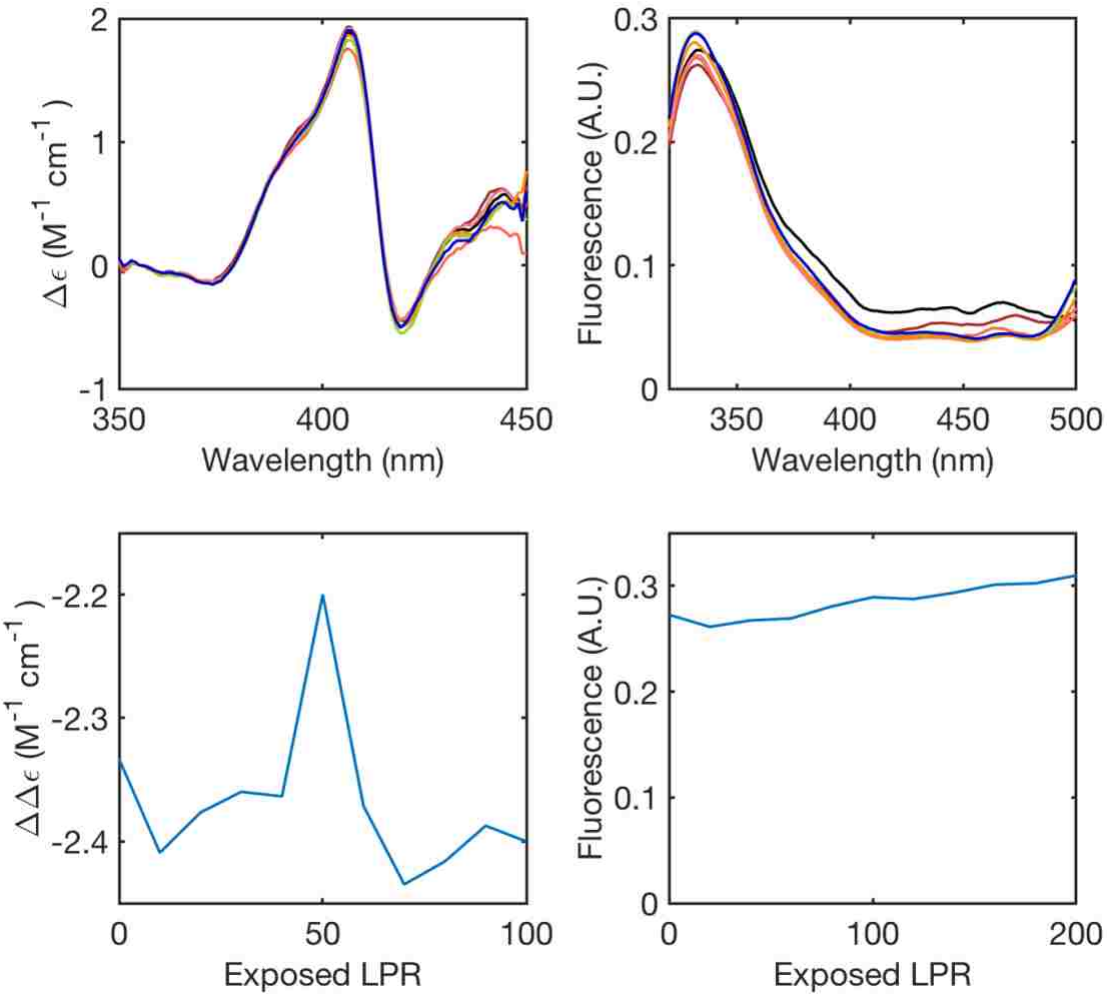

Figure 5.7. Titration of yeast iso-1-Cyt*c* with 100 nm 100% DOPC vesicles in 20 mM TES, 0.1 mM EDTA at pH 8 and 25 ˚C monitored by Soret CD (top left) and Trp59 fluorescence (top right). Soret CD amplitude ($\Delta\Delta\varepsilon = \Delta\varepsilon_{max} - \Delta\varepsilon_{min}$) plotted as a function of exposed lipid to protein ratio (LPR, bottom left). Trp59 fluorescence intensity at 331 nm plotted as a function of exposed LPR (bottom right).

5.3.6. Titration of Cyt*c* with 20% CL/80% DOPC Vesicles Demonstrates Minimal Protein-Lipid Binding.

20% CL:80% DOPC vesicles are commonly used to investigate CL binding to Cyt*c* [12,14,16,21,47] because CL represents 20% of the lipid content of mitochondria.[48] Both Soret CD and Trp59 fluorescence have been used in these studies to monitor binding of mixed lipid vesicles to Cyt*c*. Previous studies have been carried out at lower pH where the C- and L-sites also contribute to binding. At pH 8, where binding of iso-1-Cyt*c* is limited to the A-site,[7] a plot of the difference in the intensity of the positive maximum and negative minimum of the Soret CD spectrum, $\Delta\Delta\varepsilon$, does not change over the course of the titration of WT yeast iso-1-Cyt*c* with 20% CL/80% DOPC vesicles (Figure 5.8). Likewise, Trp59 fluorescence does not show the increase in intensity normally observed for partial unfolding of iso-1-Cyt*c* typically associated with binding of iso-1-Cyt*c* to CL-containing vesicles (Figure 5.8). Tracking the fluorescence intensity over the course of the titration at the emission maximum confirms the lack of a significant interaction of iso-1-Cyt*c* with 20% CL/80% DOPG via the A-site at pH 8 (Figure 5.8). Thus, neither local structural rearrangement around the heme (Soret CD), nor partial unfolding of iso-1-Cyt*c* (Trp59 fluorescence) occur when iso-1-Cyt*c* is titrated with 20% CL/80% DOPC vesicles at pH 8.

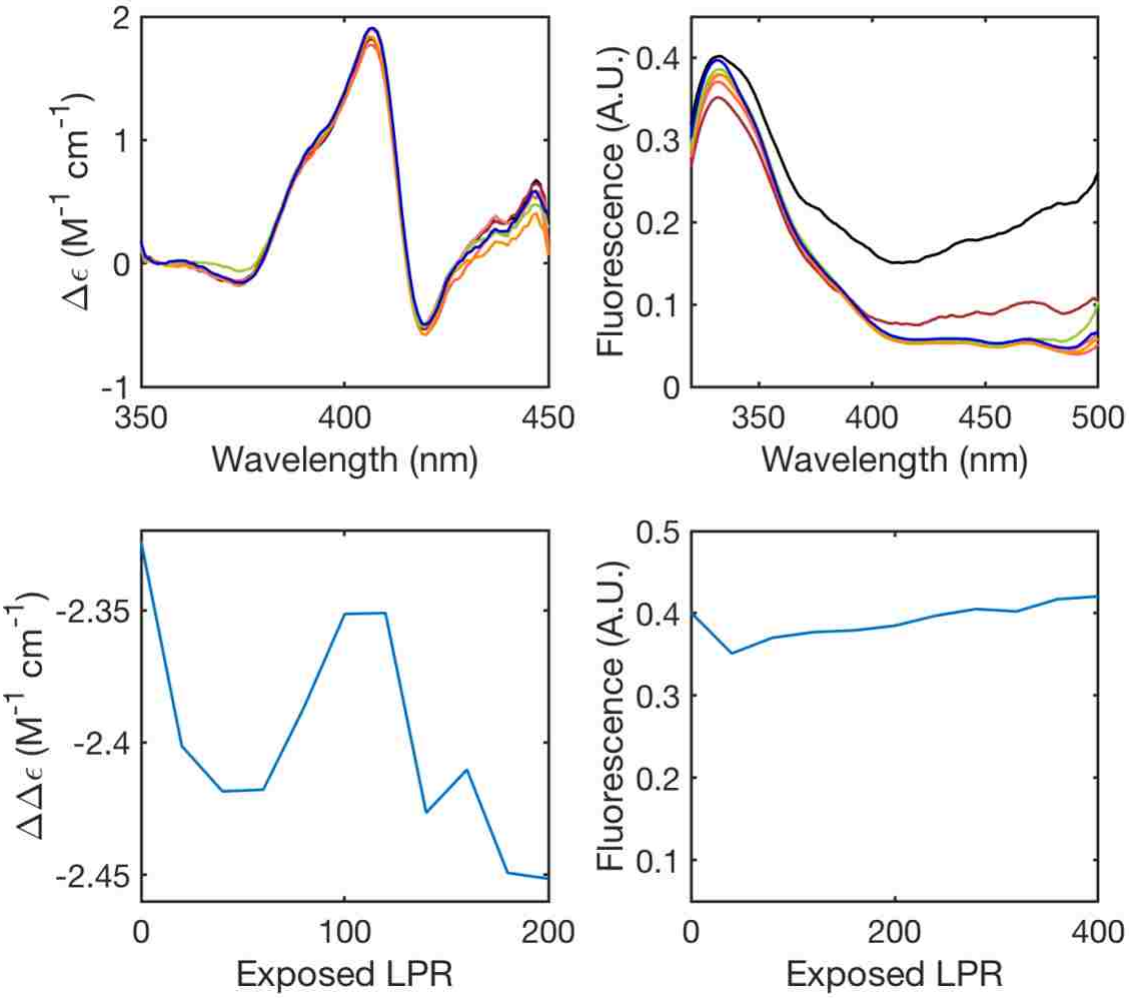

Figure 5.8. Titration of iso-1-Cyt*c* with 100 nm 20% CL/80% DOPC vesicles in 20 mM TES, 0.1 mM EDTA at pH 8 and 25 ˚C monitored using Soret CD (top left) and Trp59 fluorescence (top right). CD amplitude ($\Delta\Delta\varepsilon = \Delta\varepsilon_{max} - \Delta\varepsilon_{min}$) plotted as a function of exposed LPR (bottom left). Fluorescence intensity at 331 nm plotted as a function of exposed LPR (bottom right).

5.3.7. 100% DOPC and 20% CL/80% DOPC Do Not Illicit Electrostatic Cytochrome *c* Binding at pH 8 via the A-site.

Previous work investigating binding binding to 100% CL vesicles the A-site of Cyt*c* did showed a significant change in both the Soret CD and Trp59 fluorescence for yeast iso-1-Cyt*c*[7] (see Figure 5.8, lower panel). Using a one-site cooperative binding model (eq 5.1), Soret CD reported a K_d(app) of 10.2 in terms of exposed LPR and a cooperativity, n, of 2.2[7] and Trp59 fluorescence reported K_d(app) of 23.4 in terms of exposed LPR and n of 2.3[7] (solid curves in Figure 5.8, bottom panels). Attempts to fit the Soret CD and Trp59 fluorescence amplitudes to eq 5.1 failed for both 100% DOPC and 20% CL/80% DOPC vesicle binding at pH 8 in Figures 5.7 and 5.8. Thus, 100% DOPC and 20% CL/80% DOPC vesicles fail to induce electrostatic binding to the A-site of Cyt*c* at pH 8.

TTAPE-Me fluorescence studies show that CL/DOPC vesicles had approximately 20% of the total CL on the outside of the vesicle for CL mole fractions of 0.5 and below (Figure 3B). In the case of 20% CL/80% DOPC vesicles, 20% of the total concentration of CL on the outside corresponds to the mole fraction of only 0.04 CL on the outer leaflet. Thus, the range of exposed LPR in terms of CL concentration effectively covers the range 0 – 4 rather than 0 – 100 (0 – 20 in terms of CL concentration) for the Soret CD-monitored titrations (Figure 4) and 0 – 8 rather than 0 – 200 (0 – 40 in terms of CL concentration) in the case of the Trp59 fluorescence-monitored titrations (Figure 5.8). Given that the K_d(app) for Soret CD is ~10 in terms of exposed LPR and Trp59 fluorescence is ~23 in terms of exposed LPR for 100% CL vesicles it is not surprising that no significant binding is observed. As there will be an entropic penalty for demixing in the mixed lipid system,[49] the necessary K_d(app) is probably even higher than those observed for pure CL vesicles. Thus, it is not surprising that no binding is observed under our

conditions because of the preferential partitioning of CL to the inner leaflet of extruded vesicles. To elucidate the apparent dissociation constant corresponding to electrostatic binding it would be necessary to go to much higher exposed LPR, which would be impractical in our system. Because of this, a mixed lipid system where CL may not distribute evenly on both leaflets, may not be ideal for investigating quantitative Cyt*c* binding.

5.3.8. 100% DOPC Vesicles Do Not Illicit Electrostatic Cytochrome *c* Binding at pH 7 but 20% CL/80% DOPC Vesicles Do Facilitate Binding.

Previous work showed that 100% CL vesicles induce scattering in the presence of WT iso-1-Cyt*c* at pH 7.[7] This scattering was attributed to CL binding to multiple binding sites on Cyt*c*, notably the electrostatic A-site, and hydrogen bonding L-site.[24] Binding of vesicles to multiple sites on Cyt*c* induces large supramolecular structures of vesicles crosslinked by Cyt*c* that enhance scattering in the UV-Visible spectral region. DOPC and 20% CL/80% DOPC vesicle binding to Cyt*c* was evaluated at pH 7 using UV-Visible spectroscopy to determine if enhanced scattering due to formation of supramolecular structures occurs over the course of vesicle titrations of iso-1-Cyt*c* (Figure 5.9). No appreciable scattering off of DOPC and 20% CL/80% DOPC vesicles beyond the expected concentration-dependent scattering off the vesicles themselves[36,37] occurs during vesicles titrations of WT iso-1-Cyt*c*. The lack of scattering off of DOPC vesicles at pH 7 verifies the lack of affinity Cyt*c* has for DOPC. This finding is consistent with the lack of binding detected for DOPC vesicles at pH 8 (Figure 5.7). The lack of scattering off of 20% CL/80% DOPC vesicles (Figure 5.9) suggests CL may not be sufficiently present in the outer leaflet to induce crosslinking of vesicles. This finding is congruent with TTAPE-Me

detecting less CL on the outer leaflet of CL/DOPC vesicles than expected for unbiased partitioning of CL to the inner versus the outer leaflet of 100 nm vesicles.

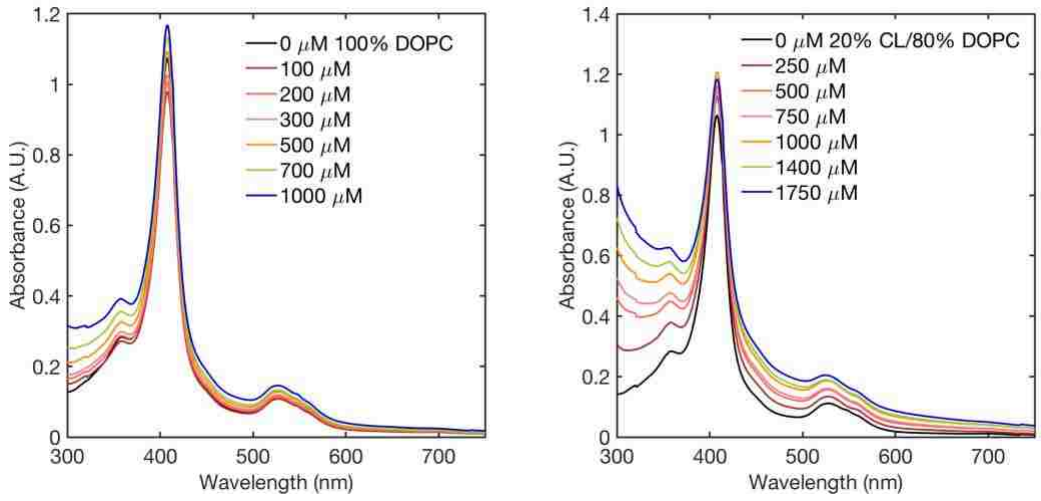

Figure 5.9. UV-Visible spectra of 100 nm DOPC (Left) and 20% CL/80% DOPC (Right) vesicles as a function of total lipid concentration in the presence of 10 μM yeast iso-1-Cyt*c* in 20 mM TES, 0.1 mM EDTA, at pH 7 and 25 °C.

Stronger binding of Cyt*c* to cardiolipin binding has been detected using mixed lipid systems at pH 7[6,10,13,17,19,21,23,30] and 7.4.[11,12,14,16,18,20,22] Under these conditions binding appears to be stronger because of the availability of sites A and L.[7] Thus, lipid binding to WT iso-1-Cyt*c* with 20% CL/80% DOPC vesicles at pH 7 was evaluated using Soret CD and Trp59 fluorescence. DOPC binding studies demonstrated no significant lipid binding to Cyt*c* at pH 7 (Figure 5.10). Neither Soret CD nor Trp59 fluorescence deviated significantly from the unbound spectral signature throughout each titration.

When WT iso-1-Cyt*c* was exposed to 20% CL/80% DOPC vesicles, the Soret CD spectra is affected as the titration progresses (Figure 5.11). The observed $\Delta\Delta\varepsilon$ is indicative of CL binding however an upper limit to the binding curve could not be resolved because sufficiently high concentrations of vesicles could not be achieved. Thus, it was not impossible to evaluate K_d(app) and *n* for extruded 20% CL/80%DOPC vesicles using Soret CD alone. Trp59 fluorescence also showed evidence of Cyt*c*-CL binding for extruded 20% CL/80% DOPC vesicles at pH 7 (Figure 5.11). The increase in Trp59 fluorescence intensity at 331 nm shows that exposure of iso-1-Cyt*c* to extruded 20% CL/80% DOPC vesicles at pH 7 leads to movement of Trp59 away from the heme and thus partial unfolding of the protein. However, with 100% CL vesicles the emission maximum red shifts from ~330 nm to ~ 340 nm, whereas a minimal red shift is apparent for the interaction of iso-1-Cyt*c* with extruded 20% CL/80% DOPC vesicles at pH 7. Thus, the nature of the interaction appears to be qualitatively different. Sufficiently high exposed LPR could not be achieved to allow the Trp59 intensity versus exposed LPR data to be fit to eq 5.1. This finding is in accordance with TTAPE-Me findings suggesting that some CL resides on the outer leaflet but much less than expected if partitioning of CL was unbiased for extruded vesicles. Thus, even though binding is stronger at pH 7, the low content of CL in the outer leaflet of extruded mixed CL/DOPC vesicles precludes quantitative assessment of binding even at pH 7. It is possible that preparation of vesicles by other methods such as sonication may affect the degree of partitioning to the inner leaflet, possibly accounting for the stronger apparent binding observed at pH 7 – 7.4 in previous studies with mixed lipid CL/DOPC vesicles.

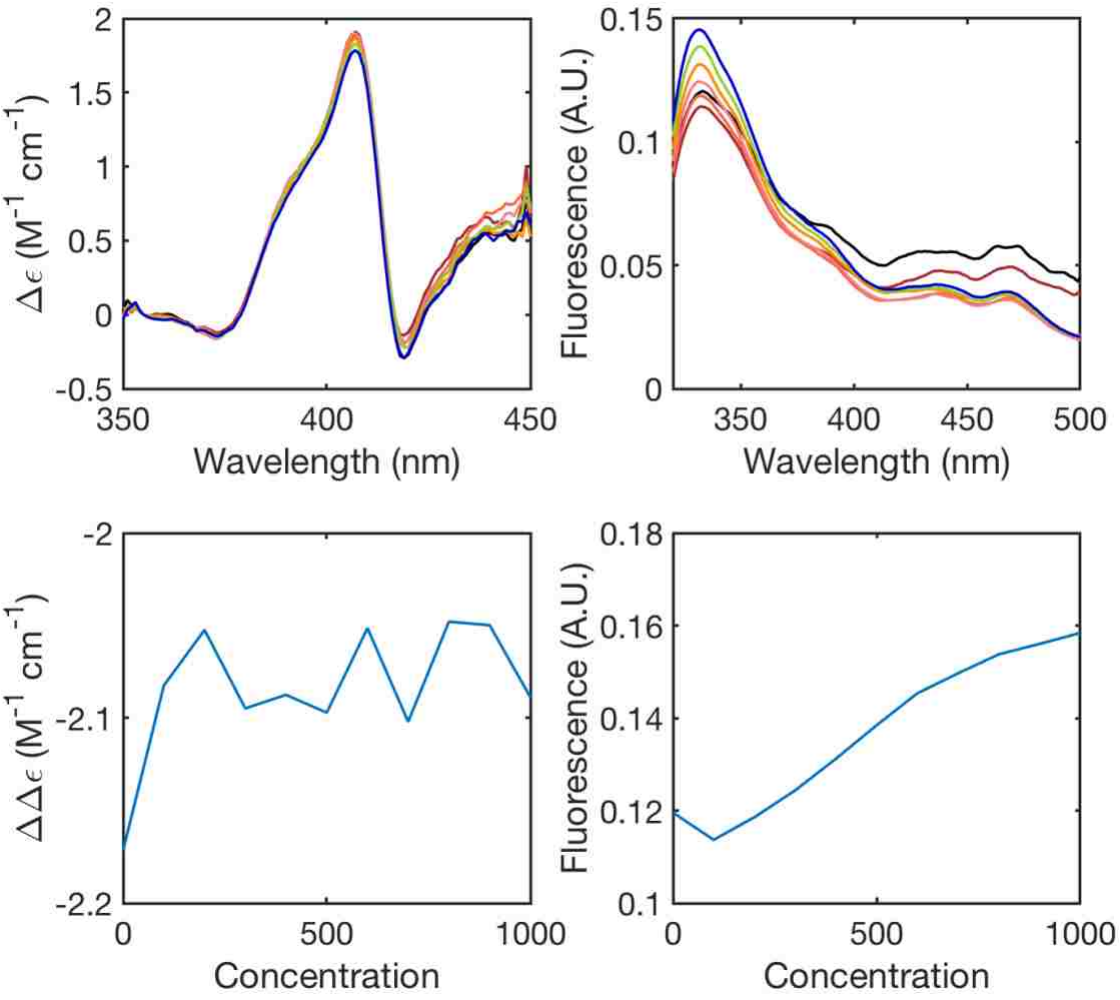

Figure 5.10. Titration of Iso-1-Cyt*c* with 100 nm 100% DOPC vesicles in 20 mM TES, 0.1 mM EDTA at pH 7 and 25 ˚C monitored using Soret CD (top left) and Trp59 fluorescence (top right). Soret CD amplitude ($\Delta\Delta\varepsilon = \Delta\varepsilon_{max} - \Delta\varepsilon_{min}$) as a function of exposed lipid to protein ratio (LPR) (bottom left). Trp59 fluorescence intensity at 331 nm as a function of exposed LPR (bottom right).

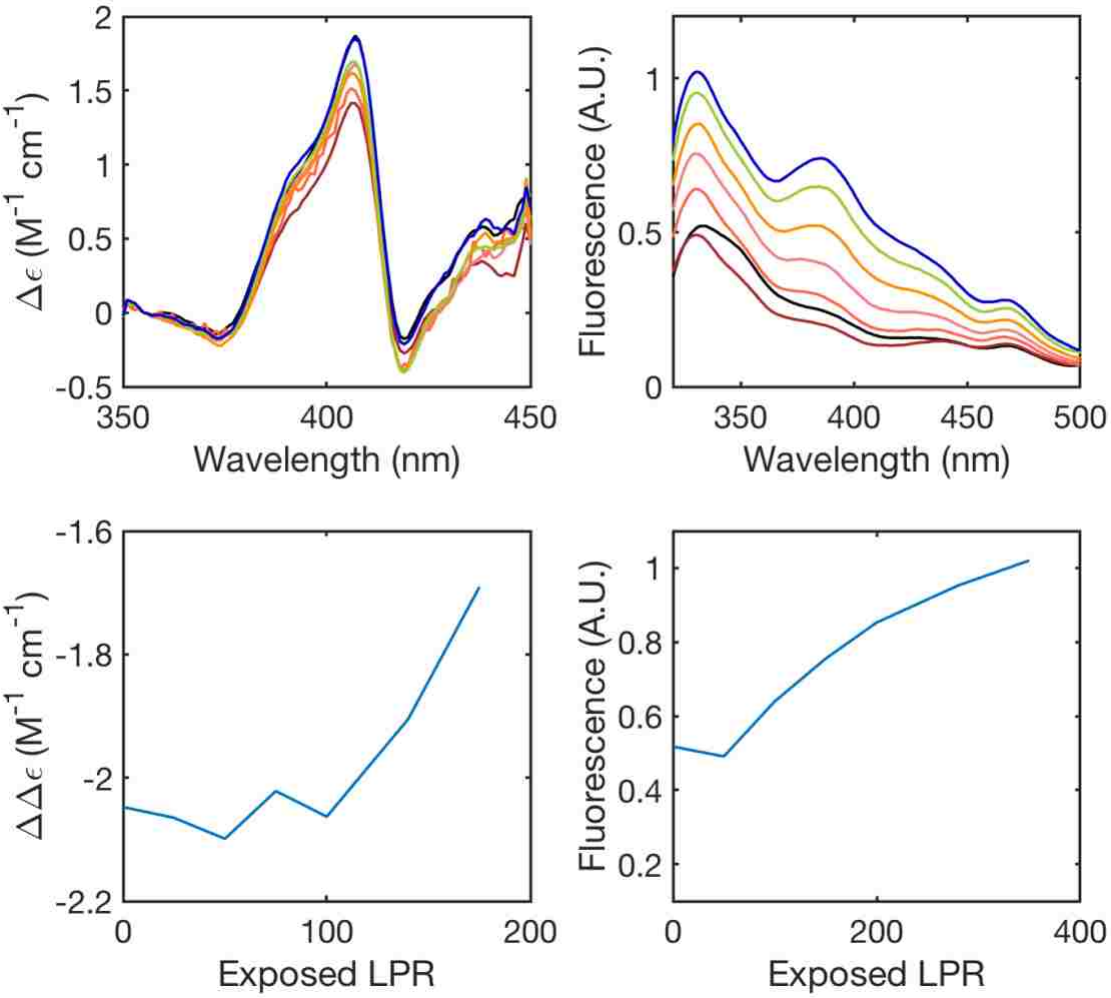

Figure 5.11. Titration of iso-1-Cyt*c* with 100 nm 20% CL/80% DOPC vesicles in 20 mM TES, 0.1 mM EDTA at pH 7 and 25 ˚C monitored using Soret CD (top left) and Trp59 fluorescence (top right). Soret CD amplitude ($\Delta\Delta\varepsilon = \Delta\varepsilon_{max} - \Delta\varepsilon_{min}$) plotted as a function of exposed LPR (bottom left). Trp59 fluorescence intensity at 331 nm plotted at as a function of exposed LPR (bottom right).

5.4. CONCLUSION

Using the fluorophore TTAPE-Me which binds specifically to lipids with anionic headgroups, we have shown that for CL/DOPC mixed lipid vesicles prepared by freeze/thaw methods followed by extrusion, the inverted cone lipid CL shows a 5:1 to preference for the concave surface of the inner leaflet of the vesicle over the convex outer leaflet at CL mole fractions less than or equal to 0.5. DOPG, a cylindrically-shaped vesicle, shows the expected 1:1 partitioning between the inner and outer leaflet, for mixed DOPG/DOPC vesicles at all mixing ratios. Thus, for extruded vesicles, lipid structure can impact the characteristics of the vesicles produced with potential impacts for studies on protein lipid interactions. We show for the interaction of iso-1-Cyt*c* with extruded 20% CL/80% DOPC vesicles at both pH 7 and 8 that the binding is much weaker than expected based on previous work with pure CL vesicles. The weaker than expected interaction of iso-1-Cyt*c* with 20% CL/80% DOPC vesicles results from the ~4% CL content in the outer leaflet caused by the 5:1 preference of CL for the inner leaflet of mixed CL/DOPC vesicles prepared by extrusion. It is possible that preparation of vesicles by other methods such as sonication may affect the degree of partitioning to the inner leaflet.

5.5. REFERENCES

(1) Burger, K. N. J. Greasing Membrane Fusion and Fission Machineries. *Traffic* **2000**, *1* (8), 605–613.

(2) Cho, W.; Stahelin, R. V. Membrane-Protein Interactions in Cell Signaling and Membrane Trafficking. *Annu Rev Biophys Biomol Struct* **2005**, *34*, 119–151.

(3) Kagan, V. E.; Bayır, H. A.; Belikova, N. A.; Kapralov, O.; Tyurina, Y. Y.; Tyurin, V. A.; Jiang, J.; Stoyanovsky, D. A.; Wipf, P.; Kochanek, P. M.; Greenberger, J. S.; Pitt, B.; Shvedova, A. A.; Borisenko, G. Cytochrome c/Cardiolipin Relations in Mitochondria: A Kiss of Death. *Free Radical Biology and Medicine* **2009**, *46* (11), 1439–1453.

(4) Orrenius, S.; Zhivotovsky, B. Cardiolipin Oxidation Sets Cytochrome c Free. *Nature chemical biology* **2005**, *1* (4), 188–189.

(5) Paradies, G.; Paradies, V.; De Benedictis, V.; Ruggiero, F. M.; Petrosillo, G. Functional Role of Cardiolipin in Mitochondrial Bioenergetics. *Biochimica et Biophysica Acta - Bioenergetics*. 2014, pp 408–417.

(6) Kagan, V. E.; Tyurin, V. A.; Jiang, J.; Tyurina, Y. Y.; Ritov, V. B.; Amoscato, A. A.; Osipov, A. N.; Belikova, N. A.; Kapralov, A. A.; Kini, V.; Vlasova, I. I.; Zhao, Q.; Zou, M.; Di, P.; Svistunenko, D. A.; Kurnikov, I. V; Borisenko, G. G. Cytochrome c Acts as a Cardiolipin Oxygenase Required for Release of Proapoptotic Factors. *Nat Chem Biol* **2005**, *1* (4), 223–232.

(7) Elmer-Dixon, M. M.; Bowler, B. E. Site A-Mediated Partial Unfolding of Cytochrome c on Cardiolipin Vesicles Is Species-Dependent and Does Not Require Lys72. *Biochemistry* **2017**, *56* (36), 4830–4839.

(8) Sinibaldi, F.; Milazzo, L.; Howes, B.; Piro, M.; Fiorucci, L.; Polticelli, F.; Ascenzi, P.; Coletta, M.; Smulevich, G.; Santucci, R. The Key Role Played by Charge in the Interaction of Cytochrome c with Cardiolipin. *JBIC Journal of Biological Inorganic Chemistry* **2017**, *22* (1), 19–29.

(9) Sinibaldi, F.; Howes, B. D.; Droghetti, E.; Polticelli, F.; Piro, M. C.; Di Pierro, D.; Fiorucci, L.; Coletta, M.; Smulevich, G.; Santucci, R. Role of Lysines in Cytochrome C-Cardiolipin Interaction. *Biochemistry* **2013**, *52* (26), 4578–4588.

(10) Rytomaa, M.; Kinnunen, P. K. J. Reversibility of the Binding of Cytochrome c to Liposomes. Implications for Lipid-Protein Interactions. *Journal of Biological Chemistry* **1995**, *270* (7), 3197–3202.

(11) Vincelli, A. J.; Pottinger, D. S.; Zhong, F.; Hanske, J.; Rolland, S. G.; Conradt, B.; Pletneva, E. V. Recombinant Expression, Biophysical Characterization, and Cardiolipin-Induced Changes of Two Caenorhabditis Elegans Cytochrome c Proteins. *Biochemistry* **2013**, *52* (4), 653–666.

(12) Pandiscia, L. A.; Schweitzer-Stenner, R. Coexistence of Native-like and Non-Native Partially Unfolded Ferricytochrome c on the Surface of Cardiolipin-Containing Liposomes. *Journal of Physical Chemistry B* **2015**, *119* (4), 1334–1349.

(13) Rytomaa, M.; Mustonen, P.; Kinnunen, P. K. J. Reversible, Nonionic, and PH-Dependent Association of Cytochrome c with Cardiolipin-Phosphatidylcholine Liposomes. *Journal of Biological Chemistry* **1992**, *267* (31), 22243–22248.

(14) Mandal, A.; Hoop, C. L.; Delucia, M.; Kodali, R.; Kagan, V. E.; Ahn, J.; Van Der Wel, P. C. A. Structural Changes and Proapoptotic Peroxidase Activity of Cardiolipin-Bound Mitochondrial Cytochrome C. *Biophysical Journal* **2015**, *109* (9), 1873–1884.

(15) Heimburg, T.; Marsh, D. Investigation of Secondary and Tertiary Structural-Changes of Cytochrome-C in Complexes with Anionic Lipids Using Amide Hydrogen-Exchange Measurements - an Ftir Study. *Biophysical Journal* **1993**, *65* (6), 2408–2417.

(16) Gorbenko, G. P.; Molotkovsky, J. G.; Kinnunen, P. K. J. Cytochrome c Interaction with Cardiolipin/Phosphatidylcholine Model Membranes: Effect of Cardiolipin Protonation. *Biophysical Journal* **2006**, *90* (11), 4093–4103.

(17) Rytömaa, M.; Kinnunen, P. K. J. Evidence for Two Distinct Acidic Phospholipid-Binding Sites in Cytochrome C. *Journal of Biological Chemistry* **1994**, *269* (3), 1770–1774.

(18) Muenzner, J.; Toffey, J. R.; Hong, Y.; Pletneva, E. V. Becoming a Peroxidase: Cardiolipin-Induced Unfolding of Cytochrome C. *Journal of Physical Chemistry B* **2013**, *117* (42), 12878–12886.

(19) Tuominen, E. K. J.; Zhu, K.; Wallace, C. J. A.; Clark-Lewis, I.; Craig, D. B.; Rytömaa, M.; Kinnunen, P. K. J. ATP Induces a Conformational Change in Lipid-Bound Cytochrome C. *Journal of Biological Chemistry* **2001**, *276* (22), 19356–19362.

(20) Hanske, J.; Toffey, J. R.; Morenz, A. M.; Bonilla, A. J.; Schiavoni, K. H.; Pletneva, E. V. Conformational Properties of Cardiolipin-Bound Cytochrome C. *Proceedings of the National Academy of Sciences of the United States of America* **2012**, *109* (1), 125–130.

(21) Pandiscia, L. A.; Schweitzer-Stenner, R. Salt as a Catalyst in the Mitochondria: Returning Cytochrome c to Its Native State after It Misfolds on the Surface of Cardiolipin Containing Membranes. *Chemical Communications* **2014**, *50* (28), 3674–3676.

(22) Hong, Y.; Muenzner, J.; Grimm, S. K.; Pletneva, E. V. Origin of the Conformational Heterogeneity of Cardiolipin-Bound Cytochrome C. *Journal of the American Chemical Society* **2012**, *134* (45), 18713–18723.

(23) Kostrzewa, A.; Páli, T.; Froncisz, W.; Marsh, D. Membrane Location of Spin-Labeled Cytochrome c Determined by Paramagnetic Relaxation Agents. *Biochemistry* **2000**, *39* (20), 6066–6074.

(24) Kawai, C.; Prado, F. M.; Nunes, G. L. C.; Di Mascio, P.; Carmona-Ribeiro, A. M.; Nantes, I. L. PH-Dependent Interaction of Cytochrome c with Mitochondrial Mimetic Membranes: The Role of an Array of Positively Charged Amino Acids. *Journal of Biological Chemistry* **2005**, *280* (41), 34709–34717.

(25) O'Brien, E. S.; Nucci, N. V.; Fuglestad, B.; Tommos, C.; Wand, A. J. Defining the Apoptotic Trigger: The Interaction of Cytochrome c and Cardiolipin. *Journal of Biological Chemistry* **2015**, *290* (52), 30879–30887.

(26) McClelland, L. J.; Mou, T.-C.; Jeakins-Cooley, M. E.; Sprang, S. R.; Bowler, B. E. Structure of a Mitochondrial Cytochrome c Conformer Competent for Peroxidase Activity. *Proceedings of the National Academy of Sciences of the United States of America* **2014**, *111* (18), 6648–6653.

(27) Rajagopal, B. S.; Silkstone, G. G.; Nicholls, P.; Wilson, M. T.; Worrall, J. A. R. An Investigation into a Cardiolipin Acyl Chain Insertion Site in Cytochrome C. *Biochimica et Biophysica Acta (BBA) - Bioenergetics* **2012**, *1817* (5), 780–791.

(28) McClelland, L.; Seagraves, S.; Khan, M.; Cherney, M.; Bandi, S.; Culbertson, J.; Bowler, B. The Response of Ω-Loop D Dynamics to Truncation of Trimethyllysine 72 of Yeast Iso-1-Cytochrome c Depends on the Nature of Loop Deformation. *Journal of Biological Inorganic Chemistry* **2015**, *20* (5), 805–819.

(29) Muenzner, J.; Pletneva, E. V. Structural Transformations of Cytochrome c upon Interaction with Cardiolipin. *Chemistry and Physics of Lipids* **2014**, *179*, 57–63.

(30) Amacher, J. F.; Zhong, F.; Lisi, G. P.; Zhu, M. Q.; Alden, S. L.; Hoke, K. R.; Madden, D. R.; Pletneva, E. V. A Compact Structure of Cytochrome c Trapped in a Lysine-Ligated State: Loop Refolding and Functional Implications of a Conformational Switch. *Journal of the American Chemical Society* **2015**, *137* (26), 8435–8449.

(31) Bergstrom, C. L.; Beales, P. A.; Lv, Y.; Vanderlick, T. K.; Groves, J. T. Cytochrome c Causes Pore Formation in Cardiolipin-Containing Membranes. *Proceedings of the National Academy of Sciences of the United States of America* **2013**, *110* (16), 6269–6274.

(32) Sinibaldi, F.; Fiorucci, L.; Patriarca, A.; Lauceri, R.; Ferri, T.; Coletta, M.; Santucci, R. Insights into Cytochrome C-Cardiolipin Interaction. Role Played by Ionic Strength. *Biochemistry* **2008**, *47* (26), 6928–6935.

(33) Pandiscia, L. A.; Schweitzer-Stenner, R. Coexistence of Native-Like and Non-Native Misfolded Ferricytochrome C on the Surfac of Cardiolipin Containing Liposomes. *Biophysical Journal* **2015**, *108* (2, Supplement 1), 91a.

(34) Leung, C. W. T.; Hong, Y.; Hanske, J.; Zhao, E.; Chen, S.; Pletneva, E. V.; Tang, B. Z. Superior Fluorescent Probe for Detection of Cardiolipin. *Analytical Chemistry* **2014**, *86* (2), 1263–1268.

(35) Hong, Y.; Häußler, M.; Lam, J. W. Y.; Li, Z.; Sin, K. K.; Dong, Y.; Tong, H.; Liu, J.; Qin, A.; Renneberg, R.; Tang, B. Z. Label-Free Fluorescent Probing of G-Quadruplex Formation and Real-Time Monitoring of DNA Folding by a Quaternized Tetraphenylethene Salt with Aggregation-Induced Emission Characteristics. *Chemistry - A European Journal* **2008**, *14* (21), 6428–6437.

(36) Elmer-Dixon, M. M.; Bowler, B. E. *Rapid Quantification of Cardiolipin and DOPC Lipid and Vesicle Concentration*; 2017; Vol. 520.

(37) Elmer-Dixon, M. M.; Bowler, B. E. Rapid Quantification of Vesicle Concentration for DOPG/DOPC and Cardiolipin/DOPC Mixed Lipid Systems of Variable Composition. *Analytical Biochemistry* **2018**, *553*, 12–14.

(38) Goldes, M. E.; Jeakins-Cooley, M. E.; McClelland, L. J.; Mou, T. C.; Bowler, B. E. Disruption of a Hydrogen Bond Network in Human versus Spider Monkey Cytochrome c Affects Heme Crevice Stability. *Journal of Inorganic Biochemistry* **2016**, *158*, 62–69.

(39) Wandschneider, E.; Hammack, B. N.; Bowler, B. E. Evaluation of Cooperative Interactions between Substructures of Iso-1-Cytochrome c Using Double Mutant Cycles. *Biochemistry* **2003**, *42* (36), 10659–10666.

(40) Pollock, W. B. R.; Rosell, F. I.; Twitchett, M. B.; Dumont, M. E.; Mauk, A. G. Bacterial Expression of a Mitochondrial Cytochrome c. Trimethylation of Lys72 in Yeast Iso-1-Cytochrome C and the Alkaline Conformational Transition. *Biochemistry* **1998**, *37* (17), 6124–6131.

(41) Smolentsev, N.; Lütgebaucks, C.; Okur, H. I.; De Beer, A. G. F.; Roke, S. Intermolecular Headgroup Interaction and Hydration as Driving Forces for Lipid Transmembrane Asymmetry. *Journal of the American Chemical Society* **2016**, *138* (12), 4053–4060.

(42) Vequi-Suplicy, C. C.; Riske, K. A.; Knorr, R. L.; Dimova, R. Vesicles with Charged Domains. *Biochimica et Biophysica Acta - Biomembranes* **2010**, *1798* (7), 1338–1347.

(43) Tian, A.; Baumgart, T. Sorting of Lipids and Proteins in Membrane Curvature Gradients. *Biophysical Journal* **2009**, *96* (7), 2676–2688.

(44) Carnie, S.; Israelachvili, J. N.; Pailthorpe, B. A. Lipid Packing and Transbilayer Asymmetries of Mixed Lipid Vesicles. *BBA - Biomembranes* **1979**, *554* (2), 340–357.

(45) Sorre, B.; Callan-Jones, A.; Manneville, J.-B.; Nassoy, P.; Joanny, J.-F.; Prost, J.; Goud, B.; Bassereau, P. Curvature-Driven Lipid Sorting Needs Proximity to a Demixing Point and Is Aided by Proteins. *Proceedings of the National Academy of Sciences* **2009**, *106* (14), 5622–5626.

(46) Tuominen, E. K. J.; Wallace, C. J. A.; Kinnunen, P. K. J. Phospholipid-Cytochrome c Interaction. Evidence for the Extended Lipid Anchorage. *Journal of Biological Chemistry* **2002**, *277* (11), 8822–8826.

(47) Soffer, J. B.; Fradkin, E.; Pandiscia, L. A.; Schweitzer-Stenner, R. The (Not Completely Irreversible) Population of a Misfolded State of Cytochrome c under Folding Conditions. *Biochemistry* **2013**, *52* (8), 1397–1408.

(48) Frey, T. G.; Renken, C. W.; Perkins, G. A. Insight into Mitochondrial Structure and Function from Electron Tomography. *Biochimica et Biophysica Acta - Bioenergetics* **2002**.

(49) Heimburg, T.; Angerstein, B.; Marsh, D. No Title. *Biophysical Journal1* **1999**, *76* (5), 2575–2586.

Chapter 6: Curvature Dependent Binding of Cytochrome *c* to Cardiolipin

6.1. INTRODUCTION

Cytochrome *c* (Cyt*c*) resides at low millimolar concentrations (0.5 – 1 mM) in the intra-cristal compartments and the intermembrane space.[1] The primary functions of Cyt*c* are as an intermediary in the electron transport chain and as a signaling agent in the intrinsic pathway of apoptosis. The earliest signal in the intrinsic pathway of apoptosis involves oxidation of the cone-shaped, non-bilayer forming lipid, cardiolipin (CL) by Cyt*c* on the inner mitochondrial membrane (IMM) of the intermembrane space (IMS).[2,3] The IMM, particularly in the intra-cristal compartments, contains many concave surfaces.[4] After oxidation of CL, Cyt*c* is released from the IMM, exits the mitochondria and forms part of the apoptosome in the cytosol, initiating apoptosis.[3,5] Because Cyt*c*-CL binding is a preemptive step to apoptosis, work has been performed in an effort to elucidate the nature and extent of this interaction. Studies have investigated the role of lipid composition in protein binding but have only minimally addressed the role membrane curvature plays in the interaction.[6–9] Here, we investigate protein binding to the concave inner surface of pure (100%) CL vesicles to assess the role of membrane curvature in Cyt*c* binding to CL.

6.2. MATERIALS AND METHODS

6.2.1. Sample Preparation.

Wild-type yeast iso-1-cytochrome *c* (iso-1-Cyt*c*) was expressed from *Escherichia coli* BL21 DE3 cells (BioRad, Phage T1-resistant strain) and purified following previously reported methods.[10] Protein was concentrated to concentrations between 0.5 and 5 mM in 20 mM TES,

0.1 mM EDTA, 0.1 mM NaCl, pH 8. For each titration point, three aliquots of 100% cardiolipin (Avanti Polar Lipids, Inc) (CL) (minimally 5 mg each) were mixed with the ionophore Nonactin in a 1:100 ratio of Nonactin:CL, and the mixtures were dried individually under compressed nitrogen for approximately 2 hours to remove chloroform. The lipid/nonactin mixture was then combined with the concentrated protein solutions to form vesicles. Mixing was performed at low speeds on a vortexer. Vortexing was sufficiently vigorous to thoroughly mix the protein with the CL/nonactin but not so vigorous that formation of bubbles occurred. Protein/lipid/nonactin mixtures were extruded to 100 nm using an Avanti Mini Extruder where two 100 nm membrane supports were used for extrusion and samples were passed through the extruder 11 times. After extrusion, samples were loaded onto a washed (20 mM TES buffer, 0.1 mM EDTA, pH 8) CM Sepharose Fast Flow column (GE Healthcare Life Sciences) and run down the column in the mobile phase. Cyt*c* external to the vesicles bound to the CM-sepharose cation-exchange resin while the negatively-charged vesicles filled with Cyt*c* eluted off the column. Eluent containing Cyt*c* filled vesicles was collected and concentrated to <1 mL using Amicon Ultra-15 Centrifugal Filter Units with 50k MWCO (EMD Millipore, Sigma). Samples were diluted to 15 mL in 20 mM TES Buffer, 0.1 mM EDTA, pH 8 and set to equilibrate on an orbital shaker for 8 hours at 4 °C. Conductivity was periodically measured to follow the flow of NaCl from inside the vesicles via the nonactin channels. When conductivity stabilized, indicating that the flow of NaCl out of the interior of the samples was complete, the CL vesicles loaded with iso-1-Cyt*c* were again run down a CM Sepharose column in 20 mM TES Buffer, 0.1 mM EDTA, pH 8, collected and concentrated using the same 50k MWCO ultrafiltration devices. Conductivity at equilibrium was approximately the conductivity of 20 mM TES, 0.1 mM EDTA buffer at pH 8. The concentration of iso-1-Cyt*c* was measured with a Beckman Coulter DU800 using previously reported

extinction coefficients,[11] and taking into account scattering off of the vesicles. A Malvern Zetasizer was used to perform Dynamic Light Scattering on all samples to determine vesicle size. Vesicle size was measured to be 100 nm ± 5 nm for all replicates at all titration points. Vesicle size was later used to calculate lipid concentration and determine exposed lipid to protein ratio (LPR) for each protein concentration point. Samples were then diluted or concentrated as needed to either 5 μM or 10 μM iso-1-Cyt*c* concentration, as appropriate, for spectroscopic measurements.

6.2.2. Circular Dichroism Spectroscopy.

Soret CD spectra were measured using previously reported methods.[10] Briefly, CD data were acquired using an Applied Photophysics Chirascan Spectrophotometer to measure the spectral region from 350 nm – 450 nm, scanning in 1 nm steps with a 3 second/nm scan rate and 1.8 nm bandwidth. Samples were contained in a 4 mm by 10 mm Hellma cuvette (Hellma Analytics) utilizing the 4 mm pathlength. Spectra were smoothed with a 6-point Savitsky-Golay smoothing function and data were analyzed using the difference between the positive maximum near 405 nm and negative minimum near 420 nm as the signal amplitude, as previously described.

6.2.3. Tryptophan Fluorescence Spectroscopy.

Trp59 fluorescence measurements were performed using previously reported methods.[10] Briefly, fluorescence data were acquired using an Applied Photophysics Chirascan Spectrophotometer modified for fluorescence data acquisition using a scanning emission monochromator (Applied Photophysics). Samples were excited at 295 nm (5 nm bandwidth) and fluorescence was measured at 90^{o} with a 305 nm cutoff filter (Newport Corp) in-line to limit

excitation bleed through. Emission was measured from 320 nm to 500 nm in 1 nm steps, with 0.5 sec per step and a 2.5 nm bandwidth. A 5 mm by 5 mm Hellma fluorescence cuvette was used for measurements. Spectra were smoothed a 6-point Savitsky-Golay smoothing function and data were analyzed to extract fluorescence peak emission intensity as previously reported.

6.2.4. Data Fitting.

A one site cooperative Langmuir-type equation (eq 6.1) was used to fit CD and fluorescence data, where the spectroscopic value, s(x)

$$s(x) = \frac{s_o + s_1\left(\frac{x}{K_d(\text{app})}\right)^n}{1+\left(\frac{x}{K_d(\text{app})}\right)^n} \qquad \text{(eq 6.1)}$$

corresponds to the amplitude measured at the exposed lipid to protein ratio (LPR), x, in the titration and s_0 and s_1 are the amplitudes of the initial (free protein) and final (lipid bound protein) states, respectively. Here, K_d(app) is the apparent dissociation constant corresponding to the exposed LPR required to induce half occupancy of the conformation associated with site A binding to CL and *n* is the associated Hill coefficient.

6.2.5. Lipid to Protein Ratio Calculations.

Lipid to protein ratio was calculated for concave binding using the initial protein concentration (protein concentration during vesicle formation) and the lipid concentration on the vesicle inner leaflet associated with vesicle size measured using DLS. After vesicle formation and removal of excess protein from the exterior of vesicles, DLS was run to measure vesicle size. Using bilayer thickness of CL(3.67 nm)[12], average surface area of an inner leaflet was calculated. Headgroup surface area of CL (1.298 nm^2)[12] was then used to determine the number of lipids on

the concave surface of the vesicle. Taking into account bilayer thickness, the average inner volume of a vesicle was calculated and the initial protein concentration was used to find the total number of proteins present on the interior of a vesicle. The LPR was calculated using both populations for each sample at each concentration point for each trial.

6.3. RESULTS AND ANALYSIS

In previous work, we showed that yeast iso-1-Cyt*c* binds to the convex surface of 100 nm, pure CL vesicles and reported the associated binding parameters for cooperative, one-site, Langmuir-type binding (Eq. 6.1, Table 6.1)[10]. These studies were carried out at pH 8, conditions selective for binding to the anionic site, A-site,[10] which has long been attributed to electrostatic binding to lysines 72 and 73,[13,14] and possibly lysines 86 and 87 (See Figure 6.1, top).[13–15] We assigned the two distinct apparent dissociation constants, K_d(app), found using Soret circular dichroism (CD) and fluorescence spectroscopy, to a two-step conformational rearrangement on the surface of the pure CL vesicles. If we interpret the K_d(app) in terms of exposed lipid to protein ratio (LPR) as reflecting the space required on the membrane surface, the first step requires the surface area of ~10 CL headgroups (~13 nm^2; CL headgroup surface is 1.298 nm^2,[12]). This surface area requirement is only slightly larger than the 9.1 nm^2 of membrane surface area the native state of Cyt*c* is expected to require,[16,17] suggesting only a modest structural rearrangement in the first step.

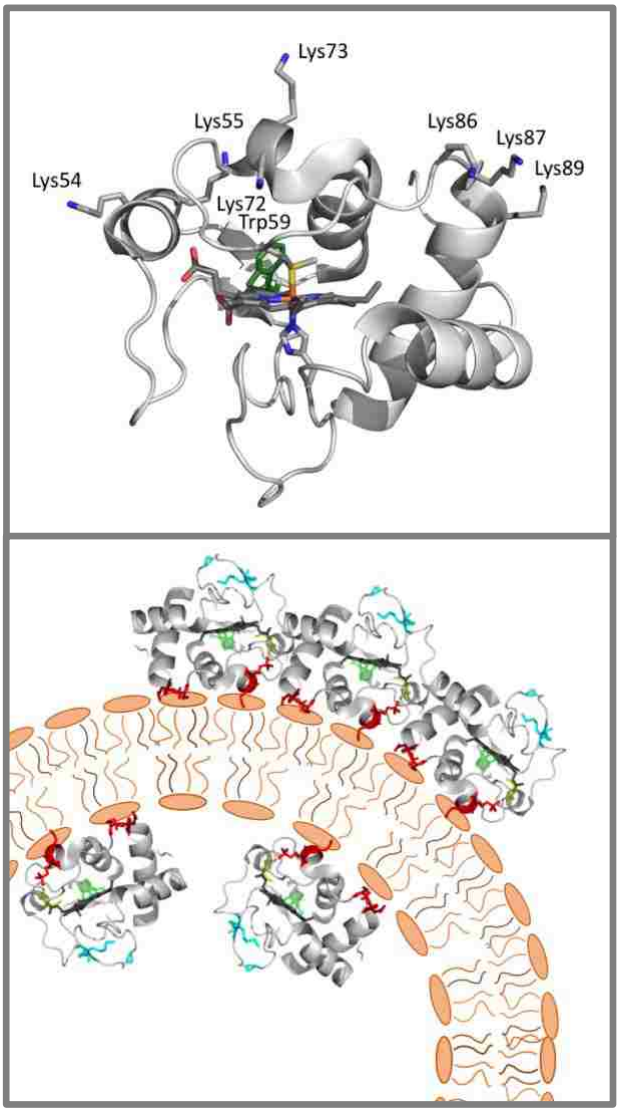

Figure 6.1. TOP: Yeast iso-1-Cyt*c* (PDB entry 2YCC) showing lysines 72, 73, 86 and 87, which are commonly assigned as constituents of the A-site (top panel, prepared using MacPymol) Neighboring lysines 54, 55 and 89 are also shown. Trp59 is shown in green behind the heme. The heme and its ligands, Met80 and His18, are also shown. **BOTTOM:** Schematic representation of spatial constraints on binding iso-1-Cyt*c* to the convex outer surface versus the concave inner surface of a pure CL vesicle.

The second step requires ~23 CL headgroups (~30 nm^2) indicative of a more significant conformational rearrangement. Fluorescence resonance energy transfer studies of partial unfolding on the surface of 1:1 CL:DOPC vesicles, which show that the C-terminal helix moves away from the heme at high LPR,[18] are qualitatively consistent with the additional membrane surface area indicated by the K_d(app) of the second conformational rearrangement we observe on pure CL vesicles. The associated Hill coefficient for each step (n ~2) suggests that the iso-1-Cyt*c* interacts directly with 2 lipid headgroups (4 negatively charged phosphates) as part of each step of the conformational rearrangement.

Table 6.1. Thermodynamic parameters for iso-1-Cyt*c* binding to 100% CL vesicles.

	CD		Fluorescence	
Membrane Curvature	K_d(app), Exposed LPR	n	K_d(app), Exposed LPR	n
Concave	54.8 ± 3.3	4.4 ± 1.0	58.2 ± 4.2	4.7 ± 1.2
Convex[10]	10.2 ± 0.2	2.2 ± 0.1	23.4 ± 0.8	2.3 ± 0.2

Reported in exposed (leaflet) lipid to protein ratio (LPR). Error corresponds to the standard error in the fit of the parameter

We have recently shown that CL partitions preferentially to the inner leaflet of CL-containing DOPC vesicles (See Chapter 5). This preferential localization suggests a variation in CL packing on concave and convex surfaces with a strong favorability for CL to pack well in vesicle inner leaflets. Conformational rearrangements of proteins on a concave membrane surface differ in two respects relative to those on a convex surface. The concave surface will cause globular proteins on the surface to tilt toward each other, rather than away from each other as on a convex surface (Figure 6.1, bottom). Thus, more surface area is expected to be necessary for protein binding to a concave membrane surface. The concave membrane surface will also better match the curvature of a globular protein, so, one might expect that more of the protein could interact with the membrane perhaps increasing the number of lipids which directly bind to the protein and thus the cooperativity of binding and/or structural rearrangements on the membrane surface.

To examine protein binding to concave membrane surfaces, we performed CL-binding titrations for iso-1-Cytc encapsulated within 100 nm, pure CL vesicles, so, that they only see the concave surface of the bilayer (For preparation of vesicle with iso-1-Cyt*c* trapped inside, see Supporting Information). Vesicle titrations of Cyt*c* binding to the concave exterior surface of CL-containing vesicles are typically done at a constant protein concentrations between 5 and 10 μM[10,19–21] in the presence of increasing amounts of vesicles. Our previous work on iso-1-Cyt*c* indicates that at this protein concentration, both Soret CD and Trp59 fluorescence monitor conformational rearrangements of iso-1-Cyt*c* already bound to pure CL vesicles.[10] Thus, titrations are best evaluated as a function of exposed LPR (available membrane surface area). For titrations as a function of exposed LPR for iso-1-Cyt*c* trapped inside vesicles, iso-1-Cyt*c* concentration must be changed to vary exposed LPR. To achieve exposed LPR across the same range as for titrations with iso-1-Cyt*c* to the convex outer surface of vesicles, the vesicles must

be formed in the presence of iso-1-Cyt*c* at concentrations ranging from 0.5 – 5 mM. Thus, the concentration of iso-1-Cyt*c* in the lumen of the pure CL vesicles in this study is similar to that observed physiologically in the IMS of mitochondria.

To monitor local and global structural rearrangement as a function of exposed LPR, Soret CD and Trp59 fluorescence spectroscopy, respectively, were used (see Supplementary Information for sample preparation and experimental methods). Soret CD is sensitive to the local heme environment, particularly heme-Met80 ligation[19] and the proximity of Phe82 to the heme.[22] Trp59 fluorescence depends on the Trp59-heme distance and is used to monitor changes in tertiary structure of Cyt*c*.[23] For binding titrations followed by Soret CD, the CL vesicle titration evaluated iso-1-Cyt*c* binding from a low exposed LPR (high iso-1-Cyt*c* concentration, Figure 6.2, top, blue spectrum) to a high exposed LPR (low protein concentration, Figure 6.2, top left, red spectrum) to assess the effect of the binding density of iso-1-Cyt*c* on the concave CL surface on the local heme environment. The amplitude of the CD signal ($\Delta\Delta\varepsilon = \Delta\varepsilon_{406} - \Delta\varepsilon_{420}$) was plotted versus exposed LPR and fit to a one-site cooperative Langmuir binding model (Eq. S1) to determine K_d(app) and n (Figure 6.2, bottom left panel, Table 6.1). Compared to binding titrations on the external convex surface of pure 100 nm CL vesicles, K_d(app) obtained from Soret CD measurements on the concave inner surface of pure CL vesicles is much higher (Table 6.1), indicating that more space is required for the Soret CD-monitored conformational change on a concave versus a convex surface. The associated Hill coefficient, n, is also twice the value reported for binding on a convex membrane surface. Trp59 fluorescence as a function of exposed LPR on the concave inner surface of the pure CL vesicle also is shown in Figure 6.2 (top right). The increase in Trp59 fluorescence intensity at the emission maximum (341 nm) was plotted versus exposed LPR and fit to Eq. 6.1 to obtain K_d(app) and n (Figure 6.2, bottom right, Table

6.2). The K_d(app) and *n* values obtained for binding on the concave inner surface of pure CL vesicles from Trp59 fluorescence data are approximately double the magnitude of the values obtained for Cyt*c*-CL binding on the convex exterior surface of pure 100 nm CL vesicles (Table 6.2). Whereas the K_d(app) and *n* parameters obtained from Soret CD versus Trp59 fluroescence data are significantly different for binding to convex membrane surfaces, they are essentially identical for binding to concave surfaces. Thus, conformational rearrangement of iso-1-Cyt*c* is concerted on the concave inner surface and stepwise on the convex outer surface of 100 nm pure CL vesicles (Figure 6.3).

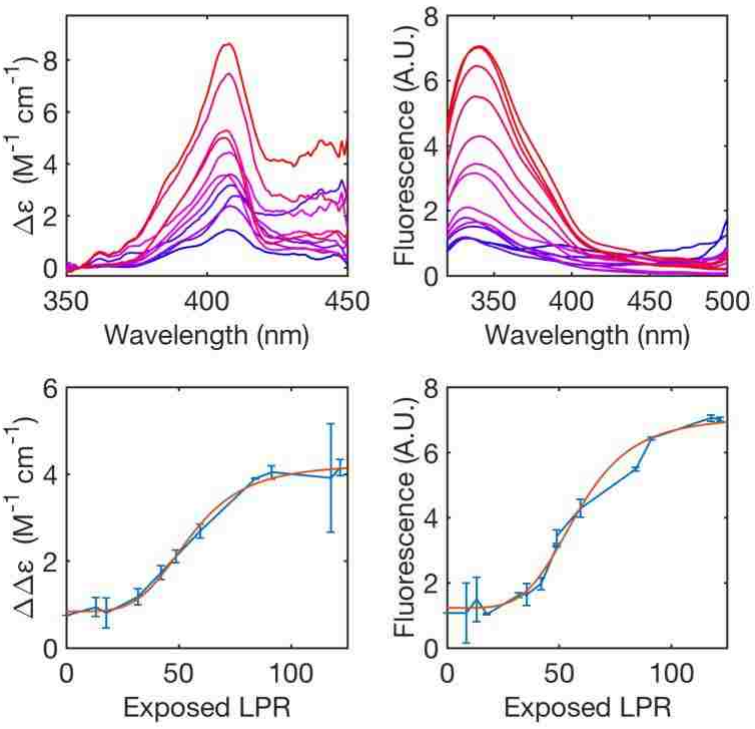

Figure 6.2. Soret CD spectra of 10 μM iso-1-Cyt*c* (top left panel) prepared from low exposed LPR (high iso-1-Cyt*c* concentration in vesicle lumen; blue spectrum is iso-1-Cyt*c* in the absence of vesicles) to a high exposed LPR (Red, low iso-1-Cyt*c* concentration in vesicle lumen) inside 100 nm, 100% CL vesicles formed in 20 mM TES buffer, 0.1 mM EDTA at pH 8. Vesicle concentration was adjusted, so that iso-1-Cyt*c* concentration was 10 μM in all samples. Average Soret CD amplitude ($\Delta\Delta\varepsilon = \Delta\varepsilon_{406} - \Delta\varepsilon_{420}$, solid black circles) as a function of exposed LPR (bottom left panel) fit to eq 6.1 (solid red curve). Trp59 fluorescence signal of 5 μM iso-1-Cyt*c* prepared at lipid concentrations ranging from a low exposed LPR (Blue) to a high exposed LPR (Red) inside 100 nm, 100% CL vesicles formed in 20 mM TES buffer, 0.1 mM EDTA at pH 8. Average Trp59 fluorescence peak signal at 441 nm as a function of exposed LPR (solid black circles) fit to Eq. 6.1 (solid red curve). Error bars of data points in the bottom panels are the standard deviation from three independent trials.

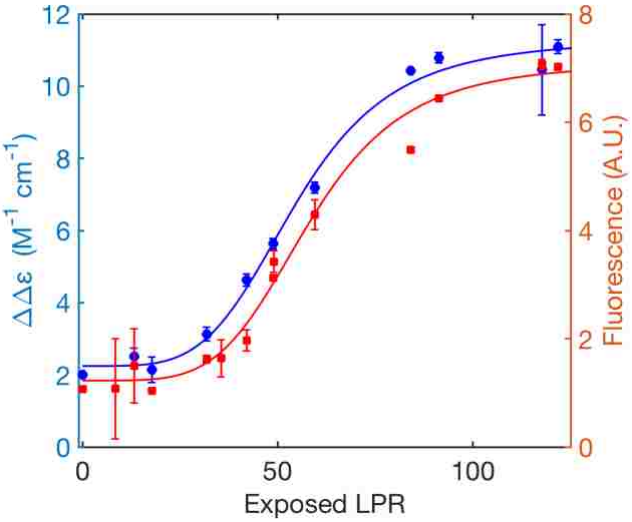

Figure 6.3. Overlay of the titration curves for WT iso-1-Cyt*c* obtained by Soret CD (blue circles) and Trp59 fluorescence (red squares) for binding to the interior concave surface of pure CL vesicles showing that binding as monitored by both spectroscopic probes is concerted.

The amplitude of the CD signal ($\Delta\Delta\varepsilon = \Delta\varepsilon_{406} - \Delta\varepsilon_{420}$) was plotted versus exposed LPR and fit to a one-site cooperative Langmuir binding model (Eq. 6.1) to determine K_d(app) and n (Figure 6.2, bottom left panel, Table 6.1). Compared to binding titrations on the external convex surface of pure 100 nm CL vesicles, K_d(app) obtained from Soret CD measurements on the concave inner surface of pure CL vesicles is much higher (Table 6.1), indicating that more space is required for the Soret CD-monitored conformational change on a concave versus a convex surface. The associated Hill coefficient, n, is also twice the value reported for binding on a convex membrane surface. Trp59 fluorescence as a function of exposed LPR on the concave inner surface of the pure CL vesicle also is shown in Figure 6.2 (top right). The increase in Trp59 fluorescence intensity at the emission maximum (341 nm) was plotted versus exposed LPR and fit to Eq. 6.1 to obtain K_d(app) and n (Figure 6.2, bottom right, Table 6.1). The K_d(app) and n

values obtained for binding on the concave inner surface of pure CL vesicles from Trp59 fluorescence data are approximately double the magnitude of the values obtained for Cyt*c*-CL binding on the convex exterior surface of pure 100 nm CL vesicles (Table 6.1). Whereas the K_d(app) and *n* parameters obtained from Soret CD versus Trp59 fluorescence data are significantly different for binding to convex membrane surfaces, they are essentially identical for binding to concave surfaces. Thus, conformational rearrangement of iso-1-Cyt*c* is concerted on the concave inner surface and stepwise on the convex outer surface of 100 nm pure CL vesicles (Figure 6.3).

The lowest exposed LPR in the titration followed by Soret CD in Figure 6.2 gives a spectrum similar to the spectrum of iso-1-Cyt*c* free in solution at pH 8 (Figure 6.4). At pH 8 when not bound to vesicles, wild type (WT) iso-1-Cyt*c* expressed from *Escherichia coli* (unlike protein expressed from the native host, *Saccharomyces cerevisiae*, Lys72 is not trimethylated causing the pK_{app} of the alkaline transition of iso-1-Cyt*c* to decrease to 8)[24] gives a Soret CD spectrum consistent with significant population of the alkaline conformer of iso-1-Cyt*c*. By contrast at an exposed LPR near 13, the negative band of the Soret CD of iso-1-Cyt*c* near 420 nm, typical of the native conformer free in solution, reappears when WT iso-1-Cyt*c* is bound to the convex exterior surface of pure CL vesicles (Figure 6.4). Thus, initial structural rearrangement that occurs on the outer surface of pure CL vesicles, which appears to make the structure of iso-1-Cyt*c* more nativelike, does not occur on the concave inner surface of pure CL vesicles. Instead, the protein appears to maintain a heme environment that is more similar to that of the protein free in solution up to an exposed LPR of almost 40.

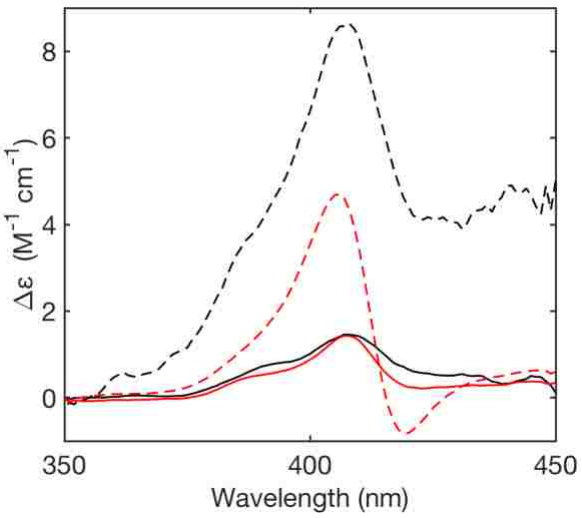

Figure 6.4. Soret CD signal corresponding to 10 μM unbound Cyt*c* in the concave (Black) and convex (Red) systems as well as signals corresponding to 10 μM bound Cyt*c* in the concave (--) and convex (--) systems.

The concerted partial unfolding on the concave inner surface occurs at about twice the exposed LPR (K_d(app) of ~56.5, Table 6.1) of the second conformational rearrangement (partial unfolding) on the convex outer surface of pure CL vesicles. This K_d(app) corresponds to a surface area of ~73 nm^2 for partial unfolding on the concave inner surface of pure CL vesicles, more than twice the surface area needed for this conformational rearrangement on the convex outer surface of pure CL vesicles. The Hill coefficient, *n*, is approximately the sum of the individual steps observed for binding to a convex membrane surface indicating that a similar total number of lipids (~4.5) interact with iso-1-Cyt*c* when it unfolds on the concave inner surface of pure CL vesicles. One factor that may lead to the concerted (concave surfaces) versus the stepwise (convex surfaces) mechanism for structural rearrangement of iso-1-Cyt*c* on membrane surfaces is that the concave surface is more stable because the cone-shape of CL is better adapted to a concave surface. Our recent studies showing that CL preferentially partitions

to the inner leaflet of 100 nm vesicles supports this contention. A more stable surface would be less prone to deformation and thus require more points of contact to initiate structural rearrangement of iso-1-Cyt*c*. The larger surface area (K_d(app)) needed for partial unfolding of iso-1-Cyt*c* on a concave versus a convex membrane surface likely has a number of contributing factors. One factor, as illustrated in Figure 6.1, is that proteins on a concave surface effectively tilt toward each other leading to more excluded volume on a concave surface and thus a requirement for more lipid surface area to allow structural rearrangements. The concave curvature may also facilitate simultaneous contact with lysine residues in or near the A site because the curvature on the surface allows for closer contact with more of the surface of iso-1-Cyt*c*. The convex exterior surface of a vesicle, by contrast, curves away from the surface of the protein. Thus, the concave surface may facilitate interaction with a broader group of lysines, in or near the A-site, permitting a more extensive concerted partial unfolding of the protein that occurs at a higher K_d(app) (larger membrane surface area).

Our recent work on the effect of Lys→Ala variants of iso-1-Cyt*c* on binding to the convex outer surface of pure CL vesicles shows that at least four lysines govern binding at the A site (Lys72, Lys73, Lys86, and Lys87). The results also indicate that neighboring lysines (Lys54, Lys55 and Lys89) also could be involved in A site binding. Thus, a large surface of lysines likely contributes to electrostatic binding via site A. The better shape complementarity between the concave inner surface of a CL vesicle and the surface of iso-1-Cyt*c* may facilitate contact with a larger group of these lysines and the negatively-charged CL headgroups leading to a larger structural rearrangement on a concave versus a convex membrane surface. Further investigation of which lysines contribute to A-site binding will be important, as will determination of whether

the relative importance of each lysine contributing to the A-site is the same on convex versus concave surfaces.

Through their work on binding of horse Cyt*c* to the concave surface of reverse micelles titrated with CL, Wand and colleagues found no evidence of partial unfolding of Cyt*c*. This conclusion was based on the observation that there are only small changes in the ^{1}H-^{15}N HSQC of horse Cyt*c* during the CL titration.[7] The diameter of the reverse micelles in this study was about 4 nm. If the entire surface area of the reverse micelle was replaced by CL during the titration, maximally 35 – 40 CL could be accommodated on the available surface area. At the 7 mM concentration of horse Cyt*c* used in these experiments, each reversed micelle would contain no more than one Cyt*c* molecule. Thus, the maximal value for the exposed LPR would be 35 – 40 and is probably less. Our data (Figure 6.2, bottom panels) also shows minimal structural perturbation to iso-1-Cyt*c* at exposed LPR values less than 40. For mitochondria in the orthodox state, the diameter of the cristae and the cristae junctions are near 30 nm.[4,25,26] The intra-cristal regions make up most of the surface area of the IMM available to Cyt*c*, providing substantial surface area with negative curvature.[26] The negative curvature of the cristae fall in between that of the 4 nm reversed micelles used by Wand and colleagues and the 100 nm CL vesicles used here. Both experiments indicate that at exposed LPR below 40 partial unfolding does not occur on concave CL-containing membrane surfaces. However, our data show that at physiological concentrations of Cyt*c* (0.5 – 1.0 mM, high exposed LPR in our study), it is possible that partial unfolding could occur on the concave surfaces in the intra-cristal compartments of the IMM.

6.4. CONCLUSION

Our findings indicate that, Cyt*c* partially unfolds on both convex and concave surfaces of pure CL vesicles. However, the membrane surface area required for partial unfolding is larger on concave than on convex membrane surfaces. The unfolding process is also more cooperative on a concave versus a convex membrane surface. The larger surface area required on the concave versus the convex surface suggests that the extent of protein unfolding on concave surfaces may be more extensive than for convex surface binding. Our results suggest that the concave curvature of the IMM will have an important impact on the conformational rearrangements of Cyt*c* on CL-containing membranes and thus in controlling the peroxidase activity of Cyt*c* in the early stages of apoptosis.

6.5. REFERENCES

(1) Timkovich, R.; Dickerson, R. E. Preliminary X-Ray Studies of a Cytochrome c from Micrococcus Denitrificans. *Journal of Molecular Biology* **1972**, *72* (1), 199,IN13,203-202,IN13,203.

(2) Kagan, V. E.; Tyurin, V. A.; Jiang, J.; Tyurina, Y. Y.; Ritov, V. B.; Amoscato, A. A.; Osipov, A. N.; Belikova, N. A.; Kapralov, A. A.; Kini, V.; Vlasova, I. I.; Zhao, Q.; Zou, M.; Di, P.; Svistunenko, D. A.; Kurnikov, I. V; Borisenko, G. G. Cytochrome c Acts as a Cardiolipin Oxygenase Required for Release of Proapoptotic Factors. *Nat Chem Biol* **2005**, *1* (4), 223–232.

(3) Orrenius, S.; Zhivotovsky, B. Cardiolipin Oxidation Sets Cytochrome c Free. *Nature chemical biology* **2005**, *1* (4), 188–189.

(4) Frey, T. G.; Renken, C. W.; Perkins, G. A. Insight into Mitochondrial Structure and Function from Electron Tomography. *Biochimica et Biophysica Acta - Bioenergetics* **2002**, *1555* (1–3), 196–203.

(5) Jiang, X. J.; Wang, X. D. Cytochrome C-Mediated Apoptosis. *Annual Review of Biochemistry* **2004**, *73*, 87–106.

(6) Pandiscia, L. A.; Schweitzer-Stenner, R. Coexistence of Native-like and Non-Native Partially Unfolded Ferricytochrome c on the Surface of Cardiolipin-Containing Liposomes. *Journal of Physical Chemistry B* **2015**, *119* (4), 1334–1349.

(7) O'Brien, E. S.; Nucci, N. V.; Fuglestad, B.; Tommos, C.; Wand, A. J. Defining the Apoptotic Trigger: The Interaction of Cytochrome c and Cardiolipin. *Journal of Biological Chemistry* **2015**, *290* (52), 30879–30887.

(8) Rytomaa, M.; Kinnunen, P. K. J. Reversibility of the Binding of Cytochrome c to Liposomes. Implications for Lipid-Protein Interactions. *Journal of Biological Chemistry* **1995**, *270* (7), 3197–3202.

(9) Kawai, C.; Prado, F. M.; Nunes, G. L. C.; Di Mascio, P.; Carmona-Ribeiro, A. M.; Nantes, I. L. PH-Dependent Interaction of Cytochrome c with Mitochondrial Mimetic Membranes: The Role of an Array of Positively Charged Amino Acids. *Journal of Biological Chemistry* **2005**, *280* (41), 34709–34717.

(10) Elmer-Dixon, M. M.; Bowler, B. E. Site A-Mediated Partial Unfolding of Cytochrome c on Cardiolipin Vesicles Is Species-Dependent and Does Not Require Lys72. *Biochemistry* **2017**, *56* (36), 4830–4839.

(11) Margoliash, E.; Frohwirt, N. Spectrum of Horse-Heart Cytochrome C. *The Biochemical journal* **1959**, *71* (3), 570–572.

(12) Pan, J.; Cheng, X.; Sharp, M.; Ho, C.-S.; Khadka, N.; Katsaras, J. Structural and Mechanical Properties of Cardiolipin Lipid Bilayers Determined Using Neutron Spin Echo, Small Angle Neutron and X-Ray Scattering, and Molecular Dynamics Simulations. *Soft Matter* **2015**, *11* (1), 130–138.

(13) Vincelli, A. J.; Pottinger, D. S.; Zhong, F.; Hanske, J.; Rolland, S. G.; Conradt, B.; Pletneva, E. V. Recombinant Expression, Biophysical Characterization, and Cardiolipin-Induced Changes of Two Caenorhabditis Elegans Cytochrome c Proteins. *Biochemistry* **2013**, *52* (4), 653–666.

(14) Muenzner, J.; Pletneva, E. V. Structural Transformations of Cytochrome c upon Interaction with Cardiolipin. *Chemistry and Physics of Lipids* **2014**, *179*, 57–63.

(15) Kostrzewa, A.; Páli, T.; Froncisz, W.; Marsh, D. Membrane Location of Spin-Labeled Cytochrome c Determined by Paramagnetic Relaxation Agents. *Biochemistry* **2000**, *39* (20), 6066–6074.

(16) Hong, Y.; Muenzner, J.; Grimm, S. K.; Pletneva, E. V. Origin of the Conformational Heterogeneity of Cardiolipin-Bound Cytochrome C. *Journal of the American Chemical Society* **2012**, *134* (45), 18713–18723.

(17) Bernad, S.; Oellerich, S.; Soulimane, T.; Noinville, S.; Baron, M. H.; Paternostre, M.; Lecomte, S. Interaction of Horse Heart and Thermus Thermophilus Type c Cytochromes with Phospholipid Vesicles and Hydrophobic Surfaces. *Biophysical Journal* **2004**.

(18) Hanske, J.; Toffey, J. R.; Morenz, A. M.; Bonilla, A. J.; Schiavoni, K. H.; Pletneva, E. V. Conformational Properties of Cardiolipin-Bound Cytochrome C. *Proceedings of the National Academy of Sciences of the United States of America* **2012**, *109* (1), 125–130.

(19) Sinibaldi, F.; Howes, B. D.; Droghetti, E.; Polticelli, F.; Piro, M. C.; Di Pierro, D.; Fiorucci, L.; Coletta, M.; Smulevich, G.; Santucci, R. Role of Lysines in Cytochrome C-Cardiolipin Interaction. *Biochemistry* **2013**, *52* (26), 4578–4588.

(20) Pandiscia, L. A.; Schweitzer-Stenner, R. Salt as a Catalyst in the Mitochondria: Returning Cytochrome c to Its Native State after It Misfolds on the Surface of Cardiolipin Containing Membranes. *Chemical Communications* **2014**, *50* (28), 3674–3676.

(21) Pandiscia, L. A.; Schweitzer-Stenner, R. Coexistence of Native-Like and Non-Native Misfolded Ferricytochrome C on the Surfac of Cardiolipin Containing Liposomes. *Biophysical Journal* **2015**, *108* (2, Supplement 1), 91a.

(22) Pielak, G. J.; Oikawa, K.; Mauk, A. G.; Smith, M.; Kay, C. M. Elimination of the Negative Soret Cotton Effect of Cytochrome c by Replacement of the Invariant Phenylalanine Using Site-Directed Mutagenesis. *Journal of the American Chemical Society* **1986**, *108* (10), 2724–2727.

(23) Tsong, T. Y. The Trp-59 Fluorescence of Ferricytochrome c as a Sensitive Measure of the Over-All Protein Conformation. *Journal of Biological Chemistry* **1974**, *249* (6), 1988–1990.

(24) Pollock, W. B. R.; Rosell, F. I.; Twitchett, M. B.; Dumont, M. E.; Mauk, A. G. Bacterial Expression of a Mitochondrial Cytochrome c. Trimethylation of Lys72 in Yeast Iso-1-Cytochrome C and the Alkaline Conformational Transition. *Biochemistry* **1998**, *37* (17), 6124–6131.

(25) Mannella, C. A. The Relevance of Mitochondrial Membrane Topology to Mitochondrial Function. *Biochimica et biophysica acta* **2006**, *1762* (2), 140–147.

(26) Gilkerson, R. W.; Selker, J. M. L.; Capaldi, R. A. The Cristal Membrane of Mitochondria Is the Principal Site of Oxidative Phosphorylation. *FEBS Letters* **2003**.

CHAPTER 7: Summary

7.1. Quantification of Lipids Enables Analytical Protein-Lipid Binding Analysis

A tool to rapidly quantify lipid concentration is required to approach protein-lipid binding quantitatively. With the intent of performing an in-depth analysis of both variant dependent and amino acid dependent lipid binding, we created a calculator that uses absorbance measurements acquired from a UV-Visible spectrophotometer and first calculates the number of vesicles in solution, then employs a lipid density measurement to approximate the total lipid concentration of the system of interest. This technique was first developed for pure lipid systems.[1] With the intent of expanding protein-lipid analysis to mixed lipid systems like those commonly employed to study the Cyt*c*-CL interaction, we modified our lipid calculator technique to make accessible lipid concentration measurements of varying compositions and concentrations of lipids.[2] Both the pure and mixed lipid calculators enable rapid quantification of lipids essential for analytical analysis of protein-lipid binding.

7.2. Evolutionary Comparison of Cytochrome *c* Variants Demonstrates Divergence of Protein Function.

Recent work has extended the role of Cyt*c* from an electron shuttle in the electron transport chain to a constituent in the pre-apoptotic pathway specifically in mammals.[3,4] In both cellular roles, Cyt*c* associates with CL on the outer leaflet of the inner mitochondrial membrane. In this work, we investigated the electrostatic protein-lipid interaction of both yeast and human Cyt*c* to determine if differing binding mechanisms exist that may explain the development of apoptotic precursor for human Cyt*c*. Our findings show that both protein variants initially dock on the

membrane and remain in a folded state at low lipid to protein ratios (when space is population limited) and display a biphasic response to binding. This biphasic response arises as the lipid to protein ratio increases, freeing up space on the membrane. Our variant dependent analysis showed that human Cyt*c* had an attenuated dissociation constant consistent with more lipid required to generate unfolding on the membrane surface than its yeast homologue. Further, we showed that the amino acid generally assumed to be responsible for this interaction (Lys72) did not contribute substantially to lipid binding, suggesting a complete characterization of electrostatic binding constituents on Cyt*c* is required to further understand the interaction being investigated.

7.3. Alanine Screening Characterizes Anionic Binding Site Constituents and Shows Concentration Charge Dependence of Lysines on Cardiolipin Binding.

As evidenced from variant dependent analysis of CL binding in chapter 3, an investigation into the constituents of the anionic site A was needed to fully understand the electrostatic interaction between Cyt*c* and CL during protein-lipid docking. To determine amino acid contribution, alanine screening was performed in and around the A site (Figure 1.2) of Cyt*c* and CL binding studies were used to assess the contribution of each substituted lysine of interest. Through these studies, we found that several lysines in the region of the A site (Lys72, Lys73, Lys86 and Lys87) had varying contributions to binding. Interestingly, complete removal of all four lysines did not completely terminate electrostatic binding suggesting that these four lysines do not completely account for electrostatic binding in this region of the protein.

7.4. Cardiolipin Membrane Distribution Demonstrates Preference of the Lipid for Concave Surfaces.

A concern in designing protein-lipid binding experiments is what exactly is being investigated especially in more complex systems where different mixtures of lipids are used. Specifically, CL is known to reside on concave surfaces but when used in binding experiments, it is assumed that the lipid homogeneously distributes itself between the concave and convex surfaces of vesicles. Further, most published work studying the Cyt*c*-CL interaction study the interaction on the convex outer leaflet of vesicles, ignoring any potential lipid driven distribution inhomogeneity. In chapter 4, we assessed the distribution of anionic lipids in mixed lipid systems comprised of the neutral lipid DOPC. To do this, we used the anionic lipid detecting fluorophore TTAPE-Me and found that CL prefers the concave interior of vesicles generated an inhomogeneity of lipid composition between vesicle membrane leaflets. This preferential localization is directly due to CL's structure, specifically it's four acyl chains. In comparison, when we assessed lipid distribution of DOPG (structurally similar to CL but possessing half the number of hydrophobic tails), we found that no preferential distribution of the anionic lipid exists. Using these findings, we then analyzed Cyt*c*-CL binding to both 100% DOPC and 20% CL/80%DOPC systems and found that protein-lipid binding was extensively attenuated. Binding did not occur appreciably in pure DOPC titrations and only modest binding was detected in the mixed lipid system. These findings further suggest that CL prefers the concave interior of vesicles, giving rise to the possibility that binding of Cyt*c* to CL on the outside of a vesicle may be intrinsically different that binding to CL on the interior of the vesicle.

7.5. Curvature Dependent Binding Analysis Demonstrates the Role of Membrane Structure in Cytochrome *c*-Cardiolipin Binding.

Because Cyt*c*-CL binding is known to occur on concave membrane surfaces, our last point of analysis of this binding interaction was to elucidate the role of membrane curvature in the protein-lipid interaction. In chapter 3, we demonstrated that a concentration dependent biphasic response to lipid exposure occurred in both yeast and human mutants exposed to convex surfaces. In comparing these findings with yeast Cyt*c* exposed to concave membrane surfaces, we have been able to show that the biphasic nature of the binding event is wholly conditional, dependent on membrane structure. This loss of biphasic binding strongly suggests that the membrane's curvature plays a direct role in the facilitation of protein docking and concerted unfolding.

7.6. Future Directions

Our findings presented in this work provide impetus for several future directions of investigation. Current work hypothesizes four potential binding sites on Cyt*c*. Given the relatively small size of the protein and in coordination with our findings that a biphasic binding event is observed under certain conditions, it is probably more likely that the four hypothesized binding sites are actually different aspects of a smaller number of binding domains. Experimental design and environmental conditions may be such that different aspects of each domain are intermittently probed but the physiological behavior of the entire domain is not seen using current methods. Alanine screening would provide insight into population of amino acids involved in lipid docking and binding. Further, a repetition of concave binding analysis using

alanine mutants would aid in elucidating the role of each amino acid involved in either docking or unfolding the protein.

Appendix I.1: INSTRUCTIONS FOR USING THE MVCC

Below is the MVCC.m file for vesicle and lipid quantification for TOCL. To use file, copy from top green '%' line to bottom '%' line into blank .m file in Matlab and save as MVCC.m in the Matlab directory.

To run MVCC file in Matlab, open Matlab and in command line, type 'MVCC' and press enter. An 'options' window will appear allowing you to choose the lipid of interest (TOCL, DOPC, POPC or POPG) if file has been copied and saved correctly. Select the lipid you wish to measure. Next a popup window will appear. Input wavelength in nanometers and absorbance in A.U. For spectrophotometer pathlengths not equal to 1 cm, scale absorbance accordingly. Input vesicle diameter in nanometers. Press enter. Calculation output will appear in command window. Output specifies first, vesicle concentration in mol/L and secondly, TOCL lipid concentration in mol/L.

Modifying Calculator for different lipids:
This calculator can be modified to calculate lipid concentration for other lipids as well. To modify the MVCC to measure a different lipid, change the following parameters: HDSA, BT and RI. These correspond to headgroup surface area (HDSA), bilayer thickness (BT) and refractive index (RI) and can be found in lines 31-33 once the code is copied into the .m file.

```
%%%%%%%%%%%%%%%%%%%%%%%%%%%%%%%%%%%%%%%%%%%%%%%%%%%%%%%%%%%%%%%%%%%%%%%%%%%%
%
%                MVCC.m (Matlab Vesicle Concentration Calculator)
%
%                Written by: Margaret Elmer-Dixon
%                Last Editted: 9/19/2016
%
%    The MVCC Calculates concentration of TOCL lipid using data input taken
%    from a UVVis spectrophotometer at a known wavelength. Vesicle diameter
%    must be specified. To calculate lipid concentration from vesicle
%    scattering, follow dialog box prompts. Output is in command window.
%
%%%%%%%%%%%%%%%%%%%%%%%%%%%%%%%%%%%%%%%%%%%%%%%%%%%%%%%%%%%%%%%%%%%%%%%%%%%%


clear all

% Construct a questdlg with three options
choice = menu('Select Lipid Composition', ...
    'TOCL','DOPC','POPC','POPG');
% Handle response
switch choice
    case 1 %'TOCL'
      lipidchoice = 'TOCL'
      HDSA = 1.298; % nm^2 (Pan, Soft Matter, 2015)
      BT = 3.67;% nm (Pan, Soft Matter, 2015)
      RI = 1.46; %(Maniti, Biochimica et Biophysica Acta, Biomembranes,
                 %1808(4):1129-1139, 2011)

    case 2 %'DOPC'
      lipidchoice = 'DOPC'
      HDSA = .674; % nm^2 (Pan, Soft Matter, 2015)
      BT = 3.87;% nm (Pan, Soft Matter, 2015)
      RI = 1.375;%1.375;% (JF Popplewell, Biochemicia et Biophysicia Acta
                 %1768 (2007) 13-20)

    case 3 %'POPC'
      lipidchoice = 'POPC'
      HDSA = .627; % nm^2 @20C (Kucerka, Biochemia et Biophysicia Acta
                   % 1808(2011) 2761-2771)
      BT = 3.98; % nm (Kucerka, Biochemia et Biophysicia Acta 1808(2011)
                 % 2761-2771)
      RI = 1.376; % 1.376(JF Popplewell, Biochemicia et Biophysicia Acta 1768
                  % (2007) 13-20)

    case 4 %'POPG'
      lipidchoice = 'POPG'
      BT = 3.73;% nm @20C (Pan, Biochemicia et Biophysicia Acta 2012,
                % 1818(9):2135-2148)
      HDSA = .644;% nm^2 @20C (Pan, Biochemicia et Biophysicia Acta 2012,
                  % 1818(9):2135-2148)
      RI = 1.45;% (Murray. J Struct. Bio. 2009, 168(1):183-189)
  end
```

```
prompt = {'Wavelength of Absorbance','Absorbance Measurement (A.U.)',…
'Vesicle Diameter (nm)'};
dlg_title = 'MVCC Input';
num_lines = 1;
defaultans={'300','1.08','100'};
answer = inputdlg(prompt,dlg_title,num_lines,defaultans);
            Wavelength = str2num(answer{1,1});
            AbsorbanceMeasured = str2num(answer{2,1});
            diameter = str2num(answer{3,1}); %nm
            radius = diameter/2; %nm
            radiusM= radius/10^9; %radius in meters


            %calculate lipid specific vesicle characteristics
            radiusInner = radius-BT; %using bilayer thickness, calculate
                                     %inner radius
            SAvesicle=4*pi*(radius^2+(radiusInner)^2); %SA of Outer and Inner
                                                       %bilayer in nm^2
            LipidDensity = SAvesicle/HDSA; %lipids per vesicle

            %calculate refractive index for each wavelength
            m1 = 1.31848+6.662./(Wavelength-129.2); % equation from 'Water
            %refractive index in dependence on temperature and wavelngth: a
            %simple approximation' Bashkatov and Genina, Optics Department
            %Saratoc state university
            m = RI+i.*1.1*10^-7;%1.45 taken from sucrose index matching
            %(Ardhammar,2002)

%calculate x parameter fommo equation 4
k = 2.*pi./Wavelength; %convert to angular wave number
xx = 2*pi*radius*m1./Wavelength;%defines size parameter

%calculate extinction efficiencies for each wavelength based on Bohren 1983.
x=xx;

    if x==0 % To avoid a singularity at x=0
    Eff=[real(m) imag(m) 0 0];
    elseif x>0 % This is the normal situation
    nmax=round(2+x+4*x^(1/3));
    n1=nmax-1;
    n=(1:nmax);cn=2*n+1; c1n=n.*(n+2)./(n+1); c2n=cn./n./(n+1);
    x2=x*x;


            %finding ABCD
            nu=(n+.5);
            z=m.*x;
            m2=m.*m;

            sqx=sqrt(0.5*pi./x);
            sqz=sqrt(0.5*pi./z);

            bx=besselj(nu,x).*sqx;
            bz=besselj(nu,z).*sqz;
            yx=bessely(nu,x).*sqx;
```

```
            hx=bx+i*yx;
            b1x=[sin(x)/x,bx(1:nmax-1)];
            b1z=[sin(z)/z,bz(1:nmax-1)];
            y1x=[-cos(x)/x,yx(1:nmax-1)];
            h1x=b1x+i*y1x;
            ax=x.*b1x-n.*bx;
            az=z.*b1z-n.*bz;
            ahx=x.*h1x-n.*hx;
            anABCD=(m2.*bz.*ax-bx.*az)./(m2.*bz.*ahx-hx.*az); % this
            %corresponds to an in Eqn 3a
            bnABCD=(bz.*ax-bx.*az)./(bz.*ahx-hx.*az); %this corresponds to bn
            %in Eqn 3b
            cnABCD=(bx.*ahx-hx.*ax)./(bz.*ahx-hx.*az);
            dnABCD=m.*(bx.*ahx-hx.*ax)./(m2.*bz.*ahx-hx.*az);


            f =[anABCD;bnABCD;cnABCD;dnABCD];%ABCD Values required for Qext
            %calculation

    anp=(real(f(1,:))); anpp=(imag(f(1,:)));
    bnp=(real(f(2,:))); bnpp=(imag(f(2,:)));
    g1(1:4,nmax)=[0; 0; 0; 0]; % displaced numbers used for
    g1(1,1:n1)=anp(2:nmax); % asymmetry parameter, p. 120, Bohren
    g1(2,1:n1)=anpp(2:nmax);
    g1(3,1:n1)=bnp(2:nmax);
    g1(4,1:n1)=bnpp(2:nmax);
    dn=cn.*(anp+bnp);
    q=sum(dn);
    Qext=2*q/x2;% this corresponds to Cext in eqn 2

    Eff=[real(m) imag(m) x Qext];

    end



            area= pi*radiusM^2; %area of scattering centers in m^2
            pathlength=.01; %pathlength in meters
            N = AbsorbanceMeasured./Qext./area./pathlength; %finds
            %N=2.303*A/Q/area/d and converts to Mol

            Nmol=N/6.022e23 %convert N avg to moles

fprintf('this is the vesicle concentration in M/L');

            lipid=Nmol*LipidDensity %lipids total

fprintf('this is the lipid concentration in M/L');
%%%%%%%%%%%%%%%%%%%%%%%%%%%%%%%%%%%%%%%%%%%%%%%%%%%%%%%%%%%%%%%%%%%%%%%%%%%%%%%%
```

Appendix I.2: INSTRUCTIONS FOR USING THE MLC

MATLAB CODE Installation and User Instructions:

1) In matlab, copy and paste the following page of code (starting with the Green commented region '%') into a .m file and save it as 'MLC.m' in the Matlab directory.
2) To run:
    a. Type 'MLC' into the command line and press 'Enter'
    b. Open MLC.m and press 'Run' at the top of the page view window.
3) The running program initiates with the following pop-up window, where the mole fraction/fraction of DOPG, DOPC and Cardiolipin (TOCL) can be specified. Note that three component systems may be calculated but have not been validated. Further, any number of absorbances and their corresponding wavelengths can be specified provided they are space separated.

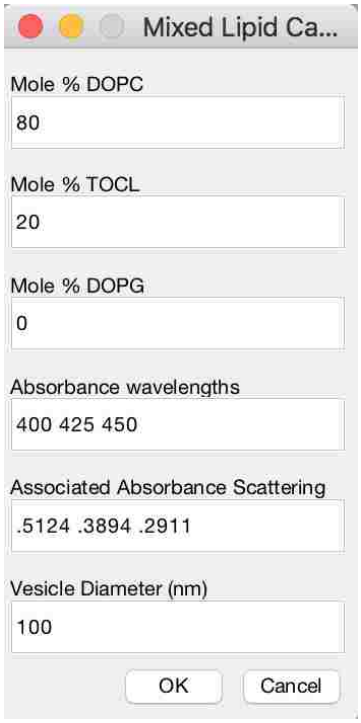

4) The output after pressing 'OK', will show up in the command window in table format. Standard deviations will be output for total lipid concentration and vesicle concentration if more than one absorbance is provided.

	Mean	STD
Mole Fraction DOPC	0.5	0
Mole Fraction CL	0.5	0
Mole Fraction DOPG	0	0
mM DOPC Lipid	1.5569	0
mM CL Lipid	1.5569	0
mM DOPG Lipid	0	0
mM Total Lipid	3.1139	0.21618
nM Vesicles	52.655	3.6556

```
%%%%%%%%%%%%%%%%%%%%%%%%%%%%%%%%%%%%%%%%%%%%%%%%%%%%%%%%%%%%%%%%%%%%%%%%%%%%
%
%               Mixed Lipid Calculator
%
%               Written by: Margaret Elmer-Dixon
%               Last Edited: 3.14.2018
%
%   The Mixed Lipid Calculator calculates concentration of lipid using data input taken
%   from a UV-Vis spectrophotometer at a known wavelength. Vesicle diameter
%   must be specified. To calculate lipid concentration from vesicle
%   scattering, follow dialog box prompts. Lipid Mixture Concentrations must be specified.
%   Output is in command window.
%
%%%%%%%%%%%%%%%%%%%%%%%%%%%%%%%%%%%%%%%%%%%%%%%%%%%%%%%%%%%%%%%%%%%%%%%%%%%%


clear all

prompt={'Mole % DOPC','Mole % TOCL','Mole % DOPG','Absorbance wavelengths','Associated Absorbance
Scattering','Vesicle Diameter (nm)'};
dlg_title='Mixed Lipid Calculator';
num_lines = 1;
defaultans = {'80','20','0','400 425 450','.5124 .3894 .2911','100'};
answer=inputdlg(prompt,dlg_title,num_lines,defaultans);

A=str2num(answer{1,1});
B=str2num(answer{2,1});
C=str2num(answer{3,1});
nm=str2num(answer{4,1});
Absorbance=str2num(answer{5,1});
Diameter=str2num(answer{6,1});

XA=A./(A+B+C);
XB=B./(A+B+C);
XC=C./(A+B+C);

      %DOPC
      HDSAa = .674; % nm^2 (Pan, Soft Matter, 2015)
      BTa = 3.87;% nm (Pan, Soft Matter, 2015)
      RIa = 1.375;%1.375;% (JF Popplewell, Biochemicia et Biophysicia Acta 1768 (2007) 13-20)
      Va =HDSAa*BTa; %nm^3

      %Cardiolipin
      BTb= 3.67;% nm (Pan, Soft Matter, 2015)
      HDSAb= 1.298; % nm^2 (Pan, Soft Matter, 2015)
      RIb= 1.46; %(Maniti, Biochimica et Biophysica Acta, Biomembranes, 1808(4):1129-1139, 2011)
      Vb=HDSAb*BTb;

      %DOPG
      HDSAc = .694; %nm^2 @20C (Pan, Biochemicia et Biophysicia Acta 2012, 1818(9):2135-2148)
      BTc = 3.63; %nm @20C (Pan, Biochemicia et Biophysicia Acta 2012, 1818(9):2135-2148)
      RIc = 1.359; %(JF Popplewell, Biochemicia et Biophysicia Acta 1768 (2007) 13-20) THIS IS FOR PG
      Vc = HDSAc*BTc;

      %SA Percent HD (surface area percent by headgroup)
      %Average HDSA (headgroup surface area) taking into account mole fraction
      HDSA = (XA*HDSAa+XB*HDSAb+XC*HDSAc);

      %Percent surface area covered by each molecule
      PA = XA*HDSAa/HDSA; %percent surface area comprised of DOPC
      PB = XB*HDSAb/HDSA; %percent surface area comprised of CL
      PC = XC*HDSAc/HDSA; %percent surface area comprised of DOPG

      %Refractive index based on the surface area occupation of each lipid
      RI = RIa*PA+RIb*PB+RIc*PC;

      % Bilayer thickness based on the weighted surface area occupation of
      % each lipid
      BT = BTa*PA+BTb*PB+BTc*PC;

      %calculate lipid specific vesicle characteristics
      diameter = Diameter;%%nm
      radius = diameter/2; %nm
      radiusM= radius/10^9; %radius in meters
      radiusInner = radius-BT; %using bilayer thickness, calculate inner radius
      SAvesicle=4*pi*(radius^2+(radiusInner)^2); %SA of Outer and Inner bilayer in nm^2
```

```
      LipidDensity = SAvesicle/HDSA; %lipids per vesicle


      for ii = 1:length(nm)
RIi(ii) = RI;
            %set indep vars
            Wavelength = nm(ii);%nm
            AbsorbanceMeasured = Absorbance(ii);%arbitrary units

            %calculate refractive index for each wavelength
            m1 = 1.31848+6.662./(Wavelength-129.2); % equation from 'Water refractive index in
%dependence on temperature and wavelngth: a simple approximation' Bashkatov and Genina, Optics
%Department Saratoc state university
            m = RI+i.*1.1*10^-7;%1.45 taken from sucrose index matching (Ardhammar,2002)

%calculate x parameter from equation 4 from Elmer-Dixon and Bowler 2017
k = 2.*pi./Wavelength; %convert to angular wave number
xx = 2*pi*radius*m1./Wavelength;%defines size parameter

%calculate extinction efficiencies for each wavelength based on Bohren 1998.
x=xx;
X(ii)=x;
    if x==0 % To avoid a singularity at x=0
    Eff=[real(m) imag(m) 0 0];
    elseif x>0 % This is the normal situation
    nmax=round(2+x+4*x^(1/3));
    n1=nmax-1;
    n=(1:nmax);cn=2*n+1; c1n=n.*(n+2)./(n+1); c2n=cn./n./(n+1);
    x2=x*x;


            %finding ABCD
            nu=(n+.5);
            z=m.*x;
            m2=m.*m;

            sqx=sqrt(0.5*pi./x);
            sqz=sqrt(0.5*pi./z);

            bx=besselj(nu,x).*sqx;
            bz=besselj(nu,z).*sqz;
            yx=bessely(nu,x).*sqx;
            hx=bx+i*yx;
            b1x=[sin(x)/x,bx(1:nmax-1)];
            b1z=[sin(z)/z,bz(1:nmax-1)];
            y1x=[-cos(x)/x,yx(1:nmax-1)];
            h1x=b1x+i*y1x;
            ax=x.*b1x-n.*bx;
            az=z.*b1z-n.*bz;
            ahx=x.*h1x-n.*hx;
            anABCD=(m2.*bz.*ax-bx.*az)./(m2.*bz.*ahx-hx.*az); % this corresponds to an in Eqn 3a from
            %Elmer-Dixon and Bowler 2017
            bnABCD=(bz.*ax-bx.*az)./(bz.*ahx-hx.*az); %this corresponds to bn in Eqn 3b from Elmer
            %Dixon and Bowler 2017
            cnABCD=(bx.*ahx-hx.*ax)./(bz.*ahx-hx.*az);
            dnABCD=m.*(bx.*ahx-hx.*ax)./(m2.*bz.*ahx-hx.*az);


            f =[anABCD;bnABCD;cnABCD;dnABCD];%ABCD Values required for Qext calculation using Eqn 2
            %from Elmer-Dixon and Bowler 2017

    anp=(real(f(1,:))); anpp=(imag(f(1,:)));
    bnp=(real(f(2,:))); bnpp=(imag(f(2,:)));
    g1(1:4,nmax)=[0; 0; 0; 0]; % displaced numbers used for
    g1(1,1:n1)=anp(2:nmax); % asymmetry parameter, p. 120, Bohren 1983
    g1(2,1:n1)=anpp(2:nmax);
    g1(3,1:n1)=bnp(2:nmax);
    g1(4,1:n1)=bnpp(2:nmax);
    dn=cn.*(anp+bnp);
    q=sum(dn);
    Qext=2*q/x2;% this corresponds to Cext in eqn 2 from Elmer-Dixon and Bowler 2017

    Eff=[real(m) imag(m) x Qext];

    end
```

```
Qx(ii)=Qext;

            area= pi*radiusM^2; %area of scattering centers in m^2
            pathlength=.01; %pathlength in cm
            N = AbsorbanceMeasured./Qext./area./pathlength; %finds N=2.303*A/Q/area/d and converts to
            %Mol

            Nmol(ii)=N/6.022e23; %convert N avg to moles
            % fprintf('this is the vesicle concentration in M/L');

            lipid(ii)=Nmol(ii)*LipidDensity; %lipids total
            % fprintf('this is the lipid concentration in M/L');
      end

 lmean = mean(lipid)*10^3;%convert from M to mMol
 lstd = std(lipid)*10^3;


 Nmean = mean(Nmol)*10^9;%convert from M to nMol
 Nstd = std(Nmol)*10^9;


 DOPCcon=XA*lmean;
 CLcon=XB*lmean;
 DOPGcon=XC*lmean;


DataName = {'Mole Fraction DOPC','Mole Fraction CL','Mole Fraction DOPG','mM DOPC Lipid',...
'mM CL Lipid','mM DOPG Lipid','mM Total Lipid','nM Vesicles'};
Mean = [XA; XB; XC; DOPCcon; CLcon; DOPGcon; lmean; Nmean];
STD = [0; 0; 0; 0; 0; 0; lstd; Nstd];
T= table(Mean,STD,'RowNames',DataName)
```

Appendix II: Tables

Table A.1.

Comparison of Cardiolipin and DOPC content in vesicles from phosphorous analysis versus Mie scattering analysis.

Date	Vesicle Lipid Content	Phosphorous,† mg/L	Lipid Concentration,† mM,	Calculated Lipid Concentration,‡ mM	% error
2/27/15	TOCL	59.7	0.995	0.957	4.0
5/14/15	TOCL	201	3.35	3.20	4.7
4/8/16	TOCL	32.2	0.537	0.515	4.3
4/8/16	TOCL	60.5	1.01	1.01	0.0
4/8/16	TOCL	112	1.87	1.87	0.0
10/27/16	DOPC	53.4	1.72	1.73	0.6
11/4/16	DOPC	48.4	1.56	1.59	1.9
11/6/16	DOPC	50.6	1.63	1.68	3.0

†Based on phosphorous content obtained from ICP measurements after phosphorous digest.
‡Calculated using Matlab vesicle concentration calculator.

Table A.2.

Comparison of DOPC content in vesicles from phosphorous analysis versus concentration calculation using initial manufacturer specified concentration

Date	Vesicle Lipid Content	Volume Lipid Dried (μl)	Phosphorous,† mg/L	Cardiolipin,† mM,	Cardiolipin,‡ mM	% error
2/27/15	TOCL*	160	59.7	0.957	1.07	12
5/14/15	TOCL*	1000	201	3.20	3.3	3.1
10/27/16	DOPC§	160	53.4	1.72	2.00	16
11/4/16	DOPC§	160	48.4	1.56	2.00	28
11/6/16	DOPC§	160	50.6	1.63	2.00	23

†Based on phosphorous content obtained from ICP measurements after phosphorous digest.
‡ Based on Manufacturer specified concentration. Samples were prepared with the intended concentration based on manufacturer labeling (Cardiolipin: 5 mg/ml, DOPC: 10 mg/ml)

Table A.3.

Wavelength Ranges for testing Various Vesicle Sizes

Vesicle Size	Wavelength Range for Testing (nm)			
(nm)	Cardiolipin	DOPC	POPC	POPG
50	200 - 350	200 - 325	200 - 325	200 - 350
100	200 - 690	200 - 650	200 - 650	200 - 690
200	200 - 1000	200 - 1000	200 - 1000	200 - 1000
400	275 - 1000	260 - 1000	260 - 1000	275 - 1000
1000	690 - 1000	650 - 1000	650 - 1000	690 - 1000

Calculations based on reported Index of refractions using Eqn. 4 from the main text.

Table A.4.
Comparison of lipid concentration in pure DOPG vesicles from lipid mass versus phosphorous and Mie scattering analyses

Expected lipid concentration based on lipid mass, mM[*]	Expected phosphorus content based on lipid mass, mg/mL[*]	Phosphorous content from ICP, mg/L[†]	Total Lipid Concentration from ICP, mM[†]	Calculated DOPG Concentration (MVCC), mM[‡]	% Error lipid mass versus ICP[§]
1.48	45.9	36.0	1.16	1.14 ± 0.02	27.5
1.00	30.6	29.2	0.94	0.89 ± 0.05	6.38
0.25	7.65	6.16	0.20	0.21 ± 0.01	25.0

[*]Based on manufacturer reported lipid mass.
[†]Based on phosphorous content obtained from ICP measurements after a cold digest to release phosphorous (see ref. [1]).
[‡]Calculated using Matlab Vesicle Concentration Calculator (MVCC). Error is the standard deviation from scattering data at multiple wavelengths.
[§]% Error for manufacturer reported lipid mass relative to ICP.

Table A.5.
Comparison of mixed lipid content in vesicles from phosphorous analysis versus Mie scattering analysis

Vesicle Mixed Lipid Content[*]	Expected lipid concentration based on lipid mass[†], mM	Expected phosphorus content based on lipid mass, mg/L[†]	Phosphorous content from ICP, mg/L[‡]	Total lipid concentration from ICP, mM[‡]	Calculated total lipid concentration (MLC), mM[§]	% Error lipid mass versus ICP[|]
20% CL	1.00	37.2	34.6	0.93	0.95 ± 0.03	7.64
20% CL	1.50	55.8	46.8	1.26	1.37 ± 0.04	19.2
20% CL	3.36	104	85.0	2.28	2.47 ± 0.08	22.5
50% CL	0.66	31.0	27.0	0.58	0.54 ± 0.03	15.0
50% CL	0.45	21.0	16.4	0.35	0.35± 0.03	28.2
20% DOPG	1.12	34.7	33.1	1.07	1.09± 0.01	4.83
20% DOPG	0.37	11.5	11.8	0.38	0.37± 0.01	3.13
20% DOPG	0.75	23.3	23.4	0.75	0.79± 0.03	0.47
50% DOPG	1.12	34.7	32.7	1.06	1.08± 0.02	6.11

[*]Mole percent, the remainder being DOPC.
[†]Based on manufacturer reported lipid mass.
[‡]Based on phosphorous content obtained from ICP measurements after a cold digest to release phosphorous (see ref. [1]).
[§]Calculated using the Mixed Lipid Calculator (MLC) using Mie scattering data. Error is the standard deviation from scattering data at multiple wavelengths.
[|]% Error for manufacturer reported lipid mass relative to ICP.

Table A.6. Sense primer sequences for preparation of iso-1-Cyt*c* variants.

Variant	Primer sequence
K73A	TCAGAGTACTTGACTAACCCAAAAGCCTATATTCCTGGTACCAAGATGGCC
K72|73A	GAGTACTTGACTAACCCAGCCGCATATATTCCTGGTACCAAGAT
K86A	GATGGCCTTTGGTGGGTTGGCGAAGGAAAAAGACAGAAAC
K87A	GGCCTTTGGTGGGTTGAAGGCGGAAAAAGACAGAAACGAC
K86|87A	TCGTTTCTGTCTTTTTCCGCCGCCAACCCACCAAAGGC